Microwave Photonic Mixers With High Spurious Free Dynamic Range

Ali Altaqui

A thesis submitted in fulfillment of the requirements for the Degree of Master of Philosophy

School of Electrical & Information Engineering

The University of Sydney

Australia

August 2014

ABSTRACT

Microwave photonic signal processing offers unprecedented features for processing high bandwidth signals. It puts forward a new prospect for overcoming the inherent bottlenecks caused by the limitations in conventional microwave signal processors. The motivation stems from the great potential of exploiting the unique, high time-bandwidth product, low loss, and immunity to electromagnetic interference (EMI) capabilities of photonic signal processing. Microwave photonic signal processing is the new paradigm for processing wideband microwave signals with high tunability and reconfigurability. Amongst the different photonic signal processors, the photonic frequency downconverter is important in many remote antenna, defence and radar systems. Two new microwave photonic mixers are presented in this thesis. The performance of these mixers is substantially improved compared to previous approaches.

A new linearised photonic mixer structure, which can fully eliminate the third order intermodulation distortion, is presented. It is based on an integrated dual-parallel Mach-Zehnder modulator to which an optimised RF split and an optimised optical phase shift is applied, in series with a Mach-Zehnder modulator driven by the LO. The mixer achieves a very high spurious free dynamic range performance, it enables essentially infinite isolation between the RF and LO ports, and it has the ability to function over a multi-octave frequency range. Experimental results demonstrate a record measured spurious free dynamic range performance of 127 dB·Hz$^{4/5}$, which is over 22 dB higher than that of the conventional dual-series Mach-Zehnder modulator based microwave photonic mixer.

In addition, another new wideband linearised photonic mixer structure is presented. It is based on using stimulated Brillouin scattering effects to suppress the optical carrier, together with a single drive integrated dual-parallel Mach-Zehnder modulator for linearisation. The new structure offers enhanced conversion efficiency through the carrier suppression technique. It also suppresses the third order intermodulation distortion to consequently increase the spurious free dynamic range performance through optimising the bias condition of the dual-parallel Mach-Zehnder modulator. Additionally, the new

structure enables multioctave operation, and infinite isolation between the RF and LO ports. Simulation results showed a spurious free dynamic range of 120.4 dB·Hz$^{4/5}$, and a conversion gain of 8.45 dB, corresponding to 15 dB, and 8.8 dB improvements respectively when compared to the conventional dual-series Mach-Zehnder modulator based microwave photonic mixer. Experimental results demonstrate a measured spurious free dynamic range performance of 120.8 dB·Hz$^{4/5}$, which corresponds to 16 dB improvement compared to the conventional photonic mixer structure.

Statement of Originality

I declare that this thesis, under the guidance of Prof. Robert Minasian and Dr. Erwin Chan, submitted in fulfillment of the requirements for the award of Master of Philosophy, in the School of Electrical and Information Engineering, University of Sydney, is original unless otherwise acknowledged or referenced in the text of the thesis. The thesis has not been presented for the award of any other qualification at any educational institution.

Signature: [redacted]

Date: 06 August 2014

ACKNOWLEDGEMENTS

It may be challenging to fill 100 pages of technical material for this thesis, but it certainly would be a great pleasure to fill 100 pages to acknowledge all of the people who made this possible.

First and foremost, I would like to show my gratitude to my supervisor, Prof. Robert Minasian, for his support, guidance, and patience throughout this research. His valuable discussion, and his eagerness to guide me have made it possible to complete this work.

Moreover, I would like to thank my associate supervisor, Dr. Erwin Chan, for his great contribution on my projects. His supervision on the experiments was particularly useful.

Finally I would like to dedicate this thesis to my loving and extremely supportive father, Dr. Abdullah Altaqui, and my beloved mother. They have been always guiding and supporting me since the start of my degree in the University of Sydney. Without their support and encouragement, I would have never pursued a degree in the field of engineering.

Table of Contents

CHAPTER 1 Introduction

1.1 Motivation

The increasing demand for the transmission and receiving of data at high speed has heralded fibre-optic communication technologies as the savior, mainly due to its low loss and its extremely wide bandwidth potential. The inability of conventional microwave systems to process information at very high frequency has motivated the development of microwave photonics, which offers a unique powerful paradigm for processing high bandwidth signals [1]. Moreover the field of microwave photonics has enabled the possibility to implement signal processing functions that are complex or even impossible to be achieved in the electrical domain [2]. This field promises to be the ultimate solution for many applications that require ever-increasing speed, bandwidth and dynamic range such as defence, wireless communications, sensors and radars. These applications also require devices that are small, lightweight and with low power consumption, while simultaneously offering large tunability and strong immunity to electromagnetic interference [3,4].

Among the different photonic signal processor operations is the important function of the microwave photonic mixer, which is essential in many applications such as antenna remoting, radio-over-fibre, and phased array antennas [5-7]. These applications often require the high frequency microwave signal to be downconverted to an intermediate frequency (IF) signal so as to enable efficient digitization of the received signal, hence simplifying the optical receiver design. A high dynamic range photonic mixer is particularly important to enable the digitization of the signal with high resolution [8]. However, over the past years, microwave photonic mixers have enjoyed limited success principally because of the inadequate dynamic range. For this reason, many researchers have been motivated to investigate new techniques to remove the spurious distortion from the photonic mixer to improve its dynamic range.

1.2 Objective

The aim of this research is centered on obtaining new concepts for photonic mixers that perform frequency downconversion directly in the optical domain, and in particular to improve the mixer spurious free dynamic range (SFDR). A detailed literature review of the previous photonic mixer structures is initially presented. Then the fundamental figure of merit of the photonic mixer is investigated, including the conversion efficiency, the noise figure and the SFDR. The new ideas are investigated using theoretical analysis and simulation to obtain the optimum design. Finally, the validity of the new ideas are verified experimentally.

1.3 Synopsis

The structure of this thesis is as follows. Chapter 2 provides a background on fibre optic communication systems, microwave photonics and microwave photonic signal processing techniques. Moreover the fundamental concept of microwave photonic mixers is introduced. The essential components for constructing a photonic mixer, as well as the mixer figure of merit parameters, are then introduced. Finally a detailed literature review of the previous work related to microwave photonic mixers is presented.

Chapter 3 presents a new linearised photonic mixer structure that can achieve a record dynamic range performance. The chapter starts with a summary of the previously reported linearised photonic mixer techniques. The limitations in the previously reported techniques are discussed. A novel structure is then presented which is based on an integrated DPMZM to which an optimised RF split and an optimised optical phase shift is applied, in series with an MZM driven by the LO. The new structure enables full elimination of the third order intermodulation distortion and consequently achieves high SFDR performance, while also enabling multioctave operation, and essentially infinite isolation between the RF and LO ports. The DPMZM is linearised by fully cancelling the third order IMD via controlling the modulator bias voltages and designing the splitting ratio of the RF signal applied to the DPMZM. Simulation results are also presented that can model general bias conditions with the aim of selecting the optimum bias to improve the conversion efficiency, or the noise figure while simultaneously achieving high SFDR performance. The tolerance of the linearised DPMZM based microwave photonic mixer is further investigated at a bias solution that relaxes the critical tolerance requirements of the linearised approach. Experimental results demonstrate a record measured SFDR of 127 dB·Hz$^{4/5}$, which is also 22.5 dB higher than that of the conventional dual-series MZM based mixer structure.

Chapter 4 presents a new linearised photonic mixer structure that can achieve high SFDR and improved conversion efficiency simultaneously. The chapter starts by introducing the fundamental concepts that are directly related to the new proposed structure. A literature review of the previously reported structures is then presented with a summary of the performance limitations for the previous approaches. A novel structure is then presented which is based on a stimulated Brillouin scattering (SBS) technique to suppress the carrier in a double sideband MZM driven by the LO and connected in series with an integrated single drive dual parallel Mach-Zehnder modulator (DPMZM) to which an optimised bias condition is applied. Detailed mathematical analysis and modeling are presented to evaluate the performance of the SBS carrier suppressed based linearised photonic mixer structure. Simulation results are also presented which show an SFDR of 120.4 dB·Hz$^{4/5}$, and a conversion gain of 8.45 dB, corresponding to 15 dB, and 8.8 dB improvements respectively when compared to the conventional dual series MZM based photonic mixer. Experimental results demonstrate a measured SFDR performance of 120.8 dB·Hz$^{4/5}$, which corresponds to 16 dB improvement compared to the conventional dual-series MZM based mixer structure.

Finally Chapter 5 presents the conclusion with a summary of the results obtained from the works in this thesis followed by suggested future works.

1.4 Publications from this work

Two papers arising from this work have been published, and are listed below:

1. Ali Altaqui, Erwin H. W. Chan, and Robert A. Minasian, "Microwave photonic mixer with high spurious free dynamic range," Applied Optics, vol. 53, no. 17, pp. 3687-3695, Jun. 2014.
2. A. Altaqui, E. H. W. Chan, and R. A. Minasian, "Wideband microwave photonic downconverters with high dynamic range and high conversion efficiency," International Conference on Transport Optical Networks ICTON 2014, Graz, Austria, 6-10 July 2014.

References

1. R. A. Minasian, E. H. W. Chan, and X. Yi, "Microwave photonic signal processing," Opt. Express, vol. 21, no. 19, pp. 22918-22936, 2013.
2. J. Capmany and D. Novak, "Microwave photonics combines two worlds," Nature Photon., vol. 1, no. 6, pp. 319–330, 2007.
3. A. J. Seeds, "Microwave photonics," Microw. Theory and techniques, vol. 50, no. 3, pp. 877-887, 2002.
4. J. Capmany, J. Mora, I. Gasulla, J. Lioret, and S. Sales "Microwave photonic signal processing," IEEE J. Lightwave Technol., vol. 31, no. 4, pp. 571-586, 2013.
5. C. H. Cox, and E. I. Ackerman, "Photonics for phased array systems," International symposium on phased array systems and technol., Waltham, MA, 12-15 Oct 2010.
6. W. S. C. Chang, RF photonic technology in optical fiber links. Cambridge, United Kingdom: Cambridge University Press, 2002.
7. C. Lim, A. Nirmalathas, K. Lee, D. Novak, and R. Waterhouse, "Intermodulation distortion improvement for fiber–radio applications incorporating OSSB+C modulation in an optical integrated-access environment," IEEE J. Lightwave Technol. 25, 1602–1612 (2007).
8. Stavros Iezekiel, "Microwave photonics: devices and applications ", John Wiley & Sons Ltd, 2009.

CHAPTER 2 BACKGROUND

2.1 Fibre Optic Communication Systems

The fast exponential growth of Internet traffic has resulted in a continuous and expanding demand for high-speed communication channels. Moreover the enormous demand for transmission of video and voice data over long-haul distances necessitates high bandwidth links. Previously, most of the communication systems have depended on the transmission of data at radio and microwave frequencies by means of either electrical cables or free space. The discovery of semiconductor lasers in the 1960s together with low loss optical fibers in the 1970s have sparked a new successful era in communications known as Fibre-Optic Communications [1]. The use of light for communications permits much greater transmission capacity because of its extremely high carrier frequency (193 THz) compared to on the order of 10GHz for microwave communications. Additionally the use of single mode fibre together with lasers operating at 1.55 μm has enabled the realization of extremely low attenuation loss (below 0.2 dB/km) compared to 20dB/km in microwave systems with coaxial cables operating at low frequencies as the transmission medium [2-3]. In addition to the wide bandwidth capability and low transmission loss, fibre-optic systems benefit from the advantages of immunity to electromagnetic interference (EMI), high degree of signal security, and small size and lightweight [4]. Fig. 2.1 shows the basic elements of fibre-optic communication system.

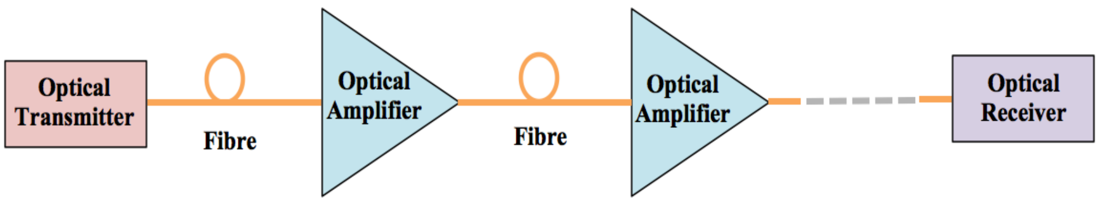

Figure 2.1: Basic components in fibre-optic communication system

The function of the optical transmitter is to convert an electrical signal into an optical signal and launches it into the optical fibre. It consists of an optical source, usually a laser, which can be either directly modulated or externally modulated through the use of electro-optic modulators [5]. Externally modulated lasers are desirable because they can reduce the degradation effects associated with directly modulated lasers such as chirping, poor spectral purity, low extinction ratio, and instability in the laser linewidth [2,6,7]. The middle section, which can be viewed as the channel, consists of optical fibres together with optical amplifiers, which are essential to counter fibre transmission loss by optically amplifying the transmitted signal. Upon reaching the destination i.e. the optical receiver, the optical signal is detected by a photodetector, which recovers the original signal by converting the optical signal back into its electrical form.

In a typical point-to-point link, the optical fibre is connected to only one source at the transmitter's end, and due to the narrow spectral width that a laser can produce; this scheme can only utilize a very narrow portion of the fibre bandwidth. A dramatic increase in the information capacity of a fibre-optic link can be realized by using an alternative viable scheme known as wavelength division multiplexing (WDM), which was introduced in the late 1970s [8]. This technology is based on exploiting the wide bandwidth potential of optical fibre through simultaneously sending multiple optical signals with different emission wavelengths into the fibre channel.

The advance of WDM technology together with high performance optoelectronic devices promises to satisfy our increasing demand for bandwidth and high quality signal. Fiber-optic communication systems continue to replace conventional microwave systems. Although, the common use of optical communication systems nowadays is for carrying baseband digital signals, some portions of the system are designed for analog applications, which aim to perform very complex functions that are impossible to be realized in microwave and RF communication systems [9]. The analog link of fiber-optic communication has become an important part of an emerging field known as microwave photonics.

2.2 Microwave Photonics

The branch of microwave photonics has progressed in parallel to the advancement of fibre-optic communication, due to the rapid availability of optical components operating at microwave frequencies and beyond. Microwave photonics describes the study of electro-optic devices and processing signal systems at microwave/ millimeter rates, or the deployment of photonic devices for signal conditioning and handling in microwave systems [10-12]. The microwave/ mm frequency for communication technology spans from the ultra high frequency (UHF) band to the extremely high frequency (EHF) band i.e. from 300 MHz to 300 GHz [13]. The key success of microwave photonics lies on the integration of microwave technology with optical technology that can readily realize low attenuation, high time bandwidth product capability, and immunity to EMI. This forms a solid foundation for wide range of microwave applications such as radars, antenna remoting for communication systems, Community Access TV (CATV), radio over fibre and most importantly signal generation and processing [14-19]. The aim of microwave photonics is to process the microwave signal with high fidelity and minimum distortion, so as to be recognized for various signal formats. The microwave signal can be digital or analog, or a pure carrier in the form of local oscillator depending on the application. In addition to microwave signal transmission in optical links, further complex functions can be performed all optically such as frequency downconversion, filtering, optical beam steering and more recently frequency measurements [20-23]. This field that exploits the optical domain advantages for performing signal acquisition and reconstruction or for signal quality improvement is known as microwave photonic signal processing.

2.3 Microwave Photonic Signal Processing

Microwave photonic signal processing supports the transmission and conditioning of microwave and radio frequency signal in the optical domain. The inherent bottlenecks arising from the limited sampling speed in traditional electrical processing technologies can be easily overcome by using photonic signal processing, which can realize unparalleled features such as high multigigahertz sampling frequencies, fast tunability and dynamic reconfigurability [24]. In addition, the compatibility of photonic signal processors with fibre optic systems enables connectivity with in-built signal processing.

Fig. 2.2 explains the fundamental principles of operation of a microwave photonic signal processor.

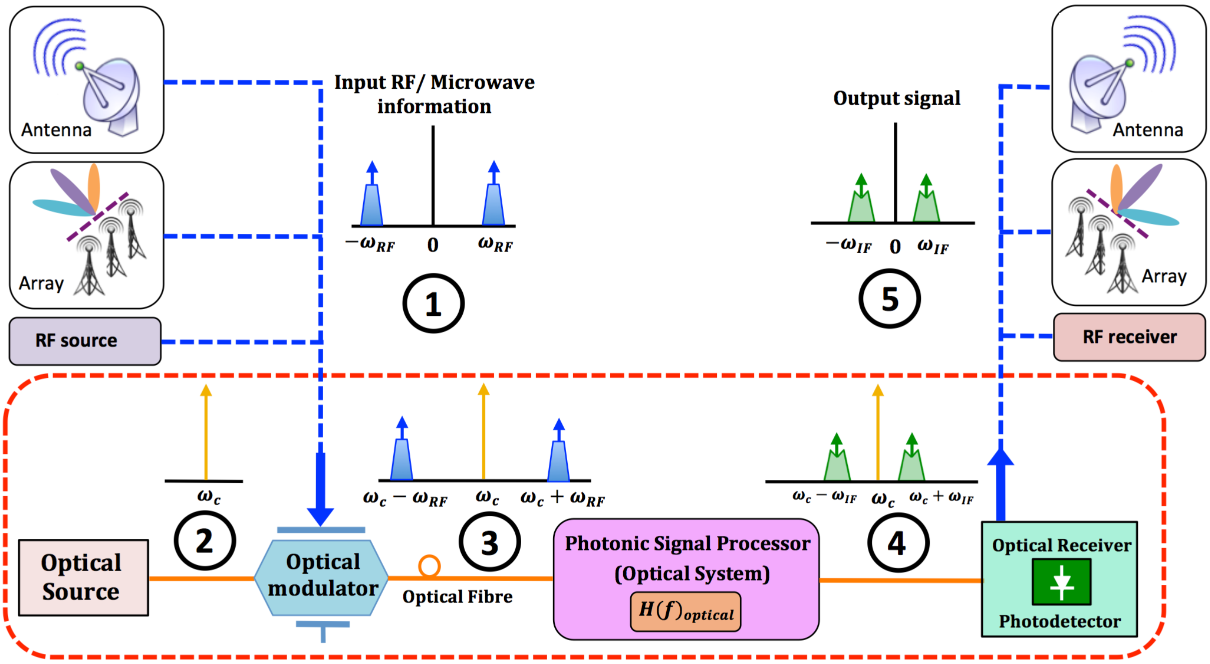

Figure 2.2: Fundamental principles of operation of microwave photonic signal processing

In Fig. 2.2 the region inside the red boundary represents the optical domain, and the region outside the red boundary represents the electrical domain. In the electrical domain, an RF source (antenna, phased array antenna or any other source) generates an input message signal in the RF/microwave frequency range ω_{RF}, which is marked in point 1 in Fig. 2.2. In the optical domain, an optical source (semiconductor laser) generates an optical carrier with extremely high carrier frequency ω_c (commonly around 193 THz), which is marked in point 2. The optical signal is modulated by the RF message signal through an optical modulator, which can be either an electro-optic intensity modulator, or an electro-optic phase modulator. The output of the optical transmitter is the modulated double sideband optical signal at frequencies $\omega_c \pm \omega_{RF}$ indicated in point 3. This signal is to be processed by a photonic signal processor that comprises several photonic devices (e.g. optical couplers, circulators, Fibre Bragg Gating (FBG), optical modulators, Erbium Doped Fibre Amplifiers (EDFA) and so on. The processor is characterised by an overall lumped optical field transfer function defined as $H(f)_{optical}$. The task of the photonic signal processor is to modify the spectral features of the sidebands so as to satisfy specific requirements set by a particular application [25]. In this example, the photonic processor is a frequency downconverter, which simply converts the RF frequency into the intermediate frequency (IF). The modified optical signal indicated in point 4 is the downconverted signal and is passed through the optical receiver, which performs the optical-electrical conversion. The output of the optical receiver is the recovered downconverted electrical signal (marked in point 5), which is also modified and ready to be sent to an RF receiver. Notice that in this example, the signal processor is considered as a mixer. However, it should be made clear that the processor is a black box that can support any functionality such as filtering, phase/frequency shifting, RF memory and so on.

2.3 Microwave Photonic mixers

2.3.1 Introduction

Microwave frequency downconversion is a fundamental function in many microwave system applications. The integration of microwave frequency mixers with fibre optic link technology is particularly attractive due to the additional advantages of low loss, high bandwidth, high isolation, and immunity to EMI. An important function of microwave photonic mixers can be seen in the challenge of digitization of high frequency microwave and millimeter wave signals, as occur in radar and defence applications, due to the sampling rate and bandwidth limitations of Analog-to-Digital (A/D) converters. The received signal needs to be digitized with high resolution, which is difficult to do at high frequencies in the RF/microwave domain. For example, to attain high performance requires 16-bit resolution A/Ds operating at clock speeds in the tens of GHz range which is beyond current capabilities. Therefore a downconversion is required to translate the signal to a low enough IF that falls within the operating range of A/D converters and can be readily digitized [26, 27].

The signal mixing in the fibre optic link can be achieved in the electrical domain or in the optical domain. Most electrical domain approaches mix the received radio frequency (RF) signal with the local oscillator (LO) after the photodetector whereas the optical domain approach mixes the RF and LO signals before the optical field is received by the photodetector. The major differences between these two approaches lie in the required photo-detector bandwidth, system noise and isolation [15, 28]. Frequency mixing in the electrical domain often the photodetector requires costly and complex high-speed electronic components, and moreover wide bandwidth photodetector is required to detect the RF frequency. In contrast, the bandwidth of the photodetector in the all optical mixing needs only to cover the intermediate frequency (IF) signal, which can be at a much lower frequency than the input RF frequency. Also since a high-speed photodetector requires small active area, this will cause additional non-linearity, and hence saturation, when the received optical power is sufficiently high. As a consequence, the dynamic range and the conversion efficiency will be limited [29]. Therefore, performing the frequency mixing in the optical domain will avoid these limitations. Furthermore, in many photonic links equipped with low-relative-intensity-noise (RIN) lasers, the system noise is limited by the shot noise of the photo-detector. The electronic domain frequency mixing, often the photodetector, can add considerable noise to the received signal. In contrast, the optical approach can mix the RF signals via a noise-free electro-optic device.

In summary, photonic frequency downconversion offers the advantages of reducing front-end hardware complexity of antenna system, efficiently extending the link frequency coverage to millimeter wave range, minimizing the effect of fibre dispersion, and enabling the digitization of the signal with high resolution at the intermediate frequency (IF) to match the capability of high performance A/D converters.

2.3.2 Fundamental principles

A frequency mixer is a non-linear device that receives two input signals, and then produces an output signal, which is at the frequency of the sum and difference of the two input frequencies. A mixer can be considered as a multiplier as shown in Fig. 2.3. One of the inputs of the mixer is the radio frequency (RF) signal, which is generally a band of frequencies generated from the antenna at the remote locations. The other input is the local oscillator (LO) signal, which is usually a single tone frequency produced from the base station. The product of these two input signals is the intermediate frequency (IF) signal which can be a down or up converted version of the RF signal.

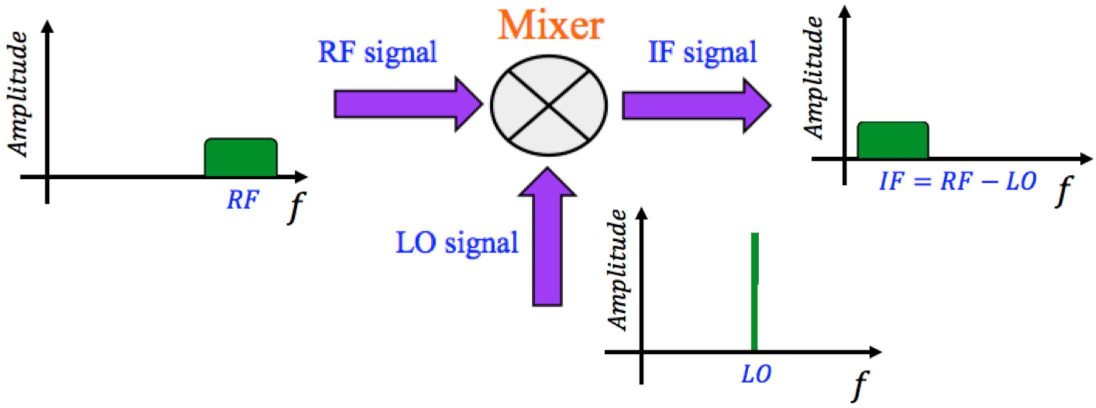

Figure 2.3: The basic principle of operation of a mixer

Assuming $S_{RF}(t) = A_{RF}\cos(\omega_{RF}t)$ and $S_{LO}(t) = A_{LO}\cos(\omega_{LO}t)$ are the two input RF and LO signals respectively, where A_{RF} is the RF amplitude, ω_{RF} is the RF angular frequency, A_{LO} is the LO amplitude, and ω_{LO} is the LO angular frequency, the output signal can be expressed as

$$
\begin{aligned}
S_{IF}(t) &= S_{RF}(t) \times S_{LO}(t) \\
&= [A_{RF}\cos(\omega_{RF}t)][A_{LO}\cos(\omega_{LO}t)] \\
&= \tfrac{1}{2}A_{RF}.A_{LO}.[\cos(\omega_{RF} - \omega_{LO})t + \cos(\omega_{RF} + \omega_{LO})t] \qquad (2.1)
\end{aligned}
$$

A common use of mixers is found in receivers where the RF signal needs to be downconverted to an intermediate frequency (IF) signal, which is at much lower frequency so as to enable efficient recovery of the received signal. In addition to the IF output, there might be other non-linear spurious components which can distort the fundamental IF signal e.g. harmonic distortion and intermodulation distortions. These non-linear components need to be removed from the system as they can significantly degrade the mixer performance.

The implementation of the multiplier operation in the optical domain can be done by using different photonic components which are characterized by their non-linear properties such as optical modulators, photodiodes, or even semiconductor optical amplifiers (SOA). The most widely used photonic component for mixing is the Mach Zehnder Modulator (MZM), which is a common type of electro-optic intensity modulators. The MZM exploits the Pockels electro-optic effect that exists in a voltage controlled wave plate (Pockels cell). An applied electric field across the pockels cell causes a change in the refractive index of the optical fibre, which consequently causes a change in the phase of the light traversing the cell. Pockels effect occurs in crystal lattice such as lithium niobate $LiNbO_3$, which is the material used to fabricate and make an MZM [2]. The fundamental purpose of the MZM is to impress the RF information signal onto the optical carrier through intensity modulation. Fig. 2.4 depicts the MZM configuration. The MZM consists of two arms, in which one arm is controlled by an applied electric field (bias voltage). The input optical carrier P_{in} is split equally into both arms of the interferometer. One of the optical lights propagating in one arm of the MZM will experience a phase shift due to the applied bias voltage. The two optical lights will then recombine to produce the output optical field P_{out}. Based on the applied bias voltage, the two optical fields may interfere constructively to produce maximum output optical power, may interfere destructively to produce minimum output optical power, or may interfere with specific phase relationship.

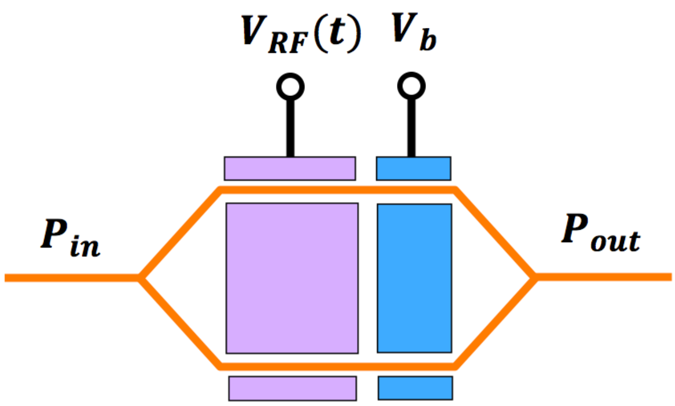

Figure 2.4: Schematic diagram of a Mach-Zehnder modulator

The general transfer function of the MZM is given by

$$P_{out} = \frac{P_{in}}{2} \cdot t_{ff}\left[1 + cos\frac{\pi}{V_{\pi}}(V_{RF}(t) + V_b)\right] \tag{2.2}$$

where t_{ff} is the insertion loss of the MZM, V_{π} is the modulator switching voltage (half wave voltage), V_b is the applied bias voltage, $V_{RF}(t) = V_{RF}\cos(\omega_{RF})$ is the applied RF signal, V_{RF} is the RF voltage amplitude, and ω_{RF} is the RF angular frequency. The insertion loss and the switching voltage of the MZM are component design parameters, which depend on the manufacturer. They are preferred to be as low as possible for specific reasons, which will be discussed later on. The input optical power and the bias voltage of the MZM are system parameters and therefore can be controlled to improve the performance of the overall system. Expanding (2.2) to express it in term of Bessel function of the first kind, the following expression is obtained

$$\begin{aligned} P_{out} = \frac{P_{in}}{2} \cdot t_{ff}\Bigg[1 &+ J_0(\beta_{RF})\cos(\varphi) \\ &+ 2\cos(\varphi)\sum_{n=1}^{\infty}(-1)^n J_{2n}(\beta_{RF})\cos(2n\omega_{RF}t) \\ &- 2\sin(\varphi)\sum_{n=0}^{\infty}(-1)^n J_{2n+1}(\beta_{RF})\cos\big((2n+1)\omega_{RF}t\big)\Bigg] \end{aligned} \tag{2.3}$$

where $\beta_{RF} = \frac{\pi}{V_{\pi}}V_{RF}$ is the RF modulation index, and $\varphi = \frac{\pi}{V_{\pi}}V_b$ is the optical phase change between the two arms of the MZM. The first two terms in (2.3) represents the amount of carrier power, the second term represents the amount of even order distortions generated from the MZM, and the last term represents the amount of the fundamental signal as well as the odd order distortions generated from the MZM. Therefore it can be seen that when $\varphi = 0$, the carrier power is maximum, and there will be no fundamental signal, and odd order. However, when $\varphi = \frac{\pi}{2}$, the amount of the carrier power will be reduced by half, and there will be no even order distortion, and finally when $\varphi = \pi$, the carrier will be suppressed, and there will be no fundamental signal nor odd order distortions. The plot of output optical field of the MZM versus the bias voltage is shown in Fig. 2.5

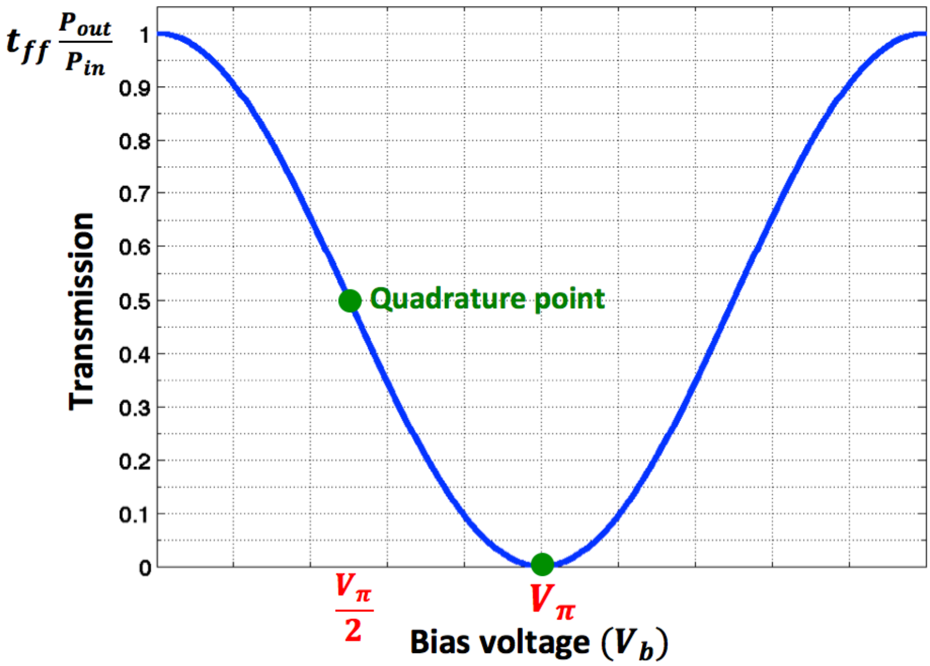

Figure 2.5: Transfer function of a Mach-Zehnder modulator

In its most common mode of operation, the MZM is biased at its quadrature point $V_b = \frac{V_\pi}{2}$, which is the most linear region. At this bias point, there is an effective orthogonality between the two optical fields i.e. the phase relationship between the two fields is 90°. The RF voltage is applied on top of this bias to modulate the optical carrier, hence producing the output modulated optical field, which is linearly proportional to the input RF voltage. At the maximum bias point $V_b = 0$, there is no phase difference between the two optical fields in the MZM, and hence constructive interference occurs. Finally at the minimum bias point $V_b = V_\pi$, the two optical fields in the MZM are out of phase i.e. the phase difference is 180°, thus destructive interference occurs, and the optical carrier will be suppressed leaving only the two RF sidebands. Although the quadrature bias scheme is commonly employed in an MZM due to the elimination of second order harmonic distortions, other bias points such as the minimum or the maximum are also useful for specific performance improvement. These bias operations technique will be discussed in detail in section 2.3.4 after introducing the mixer link performance parameters.

Next, the fundamental optical components required to form a photonic mixer are introduced. Some of these components are external to the mixer such as the laser diode and the photodiode but they are important in determining the overall mixer performance.

Other photonic components are internal to the mixer such as the optical modulators and are also important in defining the mixer performance.

Fig. 2.6 shows a general photonic mixer link. The link consists of a laser that launches a continuous wave light (optical carrier) centered at extremely high carrier frequency e.g. 193 THz. This optical carrier is then fed into the photonic mixer processor.

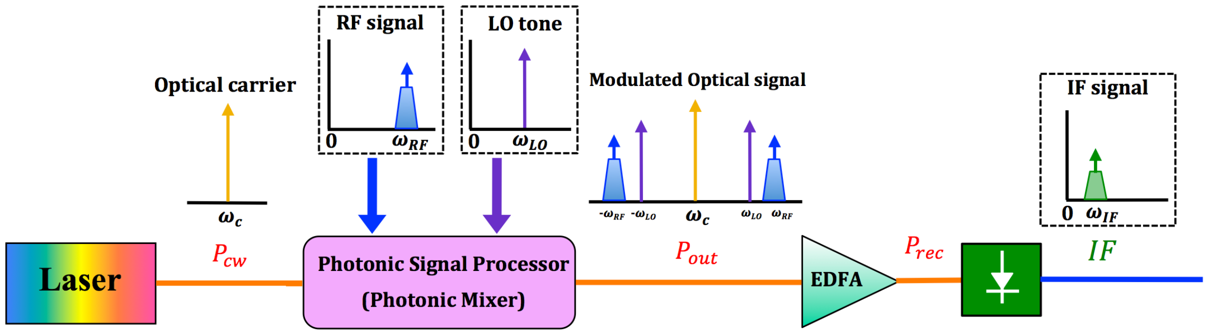

Figure 2.6: A generic photonic mixer link

The objective of the photonic mixer processor is to employ specific modulation techniques (generally intensity modulation) so as to impart the RF signal and the LO onto the optical carrier, and so that when it is detected by a photodiode, the IF signal is generated by the beating of the RF signal and the LO. This kind of mixer scheme is known as intensity modulation direct detection IM/DD. Other modulation schemes that use phase modulators to impress the RF and LO into the optical carrier can be also employed. However, due to the inherent nature of phase modulation that causes the RF and LO sidebands to be in anti-phase, the modulated optical power cannot be directly detected unless the optical carrier is suppressed, which implies the use of additional optical components to perform the carrier suppression functionality. In general the photonic mixer processor can comprise any number of optical modulators, which are connected in any arrangement e.g. series and parallel topologies. The RF signal and the LO can be applied to a single modulator unit to do the mixing function, or can be applied into separate modulator units. The output modulated optical power from the photonic mixer processor may exhibit more losses when compared to the simple RF fibre-optic link based on external modulation. This can be due to introduction of additional photonic mixer components that add their own insertion losses to the system. Therefore, an EDFA may be required to compensate for the additional losses introduced and thus improve the mixer performance. In addition to the losses, the output modulated power from the mixer includes also distortion products in addition to the desired downconverted signal, which can interfere with the fundamental signal, thus limiting the dynamic range and the signal bandwidth. The main aim of the photonic mixer link is to convey, process and downconvert the RF signal from point to point with high fidelity and minimum losses so that at the output, the IF signal can be recovered above the noise floor and can be well distinguished among the distortion products. However, as in the case of any analog system, the photonic mixer link is inevitably susceptible to various signal impairments, such as signal loss, noise and nonlinearities. These signal impairments are quantified into a number of parameters that collectively define the performance of the photonic mixer link. The most important parameters are the link gain, the noise figure and the spurious free dynamic range.

2.4 Performance parameters of the fibre optic link

The principal difference between an externally modulated fibre optic link and the photonic mixer link is the introduction of the LO modulation, which affects the amplitude and center frequency of the fundamental signal i.e. the RF signal is downshifted to the intermediate frequency. Therefore, it is intuitive to discuss the performance parameters of the externally modulated fibre optic link, and refer them to the photonic mixer link. In this section, the definition and the mathematical expressions of the performance parameters of externally fibre optic link are given. The concept of conversion efficiency is explained in Section 2.4.1. In Section 2.4.2 and 2.4.3, the dominant noise sources and the definition of noise figure are introduced. Section 2.4.4 is devoted to the nonlinear effects in fibre optic link, which includes the definitions of harmonic and intermodulation distortions. Finally, the dynamic range and the spurious free dynamic range commonly defined for fibre optic link is discussed in Section 2.4.5.

2.4.1 Conversion efficiency

A generic representation of a fibre optic link is depicted in Fig. 2.7

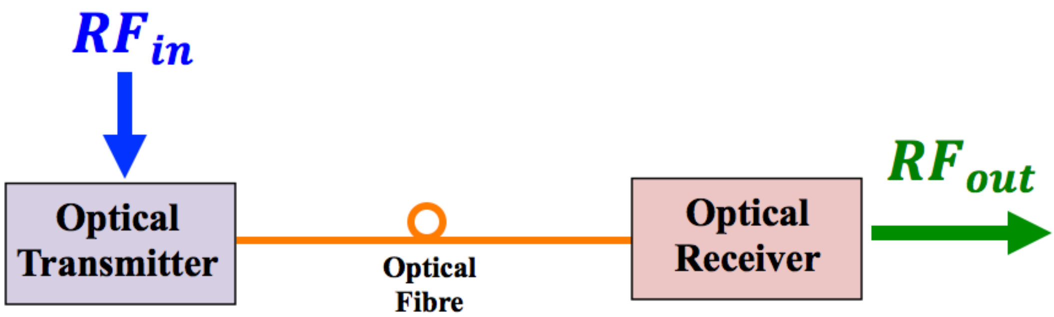

Figure 2.7: A generic representation of a fibre optic link

The link comprises a transmitter, which converts the electrical RF signal into an optical signal, an optical fiber, and a receiver, which recovers the modulated light back to the electrical domain. The conversion of the signal from electrical to optical domains and vice-versa is considerably inefficient and will inevitably lead to signal loss of input RF power. This power transmission efficiency is known as the conversion efficiency, which is fundamentally the ratio of the output RF electrical power relative to the input RF electrical power [30]. However this definition of conversion efficiency is slightly different with regard to the mixer photonic link since the signal of interest in the mixer link is the output IF signal power. Thus the conversion efficiency in a photonic mixer link is defined as the ratio between the output IF signal power relative to the input RF signal power. The general link gain expression will be derived in terms of the physical parameters of the fibre optic link and then will be compared to the photonic mixer link.

The conversion efficiency can be expressed as

$$G_{conv} = \frac{P_{out,RF}}{P_{in,RF}} \tag{2.4}$$

The final expression of the conversion efficiency depends on whether the optical transmitter is considered as directly modulated laser or externally modulated laser. In this analysis, the conversion efficiency expression will be restricted only to externally modulated fibre optic link using an MZM as shown in Fig. 2.8.

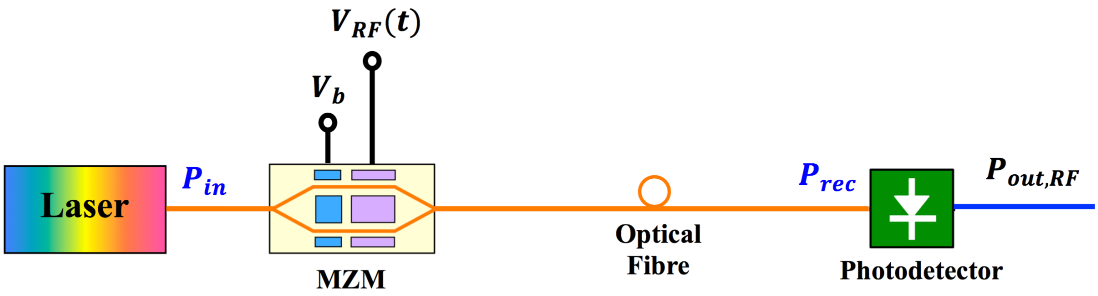

Figure 2.8: Simple model of an externally modulated fibre Optic link

In this model, the laser is operated in a continuous wave (CW) mode and the modulation is performed in the MZM. The received optical power into the photodiode can be expressed as

$$P_{rec} = \frac{P_{in}}{2} \cdot t_{ff} \left[1 + cos \frac{\pi}{V_\pi} (V_{RF}(t) + V_b)\right] \tag{2.5}$$

where P_{in} is the input optical power to the MZM, t_{ff} is the insertion loss of the MZM, V_b is the modulator bias voltage, V_π is the half wave voltage, and $V_{RF}(t)$ is the modulating RF signal. For simplicity, it is assumed that the MZM is biased at its quadrature point which is at half the modulator switching voltage i.e. $V_b = \frac{V_\pi}{2}$.

Equation (2.5) can be further analysed as following:

$$P_{rec} = \frac{P_{in}}{2} \cdot t_{ff} \left[1 + cos \frac{\pi}{V_\pi} (V_{RF} \cos(\omega_{RF} t) + \frac{V_\pi}{2})\right]$$

$$= \frac{P_{in}}{2} \cdot t_{ff} \left[1 + cos \left(m_{RF} \cos(\omega_{RF} t) + \frac{\pi}{2}\right)\right] \quad ; m_{RF} = \frac{\pi}{V_\pi} V_{RF}$$

$$= \frac{P_{in}}{2} \cdot t_{ff} [1 - \sin[m_{RF} \cos(\omega_{RF} t)] \tag{2.6}$$

where m_{RF} is the RF modulation index. Assuming a small signal analysis, equation (2.6) can be further simplified to

$$P_{rec} = \frac{P_{in}}{2} \cdot t_{ff} [1 - m_{RF} \cos(\omega_{RF} t)] \tag{2.7}$$

Therefore, the received RF optical power is given by

$$P_{rec,RF} = \frac{P_{in}}{2} \cdot t_{ff}\, m_{RF} \tag{2.8}$$

Moreover, the detected RF photocurrent is proportional to the received RF optical power and is given by

$$I_{det,RF} = \Re\, P_{rec,RF} \tag{2.9}$$

where $\Re$ is the responsivity of the photodetector in units of A/W. This parameter represents the photocurrent produced per unit of received optical power. The output RF power is simply given by

$$\begin{aligned} P_{out,RF} &= \frac{1}{2} {I_{det}}^2 R_L \\ &= \frac{1}{8}\, {t_{ff}}^2 {P_{in}}^2 (\frac{\pi}{V_\pi} V_{RF})^2 \Re^2 R_L \end{aligned} \tag{2.10}$$

where R_L is the photodiode load resistance. The input RF voltage V_{RF} can be expressed in terms of the input RF power as $V_{RF} = \sqrt{2P_{in,RF}.R_{in}}$ where R_{in} is the modulator input resistance. Thus, the conversion efficiency can be obtained as follows:

$$\therefore \boldsymbol{G_{conv}} = \frac{\boldsymbol{P_{out,RF}}}{\boldsymbol{P_{in,RF}}} = \frac{\mathbf{1}}{\mathbf{4}}\, \boldsymbol{t_{ff}}^{\mathbf{2}} \boldsymbol{P_{in}}^{\mathbf{2}} \left(\frac{\boldsymbol{\pi}}{\boldsymbol{V_\pi}}\right)^{\mathbf{2}} \boldsymbol{\Re}^{\mathbf{2}} \boldsymbol{R_L}\, \boldsymbol{R_{in}} \tag{2.11}$$

Several approaches to increase the conversion efficiency can be identified by carefully examining (2.11). The most effective approach is to increase the input optical power P_{in} into the modulator. This is a remarkable feature in external modulation compared to direct modulation wherein the link gain is independent of the optical power. In direct modulation, the link gain is determined solely by the slope efficiency, which is a physical parameter of the laser and relatively more difficult to adjust [31]. On the other hand, the input optical power to the modulator is a system parameter and therefore can be increased significantly. However, increasing the input optical power will require a higher power handling capability of both the modulator and the detector. This is challenging particularly for the photodetector, since high power handling requires a larger active area, which in turn will limit the detector bandwidth [30]. Another approach to improve the conversion efficiency is to reduce the modulator insertion loss. This option falls in the domain of component design. A typical value of insertion loss is around 3 to 5 dB, depending on how well the light is coupled from the fiber to the modulator chip and back. Furthermore, reducing the modulator switching voltage will result in improved conversion efficiency. The effort of reducing the switching voltage obviously falls in the region of component design. Lastly, the photodiode responsivity needs to be close to unity for improved conversion efficiency [30].

The conversion efficiency of the conventional structure of a photonic mixer, that comprises a series connection of two MZM in which one is driven by the RF and the other is driven by the LO, is also closely related to the conversion efficiency of the simple RF link. However, the fundamental signal becomes the IF signal rather than the RF. The introduction of another MZM to impress the LO into the modulated RF optical power will modify certain characteristics of the fundamental signal. Assuming the MZM driven by the LO is biased at quadrature, the conversion efficiency of the conventional photonic mixer can be expressed as

$$\therefore G_{conv} = \frac{P_{out,IF}}{P_{in,RF}} = \frac{1}{4}\, t_{ff}{}^{2} P_{in}{}^{2} \left(\frac{\pi}{V_\pi}\right)^2 \Re^2 R_L\, R_{in} \left[\frac{1}{4} t_{ff2}{}^{2} J_1(m_{LO})^2\right]$$

$$= \frac{1}{16}\, t_{ff}{}^{2} t_{ff2}{}^{2} J_1(m_{LO})^2 P_{in}{}^{2} \left(\frac{\pi}{V_\pi}\right)^2 \Re^2 R_L\, R_{in} \qquad (2.12)$$

where t_{ff2} is the insertion loss of the MZM driven by the LO, m_{LO} is the modulation index of the LO, and $J_1(x)$ is the Bessel function of the first order of the first kind. Notice that for the mixer conversion efficiency, the only additional system parameter that can be controlled is the LO modulation index, which can be optimised to improve the conversion efficiency.

2.4.2 Noise Performance

In this section, another factor that limits the mixer performance is introduced, which is the noise. A good start to explain and analyze the noise is by introducing the dominant noise sources in a fibre optic link (FOL) and then proceed with the discussion of the total noise power in the link. The concept of noise figure is also discussed, which is an important and a widely used performance parameter.

There are three dominant noise terms in the fibre optic link; thermal noise, shot noise and laser relative intensity noise (RIN). Conventionally, these noise terms are modeled as current sources and are assumed to be independent of each other [32]. The assumption that these sources are independent indicates that the total noise power in the FOL is proportional to the sum of the noise power components generated by the individual sources.

2.4.2.1 Thermal Noise

Thermal noise describes the random thermal motion of electrons at a particular temperature in a resistor, which is manifested as a fluctuation of current even in the absence of an applied voltage. Thus, the load resistor in the front-end of an optical receiver adds thermal noise to the current generated by the photodiode [2]. Moreover the resistor used in the modulation device at the transmitter also adds thermal noise. The difference between the two, however, is that the thermal noise in the receiver is amplified by a factor corresponding to the total link gain G_{tot} where $G_{tot} = G_{conv}.G_{amp}$, and G_{amp} is the preamplifier gain before the modulation device. Mathematically, the expression of the electrical noise power delivered by this thermal noise source to a load resistance is

$$N_{th} = 4KTB \tag{2.13}$$

where K is Boltzmann constant, T is the absolute temperature, and B is the bandwidth of the signal.

2.4.2.2 Shot Noise

Shot noise is generated at the photodetector due to the random arrival and detection of photons, which generates a random fluctuation in the detected photocurrent [2]. The electrical noise power due to the shot noise variance is given by

$$N_{shot} = 2qI_{avg}BR_L \tag{2.14}$$

where q is the electron charge, and I_{avg} is the average detected photocurrent. Compared to the thermal noise, shot noise power depends linearly on the average photocurrent, and consequently, the received optical power.

2.4.2.3 Laser Intensity Noise

The laser intensity noise describes the fluctuations in the unmodulated optical power of a laser, which mainly stems from intrinsic optical phase and frequency fluctuations caused by the spontaneous emission of photons, which are added to the coherent field of the laser. Consequently, the laser intensity noise will be observed as the fluctuation in the detected photocurrent at the receiver output [2]. The laser intensity noise power can be expressed as

$$N_{RIN} = RIN\, {I_{avg}}^2 B\, R_L \tag{2.15}$$

where RIN is the laser relative intensity noise. Notice that the N_{RIN} noise is quadratically proportional to the average detected current. Therefore at high input laser power, the RIN noise usually becomes the dominant noise power in the system.

2.4.2.4 Total Link Noise

The total noise power, which is also known as the system noise floor, can be expressed as the sum of the individual noise sources in the fibre optic link as follows:

$$\begin{aligned} N_{tot} &= N_{th} + N_{th,amp} + N_{shot} + N_{RIN} \\ &= (1 + G_{tot})KTB + 2qI_{avg}BR_L + RIN\, {I_{avg}}^2 B\, R_L \end{aligned} \tag{2.16}$$

The total noise of a fibre optic link is similar to the photonic mixer link except that the amplified thermal noise $N_{th,amp}$ is different and depends on the system conversion efficiency. Moreover, for fibre-optic links that use an EDFA to amplify the optical signal, the amplified spontaneous emission (ASE) noise is also added to the total noise floor, which contains the spontaneous-spontaneous beat noise and the single spontaneous beat noise. Assuming that an EDFA is not used in the fibre-optic link, the dominant noise source at low received optical power is the thermal noise, and the dominant noise source at high-received optical power is the laser intensity noise. These two noise sources can be decreased by using low-noise components such as lasers with low RIN characteristics. Moreover, techniques such as balanced detection are used to suppress the common mode noise i.e. RIN and ASE noise. The only noise that cannot be decreased is the shot noise, which is independent of the device properties. Therefore the objective for most photonic mixer techniques, which aim for low noise and high SNR, is to reach the shot noise limited performance.

2.4.3 Noise Figure

The Noise Figure (NF) is an important figure of merit for determining the performance quality of a fibre-optic link and is a critical parameter in many RF applications such as antenna remoting for phased arrays. It is a measure of degradation of the signal-to-noise ratio (SNR). The noise figure (NF) of a two-port device is defined as the ratio input signal to noise ratio to the output signal to noise ratio. The noise figure can be expressed in the following equation.

$$NF = \frac{SNR_{in}}{SNR_{out}} = \frac{S_{in}/n_{in}}{S_{out}/n_{out}} \tag{2.17}$$

where S_{in} is the input signal power, S_{out} is the output signal power, n_{in} is the input noise power which is solely the input thermal noise of the modulation device, and n_{out} is the total noise power N_{tot} which has been defined in equation (2.16). For a photonic mixer link, S_{out} can be viewed as the output IF signal power whereas S_{in} is the input RF signal power. Therefore S_{out} can be expressed as $S_{out} = G_{conv}\, S_{in}$, $n_{in} = KTB$ and $n_{out} = N_{tot}$, X can be rewritten as

$$NF = \frac{S_{in}/KTB}{G_{tot}\, S_{in}/P_N} = \frac{N_{tot}}{G_{conv}KTB} \tag{2.18}$$

It is worthy to mention that the noise figure NF is independent of the noise bandwidth B because the total output noise power N_{tot} in equation (2.18) is measured in the same bandwidth, B, as the thermal noise in the denominator. It is highly desired to minimize the noise figure in order to achieve high performance photonic mixer. By inspecting equation (2.18), it can be clearly deduced that to minimize the noise figure, the conversion efficiency has to be increased. One possible approach to achieve this is by introducing a low-noise, high gain pre-amplifier at the input of the modulator device and increase its gain until the noise figure approaches the limit of the pre-amplifier noise figure. This would also reduce the conversion efficiency which would lower the noise figure.

2.4.4 Nonlinear Distortions

Non-linear distortion analysis is extremely relevant to the study of photonic mixers techniques since the mixing function is done by means of a non-linear electro-optic device. The transfer function of the modulation device e.g. MZM, is intrinsically nonlinear. The derived expressions of the link gain and noise figure are sufficient when considering only the linear region of the modulator transfer functions. However, a detailed investigation of this nonlinearity is necessary since this factor considerably limits the dynamic range of the photonic mixer link. In this analysis, the modulation device is assumed to have the dominant impact on the nonlinearity. Other devices in the photonic mixer link, for instance the photo-detector, are assumed to be ideally linear. Strictly speaking, these components also contribute to fibre optic link nonlinearities. However, their influences are much smaller compared to the modulation devices [33] and, therefore, most of the time can be ignored.

Consider a general expression of the modulation device transfer function, $y(x)$, which is expanded using a Taylor series around the point x_0.

$$y(x) = \sum_{k=0}^{\infty} \frac{(x - x_0)^k}{k!} \left(\frac{d^k y}{dx^k}\right)_{x=x_0}$$

$$= \sum_{k=0}^{\infty} a_k (x - x_0)^k \tag{2.19}$$

Here a_k represents the Taylor series expansion coefficient where

$$a_k = \frac{1}{k!} \left(\frac{d^k y}{dx^k}\right)_{x=x_0} \tag{2.20}$$

Here, x is a time variant quantity, which can represent either the input current or voltage modulation to the device, whereas x_0 is related to the bias term. The most common way to describe the behavior of the nonlinear transfer function in Equation (2.19) is to perform a test known as the tone modulation. In this case the modulating signal $x(t)$ has a pure sinusoidal form. Conventionally, the tone modulation can be divided into three classes: single tone, two-tone and multitone modulations. These tone modulations are differentiated from one another by the number of signal frequencies included in the modulating signal [33]. Our discussion is limited to only single and two-tone tests. The single tone modulation uses a single frequency signal and is performed to determine the harmonic distortion generated by the nonlinear transfer function. In contrast, two-tone modulation uses a pair of closely spaced signal frequencies and is performed to determine the intermodulation distortion products. The following sections discuss the analysis of the single and two-tone tests.

2.4.4.1 Harmonic Distortion – single tone test

In a single tone test, the equation of the input signal is

$$x\,(t) = x_0 + A\,cos(\omega t) \tag{2.21}$$

where $\omega = 2\pi f$ is the angular frequency, A is the signal amplitude and x_0 is the bias current or voltage. Substituting equation (2.21) into equation (2.19) and evaluating the result for the first three terms i.e. (up to k = 3) yields

$$y(t) \approx a_0 + \frac{1}{2}a_2A^2 + \left(a_1\,A + \frac{3}{4}a_3A^3\right)cos(\omega t)24 + \frac{1}{2}a_2A^2\cos(2\omega t) + \frac{1}{4}a_3A^3\cos(3\omega t) \tag{2.22}$$

Note that in equation (2.22), the third and fourth terms have been derived from the trigonometric relations $cos^2\alpha = \frac{1}{2}(1+\cos(2\alpha))$ and $cos^3\alpha = \frac{3}{4}\cos(\alpha) + \frac{1}{4}\cos\,(3\alpha)$

The components of the response of the modulation device can be identified from equation (2.22) as

- DC component that is independent of ω.
- Signal component with frequency ω
- Harmonic distortions at frequencies of integer multiple of ω

Note that the spurious components at twice and three times the signal frequency are called second-order harmonic (HD2) and third-order harmonic (HD3) distortions, respectively.

2.4.4.2 Intermodulation Distortion – two tone test

While the single tone test already offers some insight into the device nonlinearity, a more common way to characterize this nonlinearity is to perform the so-called two-tone test. The form of the input signal in a two-tone test is as follow

$$x(t) = x_0 + A[\cos(\omega_1 t) + \cos(\omega_2 t)] \tag{2.23}$$

where $\omega_1 = 2\pi f_1$ and $\omega_2 = 2\pi f_2$ are the two-tone angular frequencies. The two frequencies f_1 and f_2 are closely spaced to each other. Now substituting equation (2.23) into equation (2.19) and computing the result up to K=3 yields the following

$$y(t) \approx a_0 + a_2A^2 + \left(a_1A + \frac{9}{4}a_3A^3\right)(\cos(\omega_1 t) + \cos(\omega_2 t)) + \frac{1}{2}a_2A^2(\cos(2\omega_1 t) + \cos(2\omega_2 t)) + \frac{1}{4}a_3A^3(\cos(3\omega_1 t) + \cos(3\omega_2 t)) + a_2A^2[\cos((\omega_1 - \omega_2)t) + \cos((\omega_1 + \omega_2)t)] + \frac{3}{4}a_3A^3[\cos((2\omega_1 - \omega_2)t) + \cos((2\omega_2 - \omega_1)t) + \cos((2\omega_1 + \omega_2)t) + \cos((2\omega_2 + \omega_1)t)] \tag{2.24}$$

Note that the trigonometric relation $cos\alpha\ cos\beta = \frac{1}{2}[\cos(\alpha - \beta) + \cos(\alpha + \beta)]$ was used to obtain the expression in equation (2.24). It is clear from equation (2.24) that besides the harmonic distortions, additional spurious components are produced at the output if two frequencies are present simultaneously. These components are called intermodulation distortions (IMDs). The second order intermodulation (IMD2) terms appear at the sum and the difference of the fundamental frequencies, ω_1 and ω_2 whereas the third-order intermodulation (IMD3) terms appear at the sum and the difference of twice of one of the fundamental frequency and the other frequency. Table 2.1 shows the amplitude and the frequencies of the components present in Equation (2.24).

Component	Frequency	Amplitude
DC	0	$a_0 + a_2A^2$
Fundamental	ω_1 , ω_2	$a_1A + \frac{9}{4}a_3A^3$
2nd order harmonic	$2\omega_1$, $2\omega_2$	$\frac{1}{2}a_2A^2$
3rd order harmonic	$3\omega_1$, $3\omega_2$	$\frac{1}{4}a_3A^3$
2nd order intermodulation	$\omega_1 - \omega_2, \omega_1 + \omega_2$	a_2A^2
3rd order intermodulation	$2\omega_1 - \omega_2, 2\omega_2 - \omega_1,$ $2\omega_1 + \omega_2, 2\omega_1 + \omega_2$	$\frac{3}{4}a_3A^3$

Table 2.1: Signal components generated from a nonlinear device under two-tone test

An important observation is that the intermodulation distortion (IMD) amplitudes are different from the harmonic distortion (HD) amplitudes even though they are primarily produced by the same mechanism. The HD2 amplitude is half of the IMD2 amplitude whereas the HD3 amplitude is one third of the IMD3 amplitude. However, in practice, the powers of these components are measured instead of the amplitudes. Considering that the amplitude is either a current or voltage parameter, the power produced here is an electrical or an RF power. Therefore the powers of the distortion terms are proportional to the square of their amplitudes. Consequently, it can be deduced that the powers of the IMD2 terms expressed in decibels are roughly 4 times higher than the HD2 powers. Likewise the IMD3 powers are 9 times higher than the corresponding HD3 powers. This is an important deduction and will be referred to when the measurements of the spurious free dynamic range is introduced. An illustrative two-tone test output spectrum of a nonlinear device is depicted in Fig. 2.9.

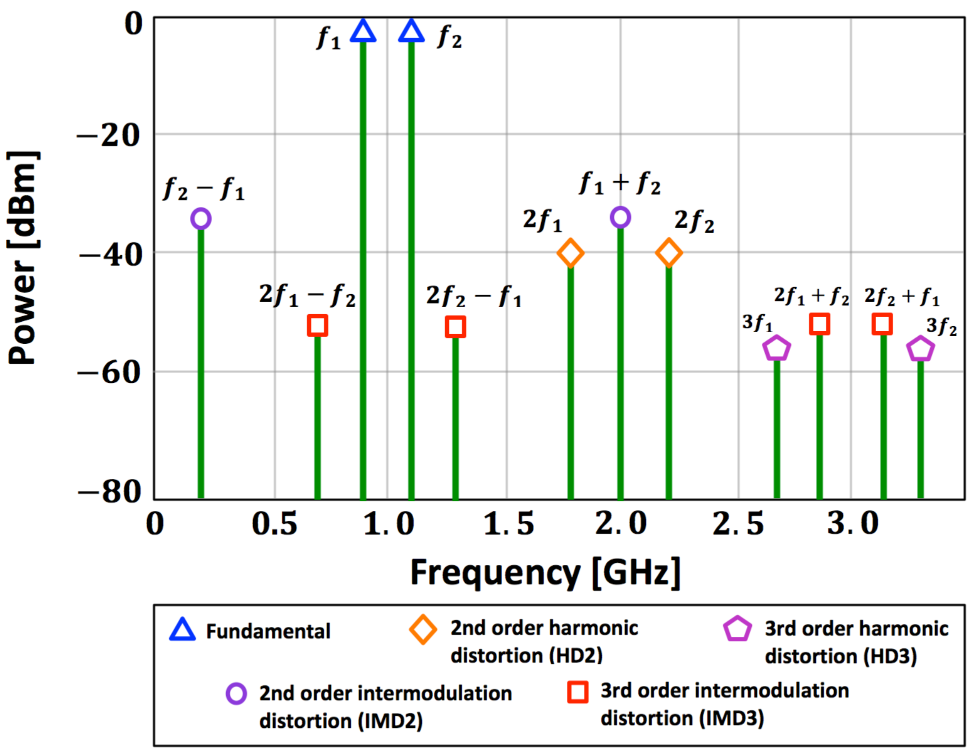

Figure 2.9: A two-tone test output spectrum

The input tone frequencies are 0.95 and 1.05 GHz and their powers are set to 0 dBm. The spectrum in Fig. 2.9 shows that the distortion products that fall closest to the fundamental signals are the IMD3 terms at $2f_1 - f_2$ and $2f_2 - f_1$. These terms are so close to the fundamental frequencies that it is almost impossible to filter them out and consequently they can cause severe interference. This implies that these spurious signals will be present in any usable signal bandwidth. Therefore, the IMD3 is considered as the main limiting distortion factor in any fibre optic link. There have been many methods reported in the literature that attempt to eliminate the IMD3 and they will be discussed in Chapter 3. With regard to the even order distortion products, the HD2 and IMD2 lie relatively far from the fundamental signals and so they are easier to filter out. However, when the signal bandwidth increases, the separation between the signals and the distortion terms reduce. The interference effect of these second order distortions becomes noticeable in a wideband system, in which the input signal is in the multi-octave range. A multi-octave signal is defined as a signal in which its highest frequency component is more than twice of its lowest frequency component. On the other hand, the effect of second order distortions can be neglected in narrowband system where the input signal operation in the suboctave range i.e. the highest frequency component of the input signal is less then twice of its lowest frequency component. Fig. 2.10 shows the interference effect of the second order distortions in a suboctave and a multioctave signal bandwidth.

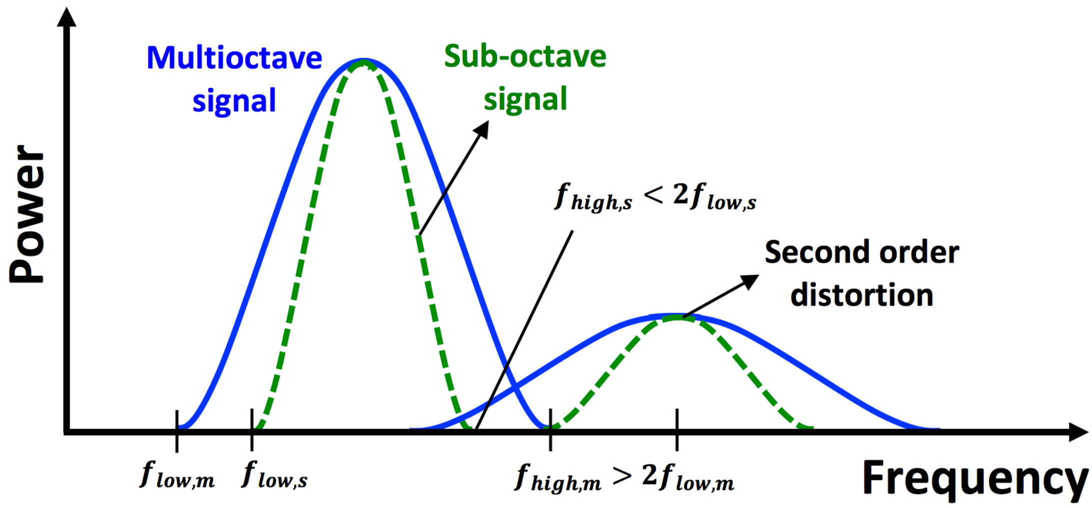

Figure 2.10: Illustration of the definition of suboctave and multioctave signal

2.4.5 Spurious Free Dynamic Range

The dynamic range is defined as the range between the maximum signal that can be conveyed by a system to the minimum detectable signal just above the noise floor [30]. In various applications such as radar systems, a high dynamic range is important because the radar can be jammed by high level jamming signals, while the radar still has to detect low level information signals. Moreover, in antenna remoting applications for wireless systems, the dynamic range plays a fundamental role in determining the capacity and size of each cell. For instance, remote units that are located near the antenna need to restrict their power and transmission rate if they exceed the upper limit of the dynamic range, whereas remote units that are located far from the antenna will not be noticeable if they fall below the lower boundary of the dynamic range. The upper boundary of the dynamic range is restricted by the presence of distortion products just above the noise floor, whereas the lower boundary of the dynamic range is restricted by the noise floor itself. At high enough signal power the distortion products (HD and IMD) become noticeable above the noise floor. This brings us to an important figure of merit known as the spurious free dynamic range (SFDR), which is defined as the range between the smallest signal that can be detected in a system just above the noise floor, and the largest signal that can be introduced without creating detectable distortion in the bandwidth of concern. Fig. 2.11 illustrates the concept of dynamic range.

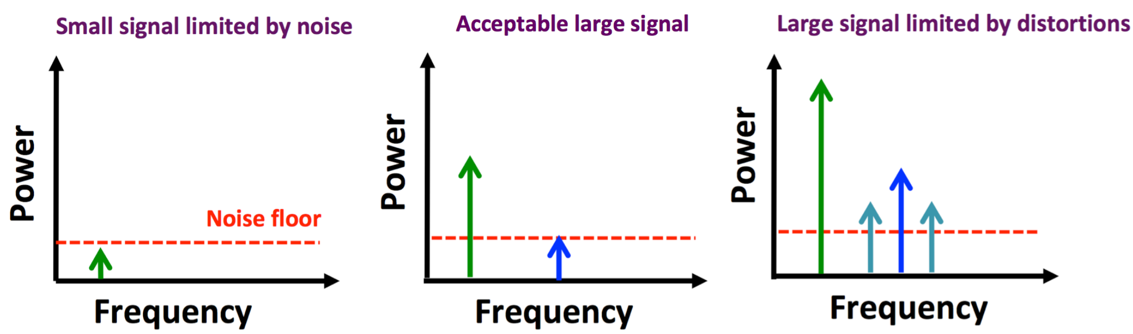

Figure 2.11: Illustration of the concept of dynamic range

Fig. 2.12 clearly illustrates the definition of SFDR where the components of the output signal, the fundamental term, the noise floor and the intermodulation distortion terms have been plotted against the input RF power, all expressed in decibels. Note that the term $SFDR_n$ has been specifically used in order to emphasize that the limiting distortion component is IMD_n. For example, $SFDR_3$ indicates the range between the minimum detectable signal just above the noise floor and the largest signal that can be introduced without creating any third order intermodulation distortion IMD_3.

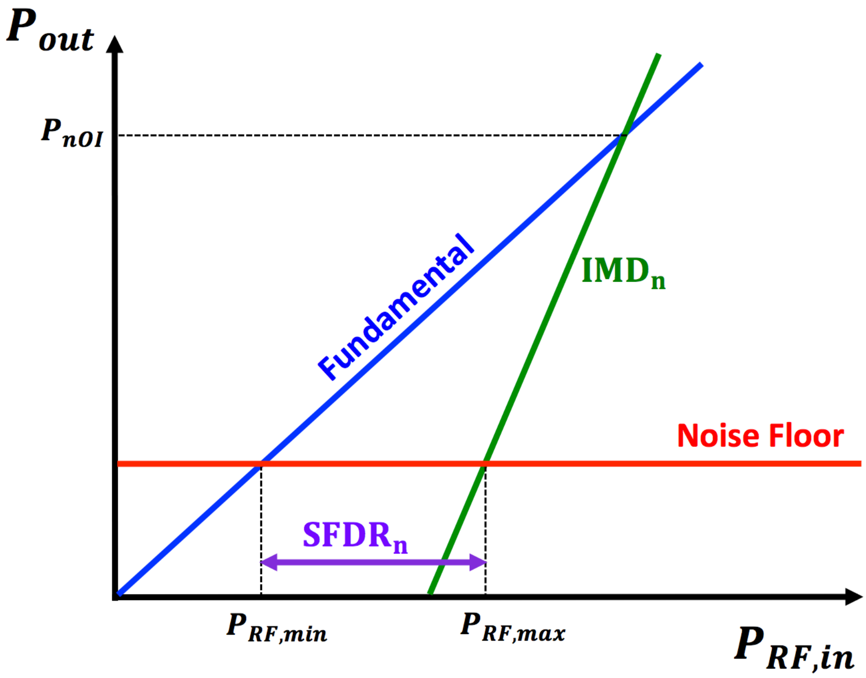

Figure 2.12: Illustration of the SFDR definition

Referring to Fig 2.12, the SFDR can be defined as the difference between $P_{RF,min}$ and $P_{RF,max}$ and can be written in a single expression [30]

$$SFDR_n = \left(\frac{P_{RF,nOI}}{N_{tot}}\right)^{\frac{n-1}{n}} \tag{2.25}$$

where $P_{RF,nOI}$ is the output RF power of the n-th order intercept point, and is defined as the intersection between the output RF signal and the n-th order IMD.

For the photonic mixer link, the fundamental signal is the IF power, and the SFDR expression is obtained by replacing $P_{RF,nOI}$ by $P_{IF,nOI}$, which is the output IF power of the n-th order intercept point. There is another useful expression for the SFDR, which relates the noise figure, the conversion efficiency and the n-th order intercept point and which can be expressed as [30]

$$SFDR_n = \frac{n-1}{n}(P_{RF,nOI} - NF - G_{conv} + 174) \tag{2.26}$$

where $P_{RF,nOI,}$ NF, and G_{conv} are all expressed in dB. Generally, $SFDR_n$ is usually expressed in $dB.Hz^{\frac{n-1}{n}}$. This is essentially the same as saying that the SFDR is measured in dB in 1 Hz bandwidth. The factor $Hz^{\frac{n-1}{n}}$ arises due to the order of the SFDR.

Finally, examining equation (2.25) and (2.26), there are several ways to improve the SFDR. For example, reducing the noise figure, or the noise floor, will yield a higher value of SFDR and therefore a better performance of the fibre optic link. Moreover, increasing the output RF n-th order intercept point by removing the dominant IMD will also improve the SFDR.

2.5 Previous work on Microwave photonic mixers

Various microwave photonic mixer approaches have been reported in the past two decades [34-56], which were based on either a combination of optical modulators arranged in different configurations, or other non-linear photonic devices such as the photodiode, or the semiconductor optical amplifier (SOA). Among the optical modulators that have been studied were the electro-optic phase modulators, the electro-optic intensity modulator or the electro-absorption intensity modulator. These photonic mixer approaches were aimed to improve one or more of the fundamental performance parameters of the mixer link i.e. the conversion efficiency, the noise figure and the SFDR. The scope of this section is limited to only detailed discussion of the unlinearized photonic mixer technologies. In other words, linearised approach that aims to cancel the IMD3 will not be included in this section. Detailed linearised photonic mixer approaches will be discussed in the next chapter together with a novel technique for a linearised photonic mixer that can achieve high SFDR performance.

2.5.1 Single MZM based photonic mixer

The earliest research with regard to photonic mixer approaches dates back to 1993 by G. K. Gopalakrishnan [34]. Two different photonic mixer approaches were proposed by Gopalakrishnan. The first approach was the single MZM based photonic mixer. Figure 2.13 shows the structure of the single MZM based photonic mixer.

As can be seen from Fig. 2.13, the structure of the single MZM is very simple and requires the same photonic components used in an externally modulated fibre optic link. The only difference is the modulating signal, which is formed by the sum of the RF signal and the LO. By means of an electrical coupler, the RF and LO are combined and applied to the MZM. The MZM needs to be biased at the most non-linear point i.e. the minimum or maximum point, in order to obtain the first order mixing product namely the IF signal.

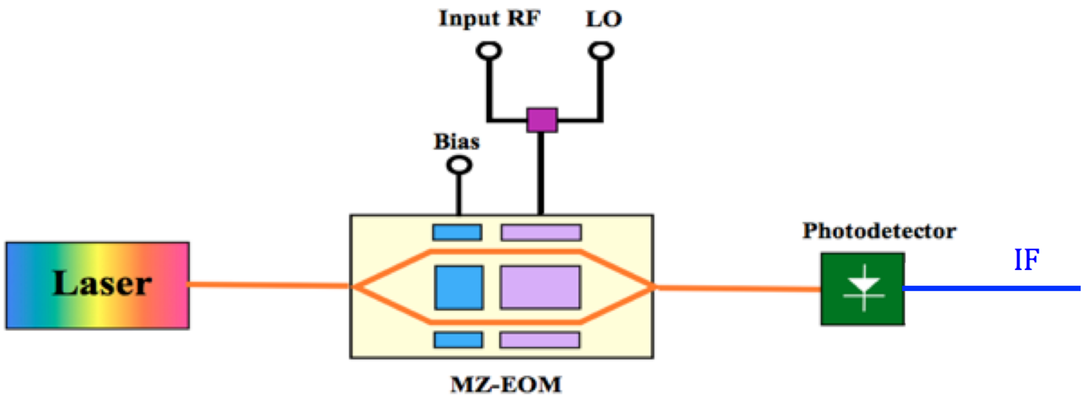

Figure 2.13: Single Mach-Zehnder modulator based photonic mixer structure

The only difference between the two bias points is that at minimum transmission point, the optical carrier and DC components are eliminated. This bias scheme offers the advantage of lower laser noise and smaller optical reflections compared to the maximum transmission bias. Compared to the conventional dual-series MZM based photonic mixer, the single MZM based photonic mixer offers the advantage of a simpler design and relatively lower conversion loss, because of the use of a single MZM to perform the mixer operation. However, the drawbacks of this structure are the extremely poor isolation between the RF and LO ports, the poor SFDR performance due to biasing at the most non-linear point, and the limited signal bandwidth due to the use of an electrical combiner. Also another disadvantage can be noticed in antenna remoting applications. Since just one modulator is used for mixing, the LO and RF signal cannot be located in separated units where one is at the base station and the other is at the remote location.

2.5.2 Dual-series MZM based photonic mixer

Another structure that was proposed by Gopalakrishnan was a combination of two cascaded MZMs, in which one is driven by the RF and the other is driven by the LO [34]. The structure of the conventional dual-series photonic mixer is depicted in Fig. 2.14

The principle of operation of this structure as a frequency mixer requires that both MZMs are biased at the quadrature point (the linear region shown in Fig. 2.5) in order to obtain the desired IF signal. This is because cascading two linear transfer functions will result in the product of each of them, which is a non-linear operation. Compared to the single MZM based photonic mixer, this structure has the advantages of infinite isolation between the RF and LO ports, due to the impressing of the RF signal and the LO into different electro-optic modulators separated by the optical interaction process.

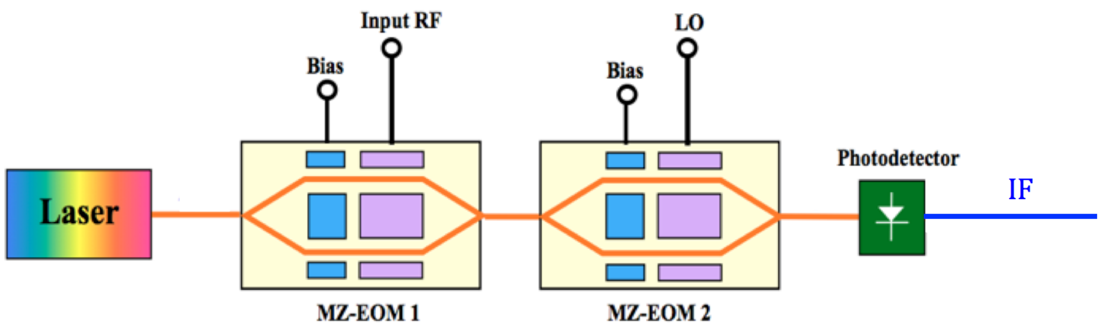

Figure 2.14: Dual-series Mach-Zehnder modulator based photonic mixer structure

Additionally, the linearity performance of this device is improved due to the biasing of the two MZMs at the quadrature points and hence all the even order distortion products are eliminated. As a consequence, the IMD3 level is reduced, which yields a decent improvement in the dynamic range performance. The disadvantage of this structure is the high conversion loss, which is mainly due to the use of an additional MZM, and also the poor noise figure performance. Detailed investigations of the conventional dual-series MZM based photonic mixer have been carried with the aim to improve the conversion efficiency, the noise figure and the SFDR.

It was suggested by A. C. Lindsay that, apart from the common techniques used to improve the conversion efficiency of the externally modulated fibre optic link, the conversion efficiency of the conventional photonic mixer structure is solely dependent on the LO modulation index, and that the optimum value is close to m_{LO}~1.8 [35]. Another technique was also proposed to improve the conversion efficiency and the SFDR by overdriving the MZM with a high LO power, which is beyond the modulator half wave voltage V_π [36]. The transfer function of the MZM, which is overdriven by the LO, will be modified in such a way as to improve the conversion efficiency and SFDR. The measured SFDR was 110 dB.$Hz^{4/5}$, and conversion loss of less than 5 dB. It was also demonstrated that it is possible to obtain the IF signal from the output of the dual-series MZM based photonic mixer by biasing the MZM driven by the LO at the minimum transmission point and applying half the LO frequency [37]. The IF in this technique was regarded as the sum and difference of a harmonic of the LO and the RF i.e. $2f_{LO} \pm f_{RF}$. This approach is efficient because it will only require a low bandwidth MZM to handle the half LO frequency, which implies a reduction in cost. Moreover, designing a lower bandwidth MZM has the advantage of low V_π, which means an improvement in the conversion efficiency, and the noise figure is possible. Finally biasing at the minimum transmission point results in a lower average detected current, which in turn reduces the shot noise and laser intensity noise.

A bias shifted approach was also proposed in [46] to improve the noise figure and SFDR performance of the dual-series MZM based photonic mixer. The MZM driven by the RF was biased close to the minimum i.e. the modulator bias angle was set to 168° (V_b = 0.93 V_π) so as to lower the contribution of shot noise and relative intensity noise. This will also reduce the link conversion efficiency, but was compensated by using a high power laser of 30 dBm. Experimental results showed a measured conversion efficiency of -15 dB, a measured noise figure of 20 dB, and a measured SFDR of 114 dB.$Hz^{2/3}$. These results were demonstrated at 2 GHz RF frequency. Although this technique made a decent improvement in the noise figure and SFDR performance, it has several drawbacks e.g. it requires a higher power laser source, and it is limited to suboctave signal bandwidth due to the low biasing scheme, which generates second order distortions. An EDFA can be also used to compensate the low conversion efficiency, however, the ASE noise generated from the EDFA can degrade both the noise figure and the SFDR.

Another technique to improve the performance of the dual-series MZM based photonic mixer was reported in [39]. It was based on a low V_π resonant electrode optical modulator. A two-section low-pass matching circuit was used to reactively match the modulator electrodes, which consequently resulted in lowering the effective V_π of the modulator. As a consequence, a high conversion gain of 3.3 dB, a low noise figure of 17.4 dB, and an SFDR of 112.9 dB.Hz$^{2/3}$ were experimentally demonstrated at 450MHz RF frequency. A further 17 dB in the conversion gain was also demonstrated by means of photodetector impedance matching. Although this technique improves the overall performance of the dual-series MZM based photonic mixer, it has the disadvantage of limiting the RF and IF signal to narrow bandwidth.

2.5.3 Electro-absorption Modulator based photonic mixer

Another device that can be used to modulate the intensity of the light is the electroabsorption modulator (EAM). Its operating principle is based on the electroabsorption effect, that is, a change in the applied electric field causes a change in the absorption spectrum, and hence a change in the bandgap energy of the semiconductor material [57]. An interesting feature of this device is that it can be also used as a photodetector, hence performing two different operations simultaneously. One approach that employs the EAM as a photonic mixer/photodetector was reported in [42], which demonstrated a conversion loss of 18.9 dB and a suboctave SFDR of 120 dB.Hz$^{4/5}$ at 10mW received optical power. The structure of the EAM based photonic mixer is shown in Fig. 2.15. A directly modulated laser was used to launch the modulated LO optical signal at a beat frequency of 900 MHz into the modulator. The EAM was also modulated by an RF signal at 1 GHz. The photodetection process occurs at the EAM, and the LO is mixed with the RF signal. At the output of the EAM, the IF signal is generated in addition to the LO and the RF signal, which then passes through a circulator toward the spectrum analyzer. When the EAM was biased at the highest slope efficiency of the photocurrent versus dc bias curve, the conversion efficiency was maximised and a measured conversion loss of 18.9 dB was demonstrated. In contrast, when the EAM was biased at the third order null point of photocurrent versus dc bias curve, the SFDR was maximised and a measured SFDR of 120 dB.Hz$^{4/5}$ was demonstrated in a suboctave bandwidth and at the expense of 3 dB reduction in the conversion loss.

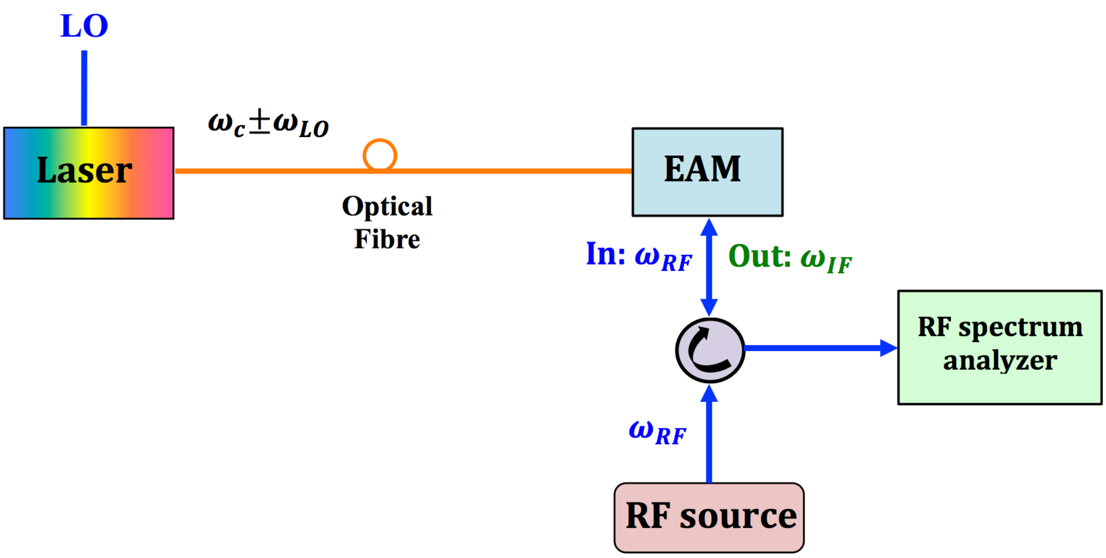

Figure 2.15: Structure of the electro-absorption modulator based photonic mixer/photodetector

Although, the SFDR performance was improved in this technique compared to the previous approaches utilizing MZM as photonic mixer, however, the limited power handling ability of the EAM prevents further improvement in the SFDR, and conversion efficiency. In addition, an EAM generally exhibits higher insertion loss compared to an MZM, and thus the performance of the conversion efficiency is also poor. Also the RF signal bandwidth is limited by the bandwidth of the electrical circulator used in this approach. Finally this approach is only limited to suboctave bandwidth as the EAM generates second order distortion at the third order null point bias.

2.5.4 Dual series phase modulators based photonic mixer with optical filtering

Another frequency downconversion method was reported in [47] and was based on direct detection of two cascaded phase modulators followed by an optical notch filter. A 30 GHz RF signal was downconverted to a 140 MHz IF signal, with a measured SFDR of 112 dB·Hz$^{2/3}$, a conversion loss of 3.5 dB, and a noise figure of 32.5 dB at 10 mA received DC photocurrent. The structure of the dual series phase modulators photonic mixer is shown in Fig 2.16.

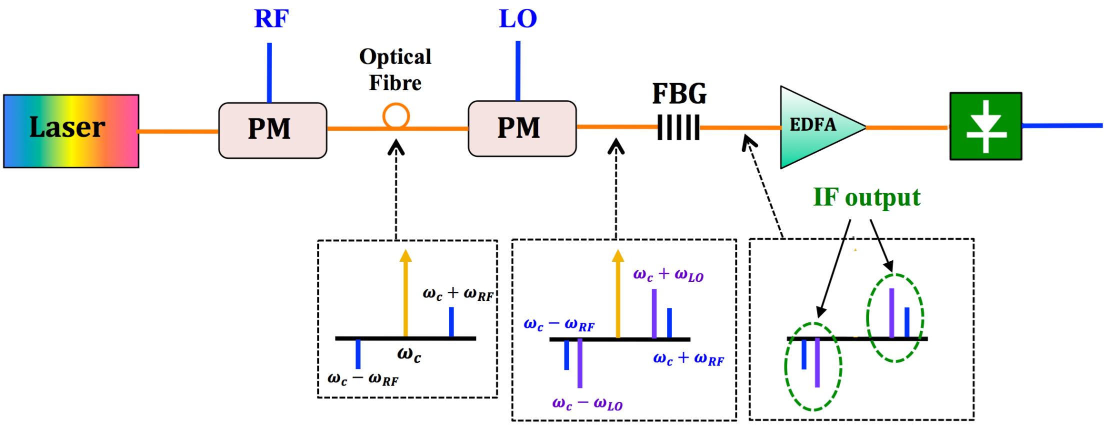

Figure 2.16: Structure of the dual-series phase modulators with optical filtering of the carrier

A DFB laser source was used to provide a 100 mW continuous wave optical power which was fed into an electro-optic phase modulator (PM) and was modulated by an RF signal at 30 GHz, the output RF modulated optical power was then fed into another PM, and was modulated by a single tone LO at 29.86 GHz. The output-modulated signal from the second PM consisted of the antiphase RF and LO sidebands as well as the optical carrier. A fibre Bragg grating (FBG) was inserted following the second PM to filter out the optical carrier. In fact, the FBG was a crucial requirement for this approach to work because if the carrier is not suppressed, the output IF products are extinguished in the detector due to the antiphased products that beat with the carrier and cancel each other. Therefore suppressing the optical carrier allowed full recovery of both sidebands when the signal beats in the photodetector to produce the IF. An EDFA was also required before the photodetector to amplify the RF and LO sidebands. The final IF output is the coherent sum of each RF signal sideband beating with the LO sideband. The conversion efficiency, noise figure and SFDR performance of this photonic mixer technique were improved by solely optimising the LO modulation index. The optimal LO modulation index to maximize the conversion efficiency was 1.08. At this modulation index, the conversion loss was measured to be 3.5 dB. The noise figure and SFDR were also optimised by setting the LO modulation index to 0.39. At this value, a measured SFDR of 112 $dB \cdot Hz^{2/3}$, and a measured noise figure of 32.5 dB were demonstrated.

This approach exploits the usual benefits of carrier suppression i.e. minimizing the DC photocurrent and hence lowering the RIN and shot noise contribution. Moreover, unlike the quadrature biased MZM which only utilizes half of the available amplitude of each sideband, this approach fully utilizes both sidebands of the RF signal and the LO by using phase modulator and carrier suppression, hence maximizing the output signal strength. Nevertheless, the dual-series PM based photonic mixer with optical filtering suffers from many drawbacks. First of all, it is limited by the critical requirement of a very narrow bandwidth and high stopband rejection level optical filter at the carrier frequency so as to filter out the optical carrier, without affecting the RF and LO components. Moreover, the optical filter must be insensitive to environmental changes so as to maintain a stable performance. Such requirements cannot be practically realized. In fact the notch filter used in this technique requires the RF signal and the LO to be several GHz removed from the carrier, making this technique suitable only for higher frequency signals. Also this technique is also limited by suboctave signal bandwidth due to the presence of second order distortion products. Finally, the SFDR performance of this technique is still not satisfactory especially for applications that require critical SFDR performance such as phased array antennas.

2.5.5 Phase modulated Radio-over-fibre link with electro-optic downconversion using a delay line interferometer.

Another technique that employs phase modulation to perform frequency downconversion was reported in [49]. The structure of this method is similar to [47] except that it uses Mach-Zehender delay line interferometer instead of a FBG, and a pair of balanced photodectectors. Fig. 2.17 depicts the structure of the dual-series PM based photonic mixer using delay line interferometer and balanced detection.

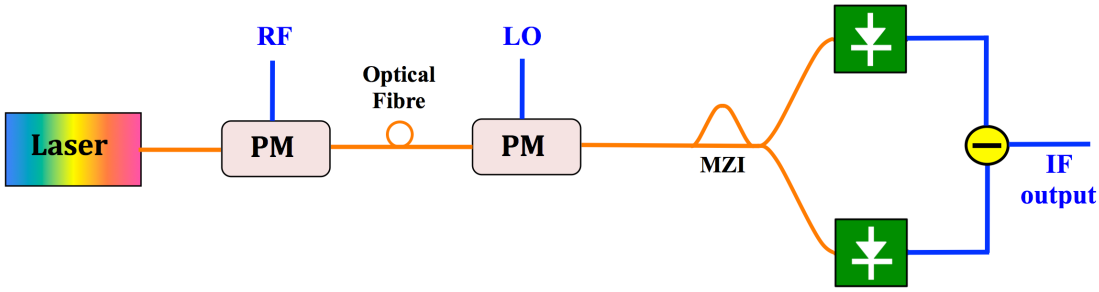

Figure 2.17: Structure of the dual-series phase modulators with a delay line interferemoeter

This simple configuration allows downconversion and common-mode noise suppression to be simultaneously realized with relatively high conversion efficiency. A laser source was used to launch the input optical power into two cascaded PMs, in which one was modulated by the RF signal at 7 GHz and the other was modulated by the LO at 6 GHz. The output modulated signal from the second PM was then passed to an asymmetric Mach-Zehnder interferometer, which was used as a delay-line filter to convert the phase modulated signal into an intensity modulated signal, which was then directly detected by a pair of balanced detection. The detected output signals are then combined to produce the downconverted signal at the IF. Two designs for the LO modulation amplitude were implemented. The first design aimed to improve the conversion efficiency by setting the LO modulation depth to 0.92, which resulted in a link gain that is 7.34 dB higher than that of the conventional dual-series MZM based photonic mixer. The second design aimed to suppress the common mode relative intensity noise (RIN) by setting the LO modulation depth to 1.2 so as to balance the photocurrents between the two detectors. At this LO modulation index, the SFDR was optimised and a measured value of 102 dB·Hz$^{2/3}$ was obtained. Clearly the SFDR performance is poor in this technique, and the use of delay line interferometer with balanced detection adds further complexity to the system. The critical requirement to filter out the optical carrier without affecting the RF and LO is also a problem in this structure.

2.5.6 Other photonic mixer devices

So far, all the previous photonic mixer approaches that have been investigated were based on using different types of optical modulators. However, the RF-IF signal conversion can be performed using other nonlinear photonic devices. In this section, we will examine the use of photodiode and semiconductor optical amplifier to perform the signal mixing.

2.5.6.1 Optical microwave double mixing using PIN photodiode

One method that uses a PIN photodiode to perform the signal conversion was reported in [43], which is based on the principle of signal double mixing in a PIN photodiode. This approach achieves as much as 30 dB of higher mixing product in a narrow band compared with the conventional direct detection approach. However it requires additional passive electrical components in the PIN photodiode circuit so as to provide the double mixing function. In conventional photonic mixers, the only useful signal at the output of the photodetector is the detected IF signal. The other detected signals such as the LO and RF are not utilized at the output of the photodetector. In this approach, however, the RF signal is also utilized. By designing a proper embedding circuit, the RF signal is reflected back into the photodiode, and hence, it is mixed again with the LO. In case of phase coherence the two mixing products are added constructively, and thus, the output IF signal is increased significantly. This method is known as optical microwave double mixing because it simultaneously utilizes two effects, i.e., a direct and indirect mixing process of the LO and the RF signal. As a result of this double effect, a 10-15 dB improvement is obtained compared to the conventional mixing process. By using additional resonance enhancement method, the mixing product can be further improved by additional 15 dB. The principle of operation of this approach is as follows. A directly modulated RF optical signal is launched into the photodiode, which is in an embedding circuit. The LO is also applied to the photodiode, and the mixing process occurs. The RF and the IF signal which are produced at the output of the photodiode, are separated by branching filters, and terminated by the admittances. The RF detected current is then reflected back to the photodiode and mixed again with the LO signal. The two mixing products, which resulted from the direct and indirect, mixing, are added if they are in phase, which can be determined by the use of proper linear conductance, and a non-linear capacitance. Clearly this technique relies heavily on the use of electrical components to obtain the double mixing effect, and thus it is only suitable for narrow band applications. Also, a high-speed photodetector is required to handle the high RF signal as opposed to conventional photonic mixer techniques, in which the photodetector needs only to handle the IF signal. Also, in order to handle high RF frequency, the photodetector needs to have a small active area, which in turn minimizes the power handling ability of the photodetector. Therefore the dynamic range cannot be significantly improved, and a further improvement in the conversion gain is difficult.

2.5.6.2 Photonic microwave mixer based on cross gain modulation in semiconductor optical amplifier

A microwave photonic mixer method was reported in [48,54] which was based on cross gain modulation (XGM) in a semiconductor optical amplifier (SOA). The use of SOA as multifunctional device permits performing all optical functions based on its nonlinearity. In this approach, two optical carriers are generated from separate laser sources, and then are externally modulated by the RF at 1 GHz and the LO at 900 MHz via the use of optical modulators. The two modulated signal are then applied to the SOA. The optical power modulated by the LO is significantly higher than the one modulated by the RF.

Therefore the modulation of the optical gain of the SOA is mainly due to the modulated LO power. The RF information signal can be shifted, via the XGM nonlinearity, to the IF signal at frequencies $f_{IF} = f_{RF} \pm f_{LO}$. The amplified signal at the output of the SOA is passed through an optical filter, and then to a PIN photodiode, which detects the output IF signal. A conversion gain of 11.5 dB, and an SFDR of 85.7 dB·Hz$^{2/3}$ were demonstrated at 100 MHz IF signal. The noise floor was measured to be -135 dBm/Hz. Clearly, the SFDR performance of this technique is extremely poor, and this is mainly due to high non-linearity arising from the SOA. The noise floor is also high, which is also due to the noise introduced by the SOA.

2.5.7 Conclusion

The previously mentioned photonic mixer structures have been mainly focused on improving the mixer conversion efficiency performance. A high conversion gain of up to 17 dB was achieved as was demonstrated in [39]. However the limited SFDR performance has been a major problem. This is due to the inherent nonlinearity in the optical modulators, which contributes significantly in the generation of spurious signals. In particular, the IMD3 is usually the dominant distortion product, and limits the upper bound of the SFDR range. If the IMD3 products are entirely eliminated, then the mixer SFDR will be enhanced significantly. High mixer SFDR performance is essential in applications such as radar, defence recievers, phased array antenna, and hybrid fixed wireless networks [18,58,59]. In the next chapter, various linearised photonic mixer techniques will be discussed, which aim of eliminating the IMD3. A novel photonic mixer approach will be also presented together with complete analytical and experimental results.

References

1. K. Kao and G.Hockham,"Dielectric-fibre surface waveguides for optical frequencies," Proc. Inst. Electr. Eng., vol. 133, no. 3, pp. 1151–1158, July 1966.
2. G. P. Agrawal, "Fibre-optic communication systems," John Wiley & Sons, 1992.
3. R. Ramaswami and K. N. Sivarajan, "Optical networks: A practical perspective," Morgan Kaufmann Publishers, 2002.
4. J. Crisp and B. Elliott, "Introduction to fibre optics," Elsevier Science & Technology, 2005.
5. C. H. Cox, L. M. Johnson, and G. E. Betts, "A theoretical and experimental comparison of directly and externally modulated fiber-optic links," Microwave Symposium Digest, 1989, IEEE MTT-S International 13-15 June 1989, vol. 2, pp. 689-692.
6. B.Cai and A.Seeds, "Optical frequency modulation links: Theory and experiments," IEEE Trans. Microw. Theory Tech., vol. 45, no. 4, pp. 505–511, Apr 1997.
7. A. Seeds, "Optical transmission of microwaves," in The Review of Radio Science, W. Stone, Ed. London, U.K.: Oxford Univ. Press, 1996, pp. 325–360.
8. B. Mukherjee, "WDM optical communication networks: progress and challenges," IEEE J. Sel. Areas Commun., vol. 18, no. 10, pp. 1810–1824, Oct 2000.
9. J. Capmany and D. Novak, "Microwave photonics combines two worlds," Nature Photon.,vol. 1, no. 6, pp. 319–330, 2007.
10. J. P. Yao, "Microwave photonics," J. Lightw. Technol., vol. 27, no. 3, pp. 314–335, Feb. 2009.
11. A. J. Seeds and K. J. Williams, "Microwave photonics," J. Lightw. Technol., vol. 24, no. 12, pp. 4628–4641, Dec. 2006.
12. J. Capmany, J. Mora, I. Gasulla, J. Lioret, and S. Sales "Microwave photonic signal processing," IEEE J. Lightwave Technol., vol. 31, no. 4, pp. 571-586, 2013.
13. D. M. Pozar, "Microwave engineering," Wesley Publishing Company, 1993.
14. R. Benjamin and A. Seeds, "Optical beam forming techniques for phased array antennas," IEE Proceedings-H, Microwaves, Antennas and Propagation, vol. 139, no. 6, pp. 526–534, 1992.
15. W. S. C. Chang, RF photonic technology in optical fiber links. Cambridge, United Kingdom: Cambridge University Press, 2002.
16. X. S. Yao and L. Maleki, "Optoelectronic microwave oscillator," J. Opt. Soc Amer. B, vol. 13, no. 8, pp. 1725–1735, 1999.
17. C. H. Cox, E. I. Ackerman, R. G. Helkey, and G. E. Betts, "Applications of analog fiber-optic links," Lasers & Elec. Opt. Society Meeting, San Francisco, USA, 10-13 Nov 1997.
18. C. H. Cox, and E. I. Ackerman, "Photonics for phased array systems," International symposium on phased array systems and technol., Waltham, MA, 12-15 Oct 2010.
19. C. H. Cox, "Steps towards photonic antennas," International conference on phased array systems and technol., Dana Point, CA, 21-25 May 2000.
20. R. A. Minasian, E. H. W. Chan, and X. Yi, "Microwave photonic signal processing," Opt. Express, vol. 21, no. 19, pp. 22918-22936, 2013.

21. C. H. Cox, and E. I. Ackerman, “Microwave photonics: past, present and future,” International Topical Meeting on Microwave Photonics, Gold Coast, Australia, 9 Sept – 3 Oct 2008.
22. J. Capmany, B. Ortega, and D. Pastor, "A tutorial on microwave photonic filters," J. Lightwave Technol. vol. 24, 201-229, 2006.
23. J. Marti, J. Capmany, “Microwave photonics and radio-over-fiber research,” IEEE microw. Magazine, vol. 10, no. 4, pp. 96-105, 2009.
24. R. A. Minasian, “Photonic signal processing of microwave signals,” IEEE. Trans. Microw. & Tech., vol. 54, no. 2, pp. 832–846, 2006.
25. C. H. Lee, “Microwave photonics,” Taylor & Francies Group, 2007.
26. D. Zibar, A. Caballero, N. G. Gonzalez, C. G. Schaeffer, and I. T. Monroy, “Digital coherent receiver employing photonic downconversion for phase modulated radio-over-fiber links,” presented at Microwave Symposium Digest, Boston, USA, 7-12 June 2009
27. Y. Li, P. Herczfeld, A. Rosen, M. Bystrom, and T. Berceli, “Optical domain down-conversion of microwave signals for high dynamic range microwave fiber optic links,” presented at the International Topical Meeting on Microwave Photonics, Grenoble, France, 3-5 October 2007.
28. Stavros Iezekiel, “Microwave photonics: devices and applications “, John Wiley & Sons Ltd, 2009.
29. E. I. Ackerman, and C. H. Cox, “RF fiber-optic link performance,” IEEE microw. Magazine, vol. 2, no. 4, pp. 50-58, 2001.
30. C. H. Cox , E. I. Ackerman, G. E. Betts and J. L. Prince, “limits on the performance of RF-over-fiber links and their impact on device design,” IEE Microw. Theory and techniques, vol. 54, no. 2, pp. 906-920, 2006.
31. C. Cox, E. Ackerman, R. Helkey, and G. Betts, “Techniques and performance of intensity-modulation direct-detection analog optical links,” IEEE Trans. Microw. Theory Tech., vol. 45, no. 8, pp. 1375–1383, 1997.
32. W. van Etten, Introduction to Random Signals and Noise. Chisester, West Sussex: John Wiley & Sons, 2005.
33. C. H. Cox, Analog Optical Links : Theory and Practice. Cambridge: Cam- bridge University Press, 2004.
34. G. K. Gopalakrishnan, W. K. Burns, and C. H. Bulmer, “Microwave optical mixing in LiNbO3 modulators,” IEEE Microw. Theory Tech., vol. 41, no. 12, pp. 2383–2391, 1993.
35. A. C. Lindsay, A. Knight, and S. T. Winnall, “Photonic mixers for wide Bandwidth RF receiever Applications,” IEEE Microw. Theory Tech., vol. 43, no. 9, pp. 2311-2317, 1995.
36. C. K. Sun, R. J. Orazi, and S. A. Pappert, “Efficient microwave frequency conversion using photonic link signal mixing,” IEEE Photonics Technol. Lett., vol. 8, no. 1, pp. 154-156, 1996.
37. C. K. Sun, R. J. Orazi, and S. A. Pappert, and W. K. Burns, “A photonic-link millimeter-wave mixer using cascaded optical modulators and harmonic carrier generation,” IEEE Photonics Technol. Lett., vol. 8, no. 9, pp. 1166-1168, 1996.
38. K. Ho, S. Liaw, and C. Lin, “Efficient photonic mixer with frequency doubling,” IEEE Photonics Technol. Lett., vol. 9, no. 4, pp. 511-513, 1997.

39. R. Helkey, J. Twichell, and C. Cox, "A down-conversion optical link with RF gain," IEEE J. Lightwave Technol., vol. 15, no. 6, pp. 956-961, 1997.
40. K. Kitayama, and R. A. Griffin, "Optical downconversion from millimeter-wave to IF-band over 50-km-long optical fiber link using an electroabsorption modulator," IEEE Photonics Technol. Lett., vol. 11, no. 2, pp. 287-289, 1999.
41. Y. Shi, and J. H. Bechtel, "High isolation balanced photonic microwave mixers," presented at Optical Fiber Communication Conference, San Diego, USA, 21-26 Deb. 1999.
42. D. S. Shin, G. L. Li, C. K. Sun, S. A. Pappert, K. K. Loi, W. S. C. Chang, and P. K. L. Yu, "Optoelectronic RF signal mixing using an electroabsorption waveguide as an integrated photodetector/mixer," IEEE Photonics Technol. Lett., vol. 12, no. 2, pp. 193-195, 2000.
43. G. Jaro, and T. Berceli, "A new high-efficiency optical-microwave mixing approach," IEEE J. Lightwave Technol., vol. 21, no. 12, pp. 3078-3084, 2003.
44. Y. Shi, W. Wang, and J. H. Bechtel, "High-isolation photonic microwave mixer/link for wideband signal processing and transmission," IEEE J. Lightwave Technol., vol. 21, no. 5, pp. 1224-1232, 2003.
45. M. Bystrom, Y. Li, N. Vacirca, P. Herczfeld, and W. Jermison " A coherent fiber-optic link with optical-domain down-conversion and digital demodulation," presented at the International Topical Meeting on Microwave Photonics, Vectoria, BC, October 2006.
46. A. Karim, and J. Devenport, "High dynamic range microwave photonic links for RF signal transport and RF-IF conversion," IEEE J. Lightwave Technol., vol. 26, no. 15, pp. 2718-2724, 2008.
47. B. Haas, and T. E. Murphy, " A carrier-suppressed phase-modulated fiber optic link with IF downconversion of 30GHz 64-QAM signals," presented at the International Topical Meeting on Microwave Photonics, Valencia, Spain, 14-16 October 2009.
48. C. Bohemond, T. Rampone, and A. Sharaiha, "Performances of a photonic microwave mixer based on cross-gain modulation in a semiconductor optical amplifier," IEEE Journals & Magazines, vol. 29, no. 16, pp. 2402-2409, 2011.
49. T. E. Murphy, and V. R. Pagan, "Phase modulated radio-over-fiber link with electro-optic downconversion using a delay-line interferometer", Proc. SPIE 7936, RF and Millimeter-Wave Photonics, 79360L (February 21, 2011);
50. R. Wang, A, Bhardwaj, and Y.Li "Efficient RF frequency down-conversion using coupled quantum well optical phase modulator," IEEE Photonics Technol. Lett., vol. 23, no. 10, pp. 645-647, 2011.
51. C. Bohemond, P. Morel, A. Sharaiha, T. Rampone, and B. Pucel, "Experimental and simulation analysis of the third-order input interception point in an all-optical RF mixer based on a semiconductor optical amplifier," IEEE J. Lightwave Technol., vol. 29, no. 1, pp. 91-96, 2011.
52. E. H. W. Chan, and R. A. Minasian, "Microwave photonic downconverter with high conversion efficiency," IEEE J. Lightwave Technol., vol. 30, no. 23, pp. 3580-3585, 2012.
53. R. Zhu, B. Hraimel, and X. Zhang, "Analysis of simultaneous photonic frequency downconversion and optical subcarrier modulation in an electroabsorption modulator," IEEE J. Lightwave Technol., vol. 30, no. 3, pp. 344-354, 2012.
54. H. Yang, J. Sun, and Q. Du, "All-optical frequency downconversion based on cross-phase modulation in high nonlinearity dispertion-shifted fiber for WDM radio over fiber application," Opt. Express, vol. 20, no. 7, pp. 8047-8054, 2012.

55. E. H. W. Chan, and R. A. Minasian, “Microwave photonic downconversion using phase modulators in a Sagnac loop interferometer,” IEEE J. sel. Topics in Quantum Electronics, vol. 19, no. 6, 2013.
56. E. H. W. Chan, and R. A. Minasian, “High conversion efficiency microwave photonic mixer based on stimulated brillouin scattering carrier suppression technique,” Opt. Lett., vol. 38, no. 24, pp. 5292-5295, 2013.
57. G. Li and P. Yu, “Optical intensity modulators for digital and analog applications,” J. Lightw. Technol., vol. 21, no. 9, pp. 2010–2030, Sept. 2003.
58. M. E. Manka, “Microwave photonics electronic warfare technologies for Australian defence,” in Proc. IEEE Int. Top. Meet. Microw. Photon., pp. 1–2, 2008.
59. C. Lim, A. Nirmalathas, K. Lee, D. Novak, and R. Waterhouse, “Intermodulation distortion improvement for fiber–radio applications incorporating OSSB+C modulation in an optical integrated-access environment,” IEEE J. Lightwave Technol. **25**, 1602–1612 (2007).

CHAPTER 3 Microwave Photonic Mixer With High Spurious Free Dynamic Range Based on DPMZM

3.1 Introduction

Microwave frequency conversion is a key function in many optical-wireless system applications. A high spurious free dynamic range (SFDR) is required in applications such as antenna remoting, radio-over-fibre (RoF), hybrid fixed wireless networks and phased array antennas [1]. High SFDR frequency downconversion is especially important for enabling the digitization of the signal with high resolution at the intermediate frequency (IF) to match the capabilities of high-performance A/D converters [2,3]. Previously reported microwave photonic mixer structures have limited SFDR performance [4-28]. This is due to the fact that the optical mixing process is obtained through inherently nonlinear elements. Therefore spurious distortions such as harmonic distortions (HDs) and intermodulation distortions (IMDs) are generated in addition to the desired down converted signal [29]. For sub octave links, the third order intermodulation distortion (IMD3) is the dominant nonlinear distortion component. As the signal bandwidth is extended to multioctave, the second order distortion products become influential to the SFDR performance [30]. Therefore, it is necessary to design a linearised mixer technique that fully suppresses the IMD3 while still maintaining multioctave operation in order to significantly enhance the SFDR over a wide bandwidth. There have been numerous linearised approaches that aim to eliminate the IMD3 [30-52]. However most of these approaches either restrict the signal bandwidth to suboctave operation, suffer from poor isolation between the RF and LO ports, do not fully suppress the IMD3 components, or increase the system complexity. In this chapter, a detailed literature review of the various reported linearised photonic mixer approaches is presented in section 3.2. Following the literature review, a novel linearised DPMZM based photonic mixer approach is presented in section 3.3. Finally, a conclusion will be given in section 3.4.

3.2 Previous work on linearised photonic mixers

In this section, the previously reported linearised photonic mixer approaches will be reviewed with the aim of evaluating their overall performance with respect to the SFDR, bandwidth of operation, and the isolation between the RF and the LO.

3.2.1 Linearised directional half coupler MZM based photonic mixer

A linearised photonic mixer technique based on the dual-series directional half coupler MZM was reported in [31]. This approach considers only a suboctave link in which the second order distortion products fall out of band, and the linearisation is performed to suppress the IMD3, which is in band with the fundamental IF signal. A third order SFDR of 122 dB·Hz$^{4/5}$ was demonstrated at an input frequency of 400 MHz, and input laser power of 25.6 dBm. Fig 3.1 depicts the structure of the linearised directional half coupler MZM based photonic mixer.

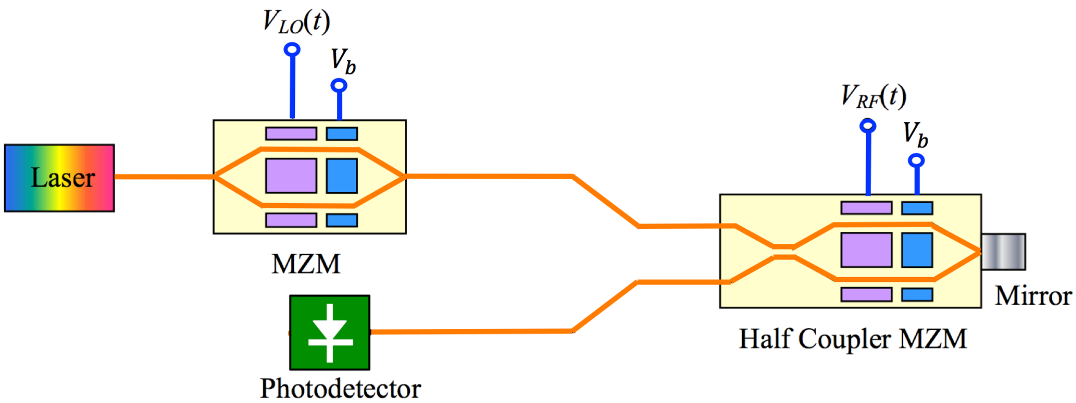

Figure 3.1: Structure of the half coupler Mach-Zehnder modulator based linearised photonic mixer

A continuous wave light was launched from the laser source into a conventional quadrature biased MZM that was driven by an LO at 420 MHz. The output LO modulated optical signal was then fed into a reflective half-coupler MZM driven by a two-tone RF signals at 399 MHz, and 401 MHz. The half-coupler MZM has a unique transfer function such that it is possible to suppress the IMD3 by adjusting the modulator bias voltage. The linearised modulator bias point was set using a feedback circuit to provide constant ratio between the input and output optical power. The center of the half-coupler modulator electrode was offset from the mirror, so there is a time delay between the modulation of the forward and reverse propagation of the optical wave. As a result the modulator voltage exhibited time dependence which affected the modulator transfer function, and consequently resulted in some frequency dependence in the optimum point for third order linearization. The output modulated RF optical power was then detected by a photodiode resulting in the downconverted IF signal at 19 MHz, and 21 MHz. The half-coupler MZM was biased to eliminate the IMD3 yielding a measured SFDR of 122 dB·Hz$^{4/5}$. Although this linearisation approach achieves a high SFDR performance, however, it suffers from several drawbacks. First of all, it was a sub-octave linearization since no elimination of second order distortions was achieved. Also this technique is not suitable in broadband applications because the half coupler modulator exhibited time delay between the modulation of the forward and reverse propagation, which caused frequency dependence on the optimum bias condition for linearisation. Finally the high SFDR performance was achieved using high input laser power of 25.6 dBm.

3.2.2 Linearised photonic mixer based on dual parallel MZM and balanced detection

Another linearised photonic mixer approach, which is based on dual parallel MZM with balanced detection, was reported in [32]. This technique realizes a multi-octave SFDR performance of 115 dB·Hz$^{4/5}$ with the additional advantage of requiring a low laser optical power of 7 dBm. The structure of the linearised photonic mixer is shown in Fig. 3.2. The RF signal and the LO were split and applied to both MZMs in an appropriate ratio to cancel the IMD3. An optical coupler was used to split the laser power into two optical paths. The laser power travelling in the upper path was much higher than that travelling in the lower path resulting in a higher IF output in the upper path. A higher RF power was applied to the lower MZM resulting in a higher intermodulation distortion in the lower arm. Both MZMs were biased at minimum resulting in a low optical carrier power, which thus minimized the average optical power into photodectectors. This in turn reduced the shot and RIN contribution. The two output optical powers from both MZMs were detected using balanced detection scheme. The resultant photocurrents from both photodiodes were then subtracted to yield the final IF output. By appropriately controlling the RF splitting ratio, the LO splitting ratio, and the optical power splitting ratio, the overall IMD3 product was suppressed. Experimental result demonstrated an SFDR of 115 dB·Hz$^{4/5}$ at 7 MHz RF, and using only 5mW laser power. This approach demonstrated a decent SFDR result, however, the performance is limited by the presence of the phase induced intensity noise (PIIN), which is generated by the optical interference in summing the two delayed optical signals in the upper and lower paths. Additionally, it has a poor isolation between the RF and LO ports since they are applied into the same unit. This also does not enable the LO and the RF signals to be placed in different location, which is a major requirement for many antenna remoting applications. Furthermore, since this technique requires two power splitters to be used to split the LO and the RF with a specific ratio, a high SFDR performance can be only achieved in a narrow bandwidth, which is determined by frequency response of the two electrical splitters.

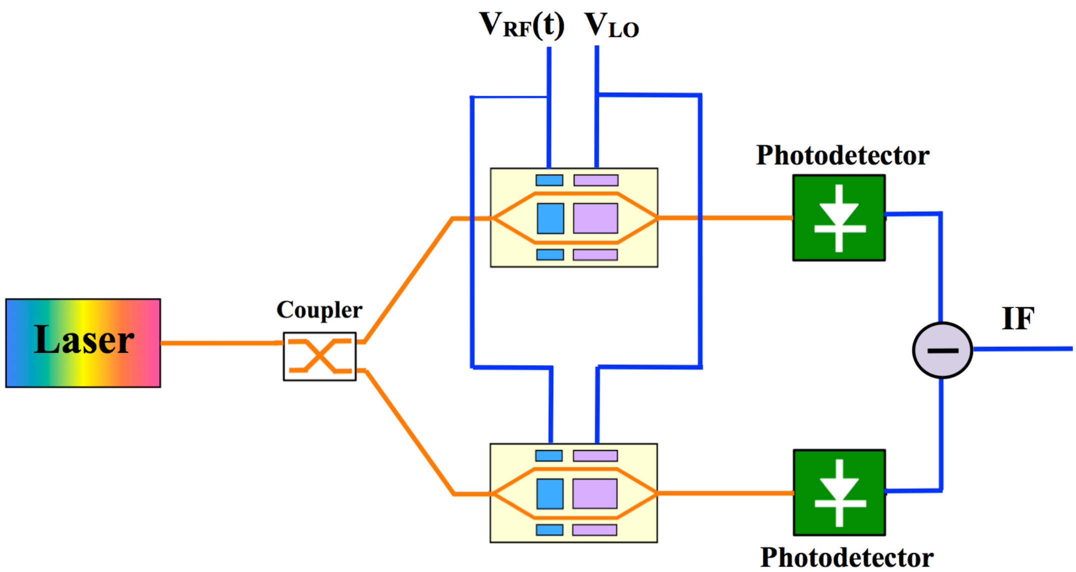

Figure 3.2: Structure of the linearized parallel Photonic mixer

3.2.3 Linearized microwave photonic mixer using dual-wavelength phase modulation and optical filtering

The linearised photonic mixer approach in [33] relies on the fact that the electro-optic coefficient of $LiNbO_3$ modulator depends on the polarization state of the light. Thus if two optical carriers with distinct wavelengths are combined and applied to the input of the modulator, this will effectively causes a single modulator to act as two modulators having different transfer functions, that can be set in opposition to cancel the third order IMD. The structure of the dual-wavelength phase modulation based linearised photonic mixer is depicted in Fig 3.3.

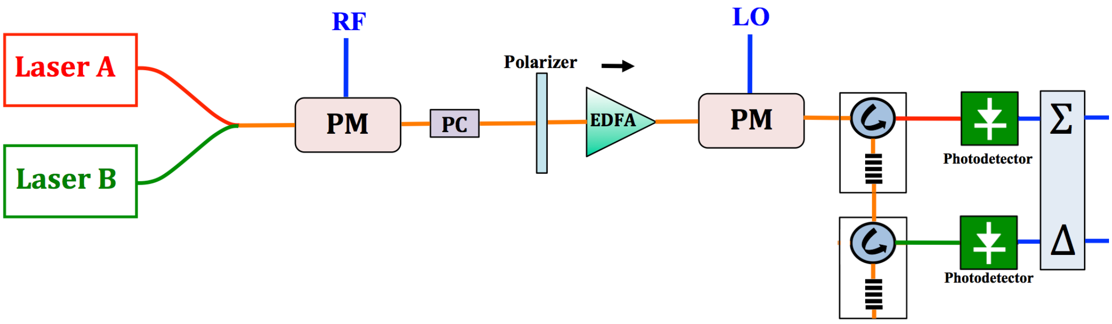

Figure 3.3: Structure of the dual-wavelength phase modulation and optical filtering based linearised phtotonic mixer

Two laser sources (A and B) are used to launch the optical carrier at wavelength λ_A and λ_B respectively. The two optical fields are polarization multiplexed and applied to the phase modulator driven by the RF. The output modulated RF optical signal is then amplified and applied to another phase modulator, which is driven by a strong microwave LO. At the output of the second PM, a pair of bandpass filters is used so as to spectrally isolate the upper sidebands of the two optical waves. The two filtered optical signals are then recovered separately by two different photodiodes. The two output photocurrents are then subtracted using a 180° hybrid coupler, and hence the final output IF is obtained. By adjusting the polarization controller prior to the PM in order to obtain specific ratio of the switching voltage of the modulator at the two different polarization states, one can eliminate the IMD3, and hence the photonic mixer is linearized. Experimental results showed a 20 GHz downconversion to 250 MHz, with a measured SFDR of 110.5 dB·Hz$^{4/5}$, a noise floor of -156 dBm/Hz, and a conversion efficiency of -49 dB. This method suggests an additional 13.5 dB improvement in the SFDR is possible if a shot noise limited performance is assumed, and a more accurate adjustment of the ratio between the two polarization states is obtained. The measured SFDR performance is still inadequate. In addition, filter drift and imperfections, as well as wavelength instability of the laser can significantly degrade the linearisation and downconversion performance of this technique.

3.2.4 Linearized photonic mixer based on balanced detection and digital signal post processing

The approach in [34] uses a combination of optical filtering and balanced detection to obtain high SFDR performance in photonic downconversion architecture. The structure is shown in Fig. 3.4.

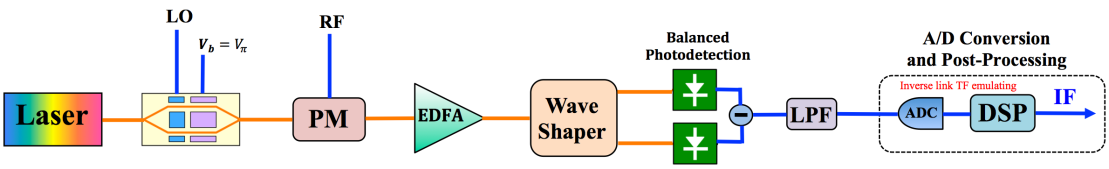

Figure 3.4: Structure of the linearized photonic mixer based on balanced detection and digital post processing

The laser optical power is fed into an MZM driven by the LO. The MZM is biased at the null point so as to suppress the carrier. Carrier suppression is of particular interest because it mitigates carrier-induced noise, maximises the signal to noise ratio (SNR), and allows efficient optical amplification of the signal sidebands, which in turn provides an overall gain, noise figure, and SFDR improvement. Also since only the second harmonic of the LO is generated at the output of the MZM, the LO frequency needed to be about half of the RF signal frequency so as to obtain the IF downconversion. The output modulated optical signal from the MZM is fed into a phase modulator, and is modulated by an RF signal. The output signal from the phase modulator is sent to a multiport reconfigurable bandpass filter. This filter is designed to select and separate only the first upper and lower sidebands of the modulated RF signals and the LO. The two outputs of the filter are connected to obtain balanced detection, which detects the optical signal, and produces the output IF signal, which is digitized and post-compensated by emulating the inverse link transfer function in the digital domain. Thus the IMD3 components are significantly suppressed. Experiments showed an RF-IF downconversion from 8 GHz to 40 MHz with a measured SFDR of 120 dB·Hz$^{4/5}$ at 12 mW received optical power, a noise floor of -162 dBm/Hz dominated by the shot noise, and a conversion loss of 28 dB. At 20 GHz RF, the SFDR was measured to be 117 dB·Hz$^{2/3}$. Although a high SFDR performance was obtained at 8 GHz, the center frequency of the bandpass filter needs to be dynamically reconfigured at different RF frequencies, which adds further complexity in the system.

3.2.5 Previous linearised Dual-Parallel Mach-Zehnder Modulator techniques

One of the most common IMD reduction techniques is the use of a dual-parallel Mach-Zehnder modulator (DPMZM). A DPMZM is a device that consists of two electro-optic intensity modulators (MZM) connected in parallel, and an embedded phase shifter as shown in Fig. 3.5 [38].

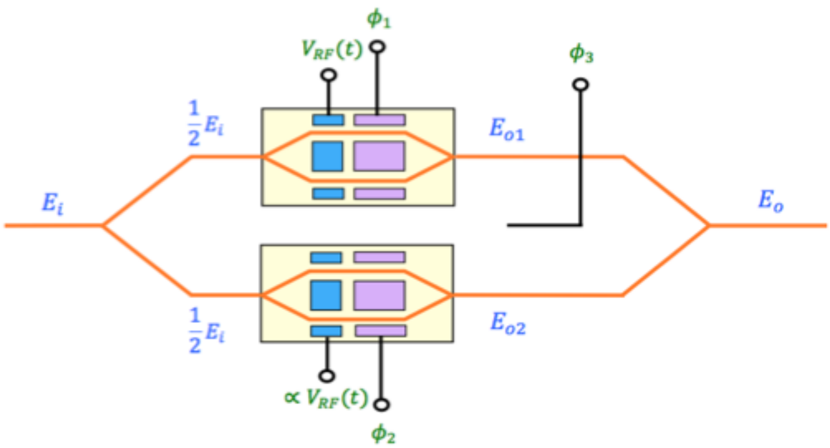

Figure 3.5: Schematic of the integrated dual-parallel Mach-Zehnder modulator

The two MZMs are used to modulate the amplitude of the optical field in the upper and lower arms of the DPMZM. The bias voltage of both MZMs can be adjusted. The phase shifter is used to control the phase between the modulated light in the upper arm of the DPMZM and the modulated light in the lower arm of the DPMZM. It is also possible to modulate the light in only one arm of the DPMZM by applying the microwave signal to only one of its two RF ports. Referring to Fig. 3.5, the transfer function of the DPMZM with respect to the bias voltages can be obtained by considering the following:

- An equal optical power split into the DPMZM,
- No RF signal is applied to the DPMZM,
- The two MZMs are operated in push-pull configuration. This setup requires half of V_π compared to the normal MZM configuration.
- The phase shifter is embedded in the lower arm of the DPMZM

The input optical field of the DPMZM is denoted by E_i and is split equally into both arms of the DPMZM. The output optical field from the upper MZM is given by

$$E_{o1} = \frac{1}{4} E_i [e^{j\varphi_1} + e^{-j\varphi_1}] \tag{3.1}$$

where $\varphi_1 = \frac{\pi V_{b1}}{V_{\pi 1}}$ is the phase change of the light in the top MZM, V_{b1} is the bias voltage of the top MZM, and $V_{\pi 1}$ is the switching voltage of the top MZM. The output optical field from the lower MZM and the phase shifter is given by

$$E_{o2} = \frac{1}{4} E_i \left[e^{j(\varphi_2+\varphi_3)} + e^{j(-\varphi_2+\varphi_3)}\right] \tag{3.2}$$

where $\varphi_2 = \frac{\pi V_{b2}}{V_{\pi 2}}$, and $\varphi_3 = \frac{\pi V_{b3}}{V_{\pi 3}}$ are the phase changes of the light in the bottom MZM and the phase shifter respectively, V_{b2} is the bias voltage of the bottom MZM, $V_{\pi 2}$ is the switching voltage of the bottom MZM, V_{b3} is the bias voltage of the phase shifter, and $V_{\pi 3}$ is the switching voltage of the phase shifter. The output optical field from the DPMZM is given by

$$E_o = E_{o1} + E_{o2} = \frac{\sqrt{t_{ff}}}{4} E_i \left[e^{j\varphi_1} + e^{-j\varphi_1} + e^{j\,(\varphi_2+\varphi_3)} + e^{j\,(-\varphi_2+\varphi_3)}\right] \tag{3.3}$$

where t_{ff} is the insertion loss of the DPMZM. The output optical power of the DPMZM is given by

$$\begin{aligned} P_o &= |E_o|^2 \\ &= \frac{t_{ff}}{16} P_i \left[e^{j\varphi_1} + e^{-j\varphi_1} + e^{j\,(\varphi_2+\varphi_3)} + e^{j\,(-\varphi_2+\varphi_3)}\right] \times \left[e^{-j\varphi_1} + e^{j\varphi_1} + e^{-j\,(\varphi_2+\varphi_3)} + e^{-j\,(-\varphi_2+\varphi_3)}\right] \end{aligned}$$

$$= \frac{t_{ff}}{16} P_i \big[4 + e^{j2\varphi_1} + e^{-j2\varphi_1} + e^{j2\varphi_2} + e^{-j2\varphi_2} + e^{j(\varphi_1+\varphi_2+\varphi_3)} + e^{-j(\varphi_1+\varphi_2+\varphi_3)} + e^{j(\varphi_1-\varphi_2-\varphi_3)} + e^{-j(\varphi_1-\varphi_2-\varphi_3)} + e^{j(\varphi_1+\varphi_2-\varphi_3)} + e^{-j(\varphi_1+\varphi_2-\varphi_3)} + e^{j(\varphi_1-\varphi_2+\varphi_3)} + e^{-j(\varphi_1-\varphi_2+\varphi_3)}\big] \quad (3.4)$$

Using the relationship $\cos(x) = \frac{e^{jx}+e^{-jx}}{2}$, equation (3.4) can be expressed as follows

$$= \frac{t_{ff}}{16} P_i [4 + 2\cos(2\varphi_1) + 2\cos(2\varphi_2) + 2\cos(\varphi_1 + \varphi_2 + \varphi_3) + 2\cos(\varphi_1 - \varphi_2 - \varphi_3) + 2\cos(\varphi_1 + \varphi_2 - \varphi_3) + 2\cos(\varphi_1 - \varphi_2 + \varphi_3)] \quad (3.5)$$

$$= \frac{t_{ff}}{8} P_i [2 + \cos(2\varphi_1) + \cos(2\varphi_2) + 2\cos(\varphi_1 + \varphi_2)\cos(\varphi_3) + 2\cos(\varphi_1 - \varphi_2)\cos(\varphi_3)] \quad (3.6)$$

Finally, the output optical power from the DPMZM can be expressed as

$$P_o = \frac{t_{ff}}{8} P_i [2 + \cos(2\varphi_1) + \cos(2\varphi_2) + 4\cos(\varphi_1)\cos(\varphi_2)\cos(\varphi_3)] \quad (3.7)$$

It is clear from (3.7) that the output optical power from the DPMZM depends on the bias voltages of the DPMZM as well as input optical power into the DPMZM. The transfer function of the DPMZM is simulated with respect to V_{b1}, V_{b2}, and V_{b3} by assuming no insertion loss in the DPMZM, 1 W of input optical power, and the switching voltages of the DPMZM are all equal to 4V. This is done by fixing two of the bias voltages and sweeping the other. We will consider the case when there is no DC offset in any of the bias voltages i.e. the maximum point is located at 0 V, and the case when there is arbitrary DC offsets of $V_{b1,\,drift}$= 0.2 V, $V_{b2,\,drift}$ = 1 V, and $V_{b3,drift}$ = 1 V as may occur in practical devices. The simulation results are shown in Fig. 3.6.

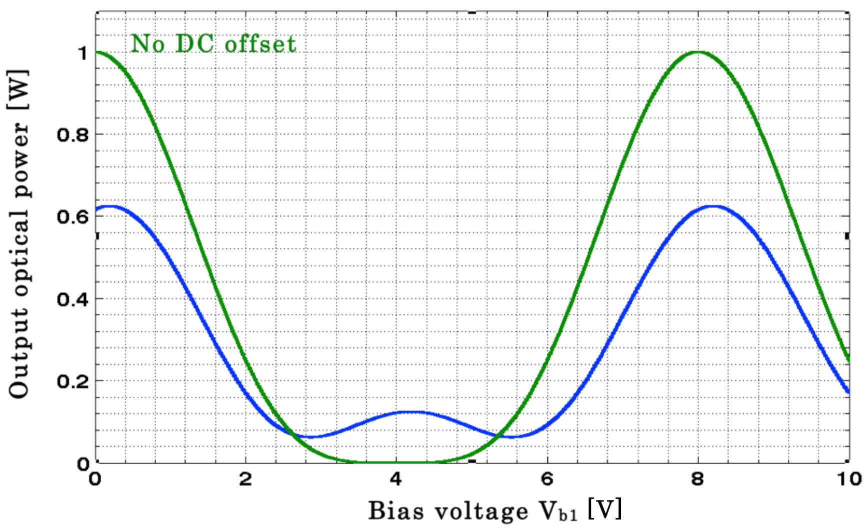

(a)

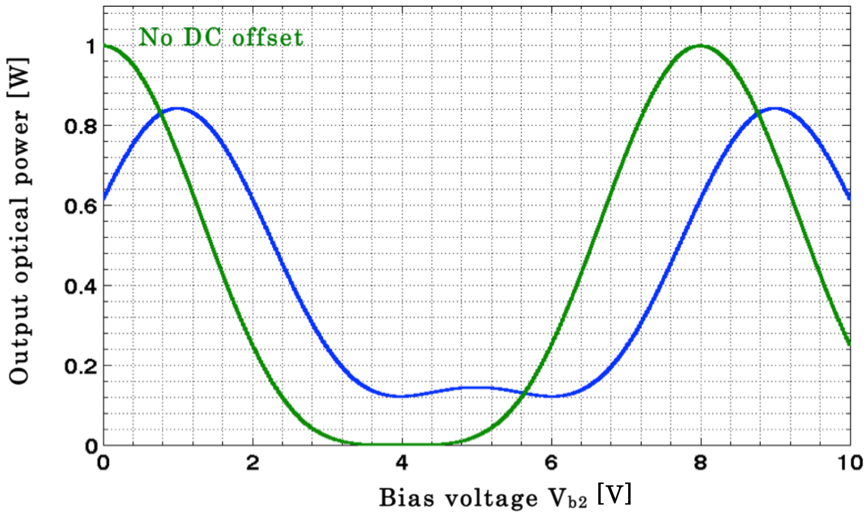

(b)

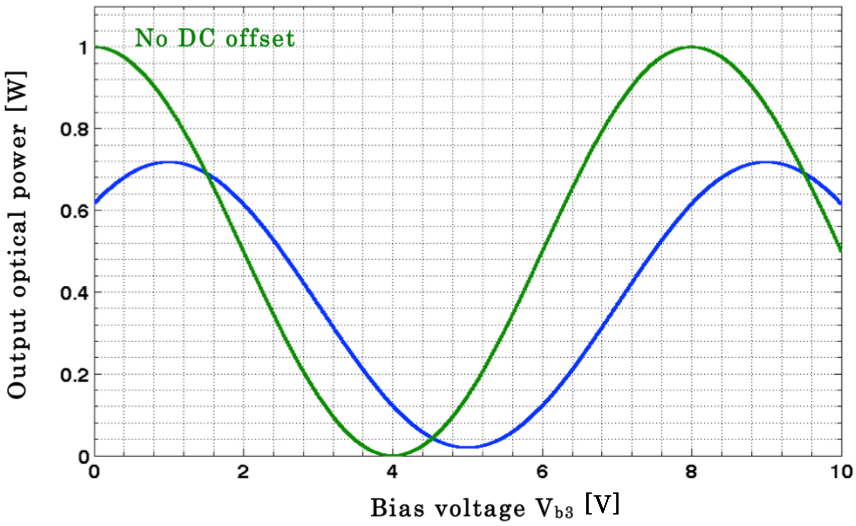

(c)

Figure 3.6: Transfer function of the DPMZM with and without DC offset for (a) V_{b1} (b) V_{b2} and (c) V_{b3}

There have been many investigations on using the DPMZM to linearize the transfer function by eliminating the distortion products particularly the IMD3. They are based on adjusting two or more of the DPMZM parameters i.e. the optical splitting ratio at the input of the DPMZM, the modulation index ratio between the upper and lower MZM, and the bias voltages of the upper MZM, the bottom MZM, and the phase shifter. The first study regarding the linearity performance of the DPMZM was conducted by Steven Krotoky in 1990 [38], which was a generalized extension of the two-polarization scheme introduced by Johnson and Russel [39]. The two MZMs can be realized by using the two orthogonal polarization states of a single MZM structure, as originally stated in [39]. As a result, the DPMZM can be integrated on a single chip, which offers an economy of optical and electrical circuit elements, and ensures that the differences in electrical delay times are negligible. Alternatively the two MZMs can be spatially connected, and this offers greater flexibility in attaining optimum performance because the optical splitting ratio can be adjusted as desired. The linearisation scheme proposed by Krotoky was centered on eliminating the dominant second order distortion in a multioctave link. It was based on fixing all the DPMZM bias voltages to $\frac{V_\pi}{2}$, and optimising both the optical splitting ratio, and the modulation index between the upper and lower MZM so as to cancel the second order distortion products. Since then, different DPMZM linearisation approaches have been reported [40-47]. The approaches in [44], and [46] are similar to [38] except that all the DPMZM bias voltages were fixed at V_π (instead of $\frac{V_\pi}{2}$) to leverage the benefits of carrier suppression, and to simultaneously linearize the DPMZM by appropriately adjusting the optical splitting ratio, and the modulation index ratio to cancel the IMD3. Of particular interest is the single drive DPMZM proposed in [47], which is based on applying the microwave signal to only one port of the DPMZM, and adjusting the DPMZM bias voltages appropriately to cancel the IMD3. The advantage of this technique is that it does not require an electrical coupler to split the RF signal, and thus the linearisation performance will not be affected by the signal frequency. In addition, choosing a different set of bias voltages (other than the quadrature or minimum) may offer additional advantages such as improved conversion efficiency, and noise figure. This linearisation technique has been demonstrated in an upconverted photonic mixer link as reported in [35]. It is based on cascading a low biased MZM with the single drive linearised DPMZM as shown in Fig. 3.7

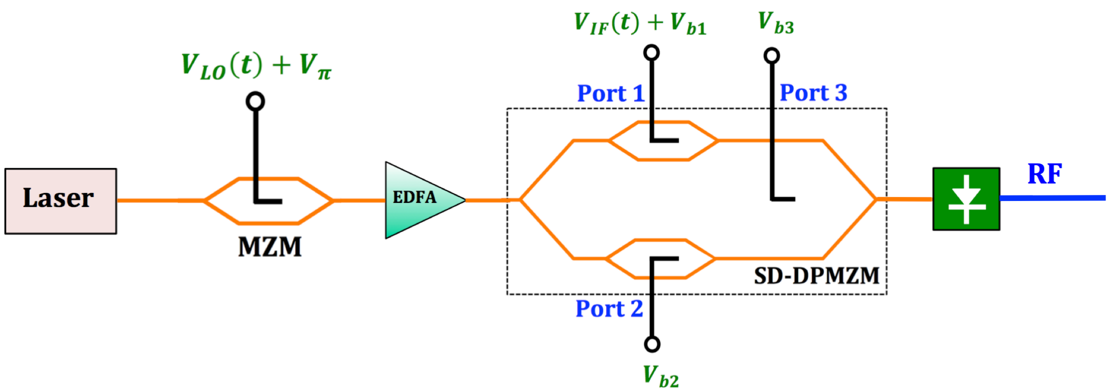

Figure 3.7: Structure of the signle drive DPMZM based photonic mixer

The laser light is modulated by a low-biased MZM, which is driven by an LO tone at frequency of about half of the RF signal frequency. The output of the MZM is a double sideband-suppressed carrier with two coherent lights at frequency separation of f_{LO}. The light from the MZM is then modulated through the single drive DPMZM. One of the MZM's in the DPMZM is driven by the IF signal as well as a DC bias voltage while the other MZM is only biased with a DC voltage. The modulated signal at the output of the DPMZM is then detected by a photodiode, which produces the upconverted RF signal. The IMD3 in the electrical domain has two origins after photodetection. The first origin is due to the beat of the optical carrier and the IMD3 component, and the second origin is due to the beat of the fundamental terms and the second order IMD terms in the optical field. Under optimized condition of the DPMZM bias voltages, these two IMD3 origins can have opposite phase and equal intensity, and thus cancel each other out, leading to low IMD3 and high dynamic range. Experimental results showed a measured SFDR of 122.7 dB·Hz$^{2/3}$, a noise floor of -161.1 dBm/Hz, and a conversion efficiency of -45 dB at 8 dBm received optical power. Although this mixer approach achieves high SFDR performance, however, it is a sub-octave linearisation scheme since no elimination of the second order distortions was achieved. Additionally, since the MZM driven by the LO was low biased, this will not only produce second order distortions but also will require higher drive of the LO power which is an additional electrical power penalty. Another fundamental issue lies in the degree of IMD3 suppression. In practice, driving only one port of the DPMZM by an RF will result in lower degrees of freedom in suppressing the IMD3 and hence lower SFDR performance. In contrast, applying the RF signal with different modulation depths into the two ports of the DPMZM will enable further suppression of the IMD3. Finally the bias voltages designed in this approach have led to a poor performance in the conversion efficiency, which is another important figure of merit. It will be shown in the next section that the bias voltages can be designed to yield improved SFDR performance and conversion efficiency simultaneously.

3.3 Novel Linearised DPMZM based photonic mixer structure

This section presents a new linearised DPMZM based photonic mixer structure that can readily overcome most of the fundamental issues in the previous photonic mixer structures such as the limited SFDR performance, the restriction to suboctave signal bandwidth, and the poor isolation between the LO and RF ports. The new structure can fully eliminate the IMD3 to consequently achieve a high SFDR performance, while also enabling multioctave operation, and essentially infinite isolation between the RF and LO ports. The concept is based on an integrated DPMZM to which an optimised RF split and an optimised optical phase shift is applied, in series with an MZM driven by the LO. The DPMZM is linearised by fully cancelling the third order IMD via controlling the modulator bias voltages and designing the splitting ratio of the RF signals applied to the DPMZM. In addition, the second order harmonic distortion is minimized so the photonic mixer can operate over a multi-octave range. Experimental results demonstrate a record measured SFDR performance of 127 dB·Hz$^{4/5}$, which is over 22 dB higher than that of the conventional dual-series Mach-Zehnder modulator based microwave photonic mixer.

3.3.1 Principle of Operation

Fig. 3.8 shows the structure of the new integrated DPMZM based linearised photonic mixer.

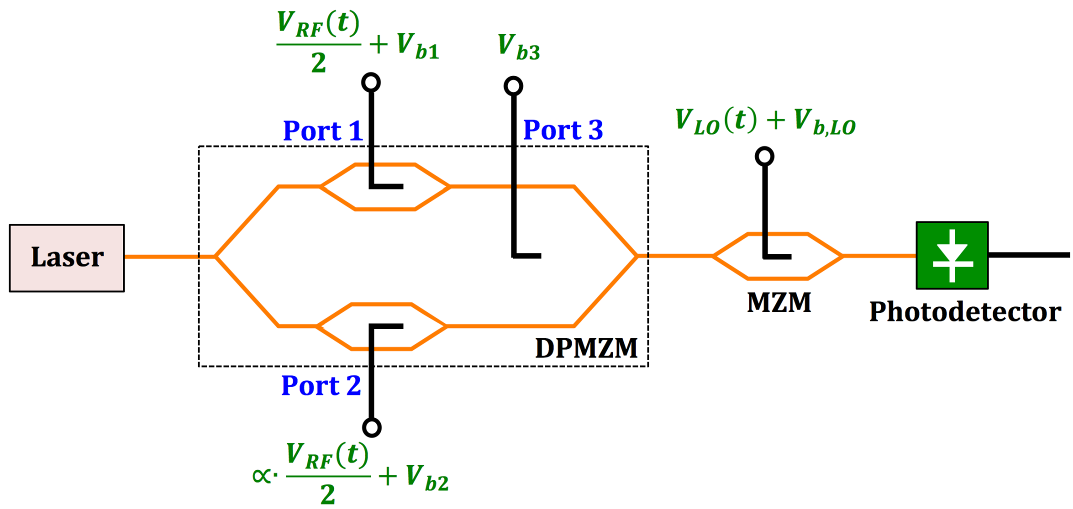

Fig. 3.8: Structure of the DPMZM based linearised photonic mixer. $V_{RF}(t)$ is the RF signal; $V_{LO}(t)$ is the LO; V_{b1}, V_{b2} and V_{b3} are the DPMZM bias voltages; and $V_{b,LO}$ is the MZM bias voltage.

Laser light is applied to the DPMZM and the input RF signal is split in the ratio of 1:α and is applied to Port 1 and Port 2 of the DPMZM so that modulation occurs with different modulation depths. An optical phase shift is applied to control the phase between the two arms of the DPMZM by setting the DC voltage applied to Port 3. The DPMZM is followed by an MZM which is driven by the LO and is subsequently detected by a low-bandwidth photodetector which generates the IF signal. The linearisation process is obtained through the integrated DPMZM. By means of an optimium design of the three bias voltages to the DPMZM together with the RF splitting ratio α, the third order IMD generated by the DPMZM is fully eliminated. The principle is illustrated in Fig. 3.9.

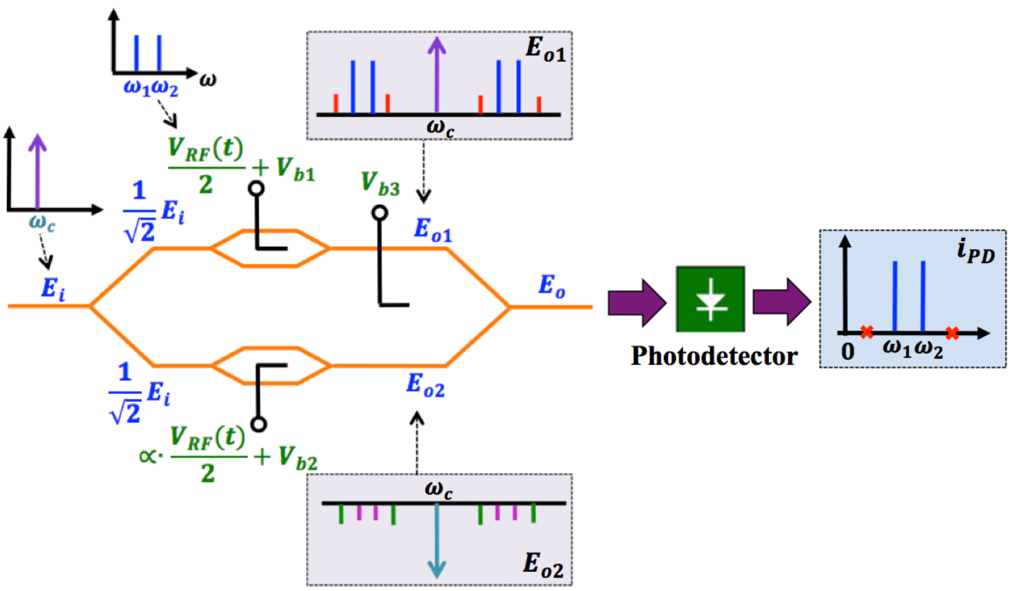

Fig. 3.9. Illustration of the linearisation process in the integrated DPMZM.

In the DPMZM, the top MZM and the bottom MZM both generate their own third order IMD components, whose value depends on the input RF modulation depth as well as the bias condtion of each MZM. The embedded phase shifter is controlled through its bias to produce a specific phase relationship between the two third order IMD components. The two modulated signals are then combined to form the output electric field. When the output electric field of the DPMZM beats at the photodetector, additional third order IMD components are generated due to either self beating of the third order IMD component of each MZM, cross beating between the third order IMD in one modulator and the optical carrier in the other modulator and vice versa, or cross beating between the two third order IMD components generated from the top MZM and the bottom MZM. The optimum design ensures that the three bias voltages of the DPMZM and the RF voltage splitting ratio are chosen so as to enable a complete cancellation of all the possible third order IMD products. Note that the example given in Fig. 3.8 considers only the simplest case where the two RF signals into the DPMZM have either in or out-of-phase relationship. The frequency downconversion process is obtained by following the DPMZM by an MZM driven by the LO, which after subsequent photodetection produces IF frequencies at $\omega_{IF} = \omega_{RF} \pm \omega_{LO}$, where ω_{RF} is the input RF frequency and ω_{LO} is the LO frequency. This MZM is biased at quadrature to avoid the even order harmonic distortion, which enables the realisation of a wideband multioctave operation of the mixer. Moreover since the RF signal and the LO are modulated in different units, this provides essentially infinite isolation between the RF and LO ports, enabling the RF signal and the LO to be located at different locations.

3.3.2 Theoretical analysis of the linearised DPMZM based photonic mixer

This section presents a general analysis for the linearised DPMZM based photonic mixer, which accounts for any bias voltages applied to the three ports of the DPMZM and any RF power splitting ratio. The mathematical expressions for the fundamental figure of merits of the mixer i.e. conversion efficiency, noise figure, and SFDR are derived, and evaluated. The mixer performance is evaluated, and techniques to improve the conversion efficiency, noise figure and SFDR are provided. It should be noted that the DPMZM analysis provided in this section considers the use of the single drive DPMZM unit which is slightly different than the push-pull unit in that it requires double the switching voltage of the push-pull configuration. Referring to Fig. 3.8, the electric field at the output of the integrated DPMZM is given by

$$E_x(t) = \frac{E_i\sqrt{t_{ff1}}}{2}\left[cos\frac{m_1(t)}{2}e^{j\frac{\varphi_3}{2}} + cos\frac{m_2(t)}{2}e^{-j\frac{\varphi_3}{2}}\right] \tag{3.8}$$

where E_i is the amplitude of the electric field at the DPMZM input, t_{ff1} is the DPMZM insertion loss, $m_1(t) = m_{RF}\,cos(\omega_{RF}t) + \varphi_1$, and $m_2(t) = \propto \cdot m_{RF}\,cos(\omega_{RF}t) + \varphi_2$ are the two inputs to the DPMZM upper and lower arm respectively, $m_{RF} = \pi(V_{RF}/V_\pi)$ is the RF modulation index, V_{RF} is the input RF signal amplitude, V_π is the half wave voltage of the modulator and is assumed to be the same for all MZMs inside the DPMZM, $\propto$ is the voltage ratio of the RF signal into Port 1 and 2 of the DPMZM, $\varphi_n = \pi(V_{bn}/V_\pi)$ is the phase difference between the two arms of the n-th MZM, V_{bn} is the DC bias voltage into Port n of the DPMZM, and ω_{RF} is the angular frequency of the RF signal. The electric field at the output of the MZM driven by the LO is given by

$$E_o(t) = \frac{E_x(t)}{2}\sqrt{t_{ff2}}\left[1 + e^{jm_{LO}(t)}\right] \tag{3.9}$$

where t_{ff2} is the MZM insertion loss, $m_{LO}(t) = m_{LO}cos(\omega_{LO}t) + \frac{\pi}{2}$ is the input to the MZM driven by the LO, and biased at quadrature, and $m_{LO} = \pi(V_{LO}/V_{\pi,LO})$ is the LO modulation index, where V_{LO} is the input LO amplitude, $V_{\pi,LO}$ is the half wave voltage of the LO modulator. The output photocurrent can be obtained from (3.9) and is given by

$$I_{PD} = |E_o(t)|^2\Re =$$
$$\frac{t_{ff1}\cdot t_{ff2}\cdot P_{in}}{16}\left[1 + cos\,m_{LO}\,(t)\right]\left[2 + cos\,m_1(t) + cos\,m_2(t) + 4\,cos\left(\frac{m_1(t)}{2}\right)cos\left(\frac{m_2(t)}{2}\right)cos(\varphi_3)\right]\Re \tag{3.10}$$

where $\Re$ is the responsivity of the photodiode, and P_{in} is the laser power into the DPMZM. We first derive the expression for the conversion efficiency of the mixer. The IF coefficient can be obtained from (3.10) and is given by

$$\Gamma_{IF} = J_1(m_{LO})\left[a\,J_1(m_{RF}) + b\,J_1(\propto m_{RF}) + c\,J_1\left(\frac{\propto m_{RF}}{2}\right) + d\,J_1\left(\frac{m_{RF}}{2}\right)\right] \tag{3.11}$$

where $J_m(x)$ is the Bessel function of the m-th order of the first kind, and $a = sin(\varphi_1)$, $b = sin(\varphi_2)$, $c = 4\cos\left(\frac{\varphi_1}{2}\right)\sin\left(\frac{\varphi_2}{2}\right)\cos(\varphi_3)$, and $d = 4\sin\left(\frac{\varphi_1}{2}\right)\cos\left(\frac{\varphi_2}{2}\right)\cos(\varphi_3)$. For small RF signal, equation (3.11) can be approximated to

$$\Gamma_{IF} = J_1(m_{LO}) \times m_{RF} \times [(2b + c) \propto +(2a + d)] \quad (3.12)$$

The output IF electrical power of the DPMZM based photonic mixer can be obtained from (3.10), and is given by

$$P_{IF,out} = \frac{1}{32} t_{ff1}{}^2 \cdot t_{ff2}{}^2 \cdot P_{in}{}^2 . m_{RF}{}^2 . J_1(m_{LO})^2 \Re^2 R_L [(2b + c) \propto +(2a + d)]^2 \quad (3.13)$$

where R_L is the photodiode load resistance. The conversion efficiency can then be obtained as follows

$$G_{conv} = \frac{P_{IF,out}}{P_{RF,in}} = \frac{1}{16}\left(\frac{\pi}{V_\pi}\right)^2 t_{ff1}{}^2 \cdot t_{ff2}{}^2 \cdot P_{in}{}^2 . J_1(m_{LO})^2 \Re^2 R_L R_{in} [(2b + c) \propto +(2a + d)]^2 \quad (3.14)$$

where R_{in} is the modulator input resistance. It can be seen from (3.14) that the conversion efficiency depends on three system parameters namely the input optical power P_{in}, the LO modulation index m_{LO}, and the IF coefficient $(2b + c) \cdot \propto +(2a + d)$. Increasing the input optical power will significantly improve the conversion efficiency. The optimum LO modulation index for maximum conversion efficiency is known to be approximately $m_{LO} \sim 1.84$ [5]. The IF coefficient can be maximised by designing the RF voltage splitting ratio to be as large as possible. This can be done by applying an RF modulation depth to port 2 of the DPMZM, that is much greater than that applied to port 1 of the DPMZM. Also the bias voltages of the DPMZM can be designed for improved conversion efficiency. The IF amplitude of the DPMZM based photonic mixer structure is compared with the IF amplitude of the conventional dual-series MZM based photonic mixer to determine whether there is penalty or gain in the conversion efficiency. The output IF power for the dual series mixer is given by

$$P_{IF,out}[DSM] = \frac{1}{32} t_{ff1}{}^2 \cdot t_{ff2}{}^2 \cdot P_{in}{}^2 . m_{RF}{}^2 . J_1(m_{LO})^2 \Re^2 R_L \quad (3.15)$$

Then the conversion efficiency ratio between the DPMZM based photonic mixer, and the dual series based photonic mixer is given by

$$\eta = \frac{P_{IF,out}[DPMZM]}{P_{IF,out}[DSM]} = [(2b + c) \propto +(2a + d)]^2 \tag{3.16}$$

Thus to yield an improved conversion efficiency, the IF coefficient needs to be $(2b + c) \propto +(2a + d) > 1$. A bias scheme that simultaneously improves the conversion efficiency and the SFDR performance will be presented in the next section. We derive also the expression for the SFDR for the linearised DPMZM based photonic mixer. For a two tone RF input $m(t) = m_{RF}[\cos(\omega_1 t) + \cos(\omega_2 t)]$ where ω_1 and ω_2 are two closely spaced angular RF signal frequencies, the output electrical signal after photodetection will consist of the two tone IF signals at frequencies $\omega_1 - \omega_{LO}$ and $\omega_2 - \omega_{LO}$ as well as the in-band third order IMD at frequencies $2\omega_1 \pm \omega_2 - \omega_{LO}$. The mixer SFDR performance is limited by the presence of the third order IMD, which is the largest distortion product. Thus it is important to find an expression for the amplitude of the third order IMD to evaluate the SFDR performance. The IMD coefficient at frequencies $2\omega_1 \pm \omega_2 - \omega_{LO}$ can be obtained from (3.10), and is given by

$$IMD = J_1(m_{Lo}) \Big[a\, J_1(m_{RF}) J_2(m_{RF}) + b\, J_1(\propto . m_{RF}) J_2(\propto . m_{RF}) + c\, J_1\left(\tfrac{\propto m_{RF}}{2}\right) J_2\left(\tfrac{\propto m_{RF}}{2}\right) + d\, J_1\left(\tfrac{m_{RF}}{2}\right) J_2\left(\tfrac{m_{RF}}{2}\right) + c\, J_1\left(\tfrac{\propto . m_{RF}}{2}\right) J_2\left(\tfrac{m_{RF}}{2}\right) + c\, J_1\left(\tfrac{\propto m_{RF}}{2}\right) J_1\left(\tfrac{m_{RF}}{2}\right)^2 + d\, J_1\left(\tfrac{m_{RF}}{2}\right) J_2\left(\tfrac{\propto m_{RF}}{2}\right) + d\, J_1\left(\tfrac{m_{RF}}{2}\right) J_1\left(\tfrac{\propto m_{RF}}{2}\right)^2\Big] \tag{3.17}$$

where $J_m(x)$ is the Bessel function of the m-th order of the first kind. The terms in (3.17) have different origins. The first and second terms in (3.17) represent the IMD generated by the self-beating of the modulated optical signal in each arm of the DPMZM. The third and fourth terms correspond to the cross-beating between the modulated optical signal in one arm and the optical carrier in the other arm of the DPMZM, and the last four terms are generated by the cross-beating of the modulated optical signal in the upper arm with the modulated optical signal in the lower arm. Equation (3.17) can be expanded by using the following relationship:

$$J_m(x) = \sum_{n=0}^{\infty} \frac{(-1)^n}{n!\,(n+m)!} \left(\frac{x}{2}\right)^{2n+m} \tag{3.18}$$

We take only the first two terms i.e. the qubic and the quintic terms from (3.17), the IMD is given by

$$IMD = \frac{m_{RF}{}^{3}}{64}.J_1(m_{LO}).[(8b+c)\propto^3 + 3d\propto^2 + 3c\propto + (8a+d)] - \frac{m_{RF}{}^{5}}{3686}.J_1(m_{LO}).[(32b+c)\propto^5 + 5d\propto^4 + 10c\propto^3 + 10d\propto^2 + 5c\cdot\propto + (32a+d)] + \text{higher order terms} \tag{3.19}$$

Equation (3.19) shows that for small signal inputs, the quintic term and the higher order terms are negligible, and the cubic term is significant. The SFDR, limited by the cubic nonlinearity can be obtained from (3) and is given by

$$SFDR = \left(\frac{P_{IF,TOI}}{N_{total}}\right)^{\frac{2}{3}} \tag{3.20}$$

where N_{total} is total noise power at the output of the DPMZM based linearised photonic mixer, which includes the laser intensity noise, the photodiode thermal noise, and the shot noise, and $P_{IF,TOI}$ is the output IF third order intercept power and can be expressed as

$$P_{IF,TOI} = \frac{t_{ff1}{}^{2}\cdot t_{ff2}{}^{2}\cdot P_{\mathrm{in}}{}^{2}.\kappa_{TOI}.J_1(m_{LO})^2\Re^2 R_L}{32}\cdot[(2b+c)\propto + (2a+d)]^2 \tag{3.21}$$

where κ_{TOI} is the third order intercept point and is given by

$$\kappa_{TOI} = 32\cdot\frac{(2b+c)\propto + (2a+d)}{(8b+c)\propto^3 + 3d\propto^2 + 3c\propto + (8a+d)} \tag{3.22}$$

From (3.20), it is clear that the SFDR can be improved by eliminating the cubic term in (3.19), or by lowering the system noise floor. An analysis of (3.19) shows that for a given bias condition, there exist three RF voltage splitting ratio solutions that enable the cancellation of the cubic term in the IMD component. Once the cubic term is cancelled, then the residual quintic term in (3.19) becomes dominant especially at higher signal levels. Consequently, the SFDR, limited by the quintic nonlinearity, is given by

$$SFDR = \left(\frac{P_{IF,FOI}}{N_{total}}\right)^{\frac{4}{5}} \tag{3.23}$$

where $P_{IF,FOI}$ is the output IF fifth order intercept power, which can be expressed as

$$P_{IF,FOI} = \frac{t_{ff1}{}^{2}\cdot t_{ff2}{}^{2}\cdot P_{in}{}^{2}.\kappa_{FOI}{}^{2}.J_1(m_{LO})^2\Re^2 R_L}{32}[(2b+c)\cdot\propto + (2a+d)]^2 \tag{3.24}$$

where κ_{FOI} is the fifth order intercept point and is given by

$$\kappa_{FOI} = \left[\frac{1843.[(2b+c)\propto + (2a+d)]}{(32b+c)\cdot\propto^5 + 5d\cdot\propto^4 + 10c\cdot\propto^3 + 10d\propto^2 + 5c\cdot\propto + 32a + d}\right]^{\frac{1}{2}} \tag{3.25}$$

The SFDR limited by the quintic nonlinearity can be improved by increasing the output IF fifth order intercept power. This can be done by either increasing the laser power into the DPMZM P_{in}, increasing the fifth order intercept point κ_{FOI}, optimising the LO modulation index m_{LO}, or increasing the IF coeffecient i.e. $(2b + c) \cdot \propto +(2a + d)$. The SFDR can be also improved by reducing the noise floor of the system. It is important to note that the maximum improvement in the SFDR value is dependent on the RF modulation index. At higher modulation indices, the fifth order intermodulation product at $2\omega_1 \pm \omega_2 - \omega_{LO}$ is not negligible due to the contribution of the seventh order non-linearity to the IMD component shown in (3.19). This in turn sets an upper bound to the SFDR value. It is also important to consider the noise figure analysis of the linearised DPMZM based photonic mixer. The noise figure is given by

$$NF = \frac{N_{tot}}{G_{preamp} G_{conv} KTB} \tag{3.26}$$

where K is Boltzmann constant, T is the absolute temperature, B is the bandwidth of the signal, and G_{preamp} is the RF pre-amplifier gain at the input of the DPMZM. The total noise of the system in given by

$$N_{tot} = N_{RIN} + N_{shot} + N_{thermal} = RIN\,(P_{avg}\Re)^2 B\, R_L + 2q(P_{avg}\Re)BR_L + 4KTB \tag{3.27}$$

where P_{avg} is the average optical power incident on the photodetector, and is given by

$$P_{avg} = \frac{t_{ff1} \cdot t_{ff2} \cdot P_{in}}{16} . [2 + cos(\varphi_1) + cos(\varphi_2) + 4\, cos\left(\frac{\varphi_1}{2}\right) cos\left(\frac{\varphi_2}{2}\right) cos(\varphi_3)] \tag{3.28}$$

Various approaches can be adopted to improve the noise figure of the linearised DPMZM based photonic mixer. One obvious approach is to increase the RF pre-amplifier gain until the noise figure of the system approaches the preamplifier noise figure. Another approach is to use the method of carrier suppression to reduce the RIN and shot noise contribution. The dominant contribution to P_{avg} in (3.28) is the optical carrier power, which is useless for the downconversion process. Two bias schemes can be used to suppress the optical carrier. The first is independent of the phase shifter and is based on biasing the upper and lower MZMs at the minimum transmission point. The second bias scheme is to set the phase shifter to minmum, and bias the upper and lower MZMs at quadrature. However, both bias schemes will also eliminate the desired IF signal. Another way to minimise the optical carrier is to bias the phase shifter at minimum, and then set φ_2 to be close to φ_1. The RF splitting ratio can then be adjusted so as to increase the IF signal, and reduce the optical carrier power.

3.3.3 Simulation results of the linearised DPMZM based photonic mixer

In this section, different bias solutions for linearisation are investigated, which set $(8b + c) \propto^3 + 3d \propto^2 + 3c \propto +(8a + d) = 0$ so as to eliminate the third order IMD product and consequently improve the SFDR performance. The bias solutions also consider improvement in the conversion efficiency and noise figure. The simulation parameters are shown in Table 3.1

Parameter	Name	Value
q	Electron Charge	$1.6{\times}10^{-19}$ C
B	Receiver Noise Bandwidth	1 Hz
T	Absolute Temperature	298 K
K	Boltzmann Constant	$1.38{\times}10^{-23}$ J/K
RIN	Relative Intensity Noise	$1{\times}10^{-16}$ Hz^{-1}
P_{in}	Input Laser Power	20 dBm
$P_{RF,in}$	Input RF power	-10 dBm
R_{in}	Input Resistance	50 Ω
R_L	Load Resistance	50 Ω
t_{ff1}	DPMZM Insertion Loss	5 dB
t_{ff2}	MZM Insertion Loss	5 dB
m_{LO}	LO Modulation Index	1.84

Table 3.1: Matlab simulation parameters for the linearised DPMZM based photonic mixer

In the next three subsections, we will investigate three different solutions for cancelling the IMD3. The first solution in section 3.3.3.1 is designed to improve the conversion efficiency, and the SFDR simultaneously. The second solution in section 3.3.3.2 is designed to improve the noise figure together with the SFDR. The last solution in section

3.3.3.3 is designed for minimum insertion loss in the DPMZM, and is used in the experiment of the linearised DPMZM based photonic mixer.

3.3.3.1 Design bias condition for improved conversion efficiency and high SFDR

The first bias solution is designed to improve the link conversion efficiency while simultaneously eliminating the IMD3. As was stated previously, it is desirable to have a large value of $\propto$ in order to maximise the conversion efficiency. Therefore the first bias solution is chosen so that it linearizes the DPMZM at $\propto = -2$. The bias voltage of the top MZM was biased at quadrature, while the bias voltage of the phase shifter was set to minimum. The bias voltage of the bottom MZM was found to be V_{b2}=0.814$V\pi$ so as to cancel the cubic term in (3.19). Fig. 3.10 shows the simulation results for the output IF signal power P_{IF}, and the IMD3 power as a function of the RF splitting ratio $\propto$., when the bias voltages are set to V_{b1}=0.5$V\pi$, V_{b2}=0.814$V\pi$, and V_{b3}=$V\pi$.

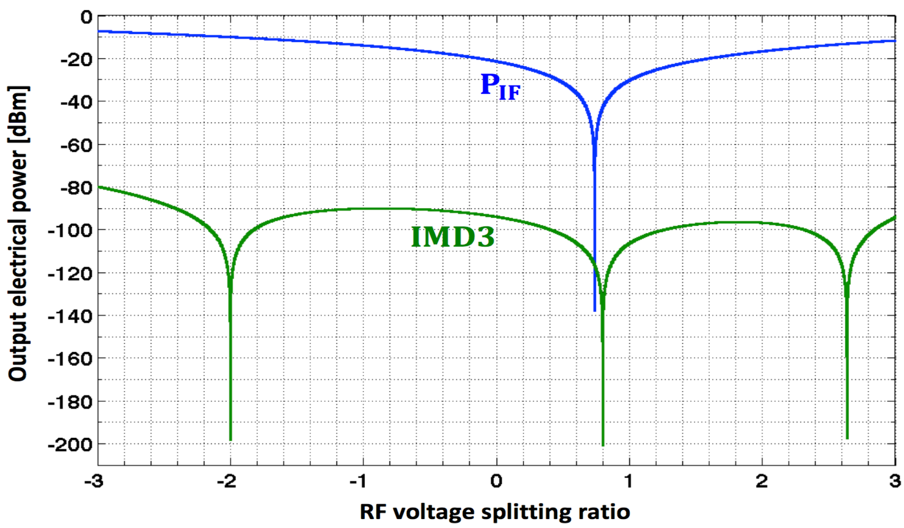

Fig 3.10: Output power spectrum at different RF splitting ratios.

Clearly there are three different RF voltage splitting ratios that enable the cancellation of the IMD3 components completely i.e. $\propto = -2, \propto = 0.8$, and $\propto = 2.63$. It is desirable to choose the splitting ratio at $\propto = -2$ since the IF signal has the highest power compared to that when using the other two RF splitting ratios for cancelling the IMD3. This indicates that the RF modulation depth into port 2 of the DPMZM is twice that of the RF modulation depth into port 1 of the DPMZM, and it is in antiphase. The antiphase can be implemented by using a 180° hybrid coupler. The SFDR performance of this bias scheme and at $\propto = -2$, is shown in Fig 3.11 with respect to variation in the input laser power.

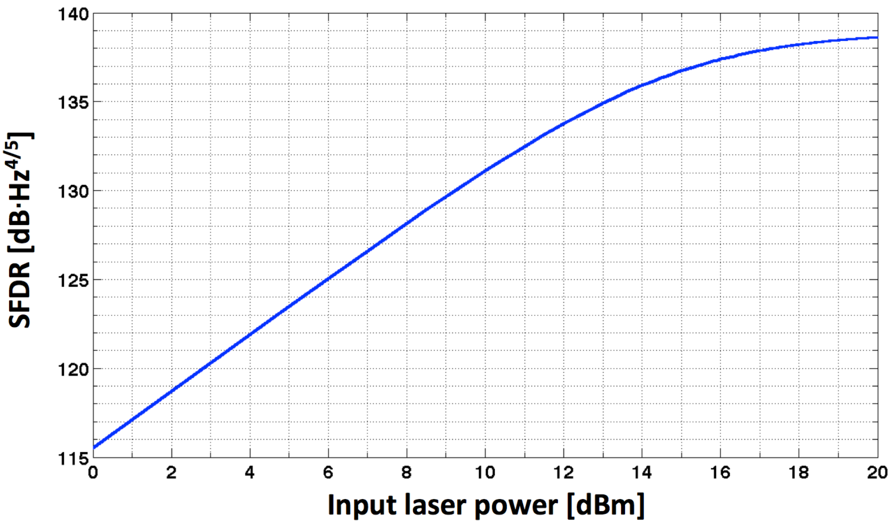

Fig 3.11: SFDR performance with respect to laser power for the linearised DPMZM based photonic mixer

It can be seen from 3.11 that for low laser power, the SFDR can be increased by increasing the input laser power. The link noise is dominated by the shot noise until P_{in}=13 dBm. When the laser power exceeds 13 dBm, the laser intensity noise starts to dominate the system noise floor, preventing further improvement in the SFDR by increasing the input laser power. The SFDR was calculated to be 131 dB·Hz$^{4/5}$ at input laser power of 10 dBm. The SFDR is further increased to 138.6 dB·Hz$^{4/5}$ at input laser power of 20 dBm. The conversion efficiency is also invistigated as a function of the input laser power, and is shown in Fig. 3.12.

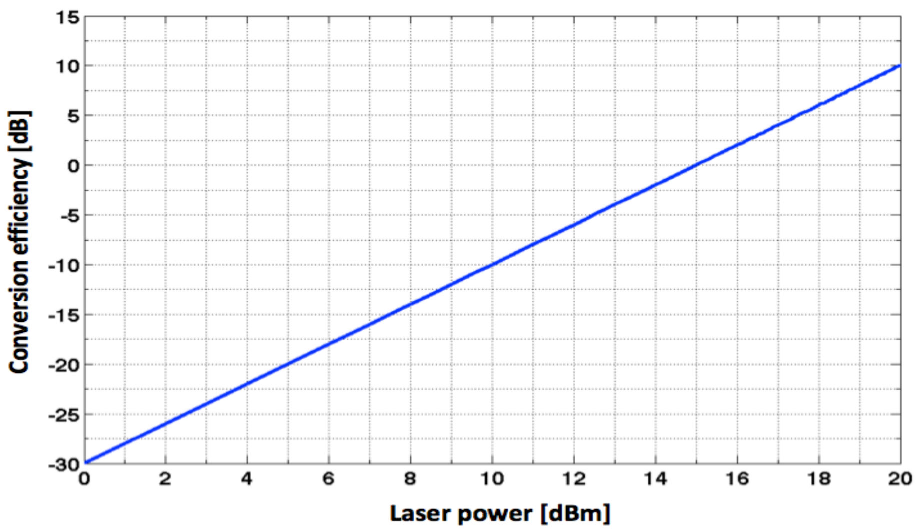

Fig 3.12: Conversion efficiency performance with respect to laser power for the linearised DPMZM based photonic mixer

Clearly the conversion efficiency in dB is linearly proportional the laser power in dBm. A 1 dB increase in the laser power results in 2 dB improvement in the conversion efficiency. This is because the conversion efficiency is proportional to the square of the laser power as was shown in (3.14). The conversion efficiency was calculated to be -10 dB at a laser power of 10 dBm, and at a high input laser power of 20 dBm and average optical power into photodetector of 7 dBm, we can obtain a net conversion gain of 10 dB. Therefore this bias scheme shows the capability of high conversion gain. Equation (3.16) was used to compute the ratio of the conversion efficiency of the linearised DPMZM based photonic mixer to the conventional dual series MZM based photonic mixer, and was found to be $\eta = 19.36$, which indicates a 12.8 dB improvement in the conversion efficiency. Finally the noise figure was simulated as a function of the input laser power and is shown in Fig. 3.13

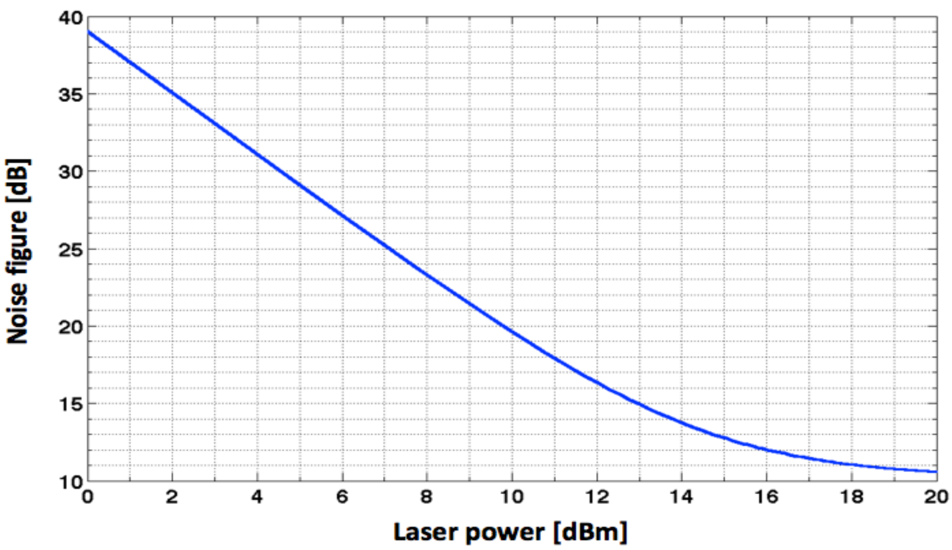

Fig 3.13: Noise figure performance with respect to laser power for the linearised DPMZM based photonic mixer

As shown from Fig. 3.13, the noise figure improves by 2 dB for every 1 dB increase in the laser power until P_{in} = 13 dBm. As the laser power is further increased, the value of the noise figure approaches 10 dB. The noise figure was calculated to be 19.6 dB at laser power of 10 dBm. In summary the bias condition at $V_{b1}=0.5V\pi$, $V_{b2}=0.814V\pi$, and $V_{b3}=V\pi$, and at splitting ratio of $\propto = -2$ can achieves an SFDR of 131 dB·Hz$^{4/5}$, a conversion efficiency of -10 dB, and a noise figure of 19.6 dB at input laser power of 10 dBm

3.3.3.2 Design bias condition for improved noise figure and high SFDR

It was mentioned previously that one way to improve the noise figure is to reduce the total noise floor of the linearised DPMZM based photonic mixer. It was also shown that a method to minimise the RIN and shot noise contribution is by using the technique of carrier suppression. This can be achieved by biasing the phase shifter at minimum, and then setting bias voltage in port 1 of the DPMZM to be close to bias voltage to the port 2 of the DPMZM. The RF voltage splitting ratio can then be adjusted so as to increase the IF signal, and reduce the optical carrier power. The DPMZM bias condition can be designed to minimise the carrier power at V_{b1}=0.7Vπ, V_{b2}=0.8Vπ, and V_{b3}=Vπ. A plot of the output IF signal power, and the IMD3 power as a function of the RF voltage splitting ratio is shown in Fig. 3.14.

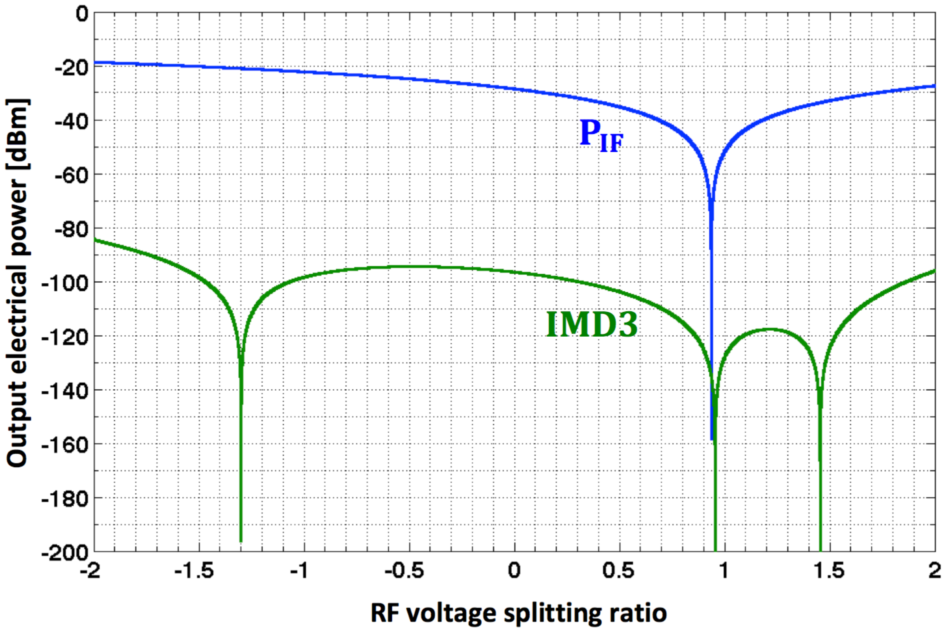

Fig 3.14: Output power spectrum at different RF splitting ratios.

Again there are three different RF voltage splitting ratios that cancel the IMD3 completely. The splitting ratio at $\propto = -1.3$ is chosen because the ouput IF power is maximised compared to the other two splitting ratios. The SFDR, conversion efficiency, and noise figure performance at V_{b1}=0.7Vπ, V_{b2}=0.8Vπ, V_{b3}=Vπ, and $\propto = -1.3$ is shown in Fig. 3.15 as a function of laser power.

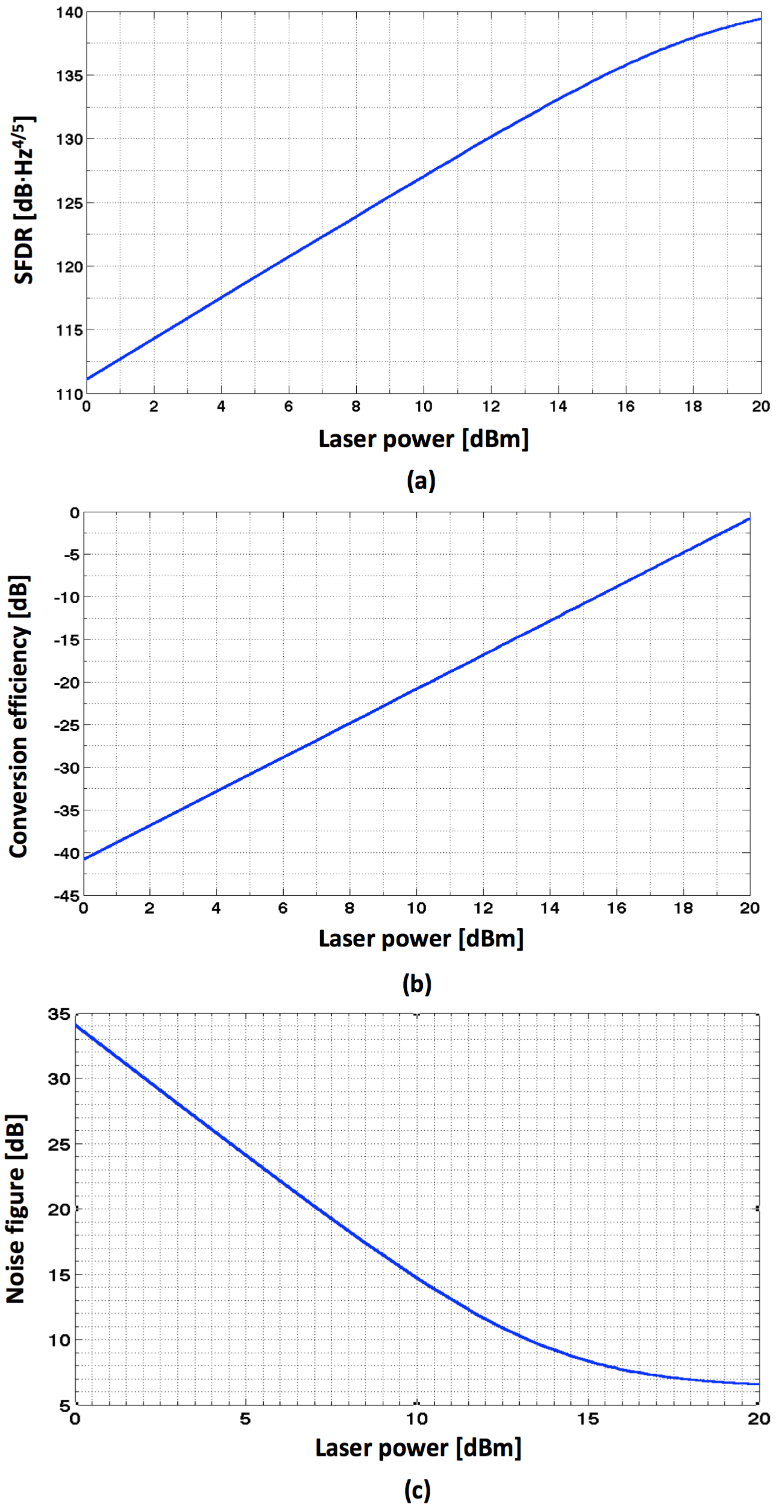

Fig 3.15: Performance of (a) SFDR, (b) Conversion efficiency and (c) Noise figure with respect to laser power

Fig. 3.15 (a) shows that the SFDR increases linearly up to P_{in} = 16 dBm, and then starts to saturate when the laser power is increased further. The SFDR was calculated to be 127.2 dB·Hz$^{4/5}$ at input laser power of 10 dBm, and is increased to 139 dB·Hz$^{4/5}$ at laser power of 20 dBm. Compared to the previous bias approach, the SFDR performance is worse at low input optical power, but showes significant improvement at high input laser power. This is due to the fact that this bias condition is designed to minimise the RIN and shot noise contribution, and hence further extending the linear relationship between the SFDR and the laser power. Fig. 3.15 (b) shows the conversion efficiency with respect to the laser power. The conversion efficiency is calculated to be -21.4 dB at laser power of 10 dBm, which is 11 dB less than that of the previous bias condition for optimised conversion efficiency. On the other hand the noise figure is improved when compared to the first bias approach as shown in Fig. 3.15 (c). The noise figure was calculated to be 14.8 dB at laser power of 10 dBm, which is about 5 dB better than the first bias condition.

3.3.3.3 Design bias condition for the minimum DPMZM optical power loss

Although the two previous bias conditions achieve either a high conversion efficiency, or a good noise figure together with high SFDR performance, they introduce a high optical power loss. The first bias scheme i.e. $V_{b1}=0.5V\pi$, $V_{b2}=0.814V\pi$, and $V_{b3}=V\pi$ introduces an optical power loss of 13.6 dB in addition to the DPMZM insertion loss. The second bias scheme i.e. $V_{b1}=0.7V\pi$, $V_{b2}=0.8V\pi$, and $V_{b3}=V\pi$ exhibits optical power loss of 22.8 dB in addition to the DPMZM insertion loss. In practical perspective, these optical losses are intolerable, and a high power laser cannot counter this problem due to the limited power handling capability of the DPMZM used in the experiment (Sumitomo T. SBX1.5-10-P-FK), which is up to 10 dBm. The link will also exhibit additional optical power losses due to the MZM, and the fibre connection. Using an EDFA can solve the problem, however, the EDFA gain needs to be > 25 dB so as to overcome all the optical losses in the link. As a result this may degrade the performance of noise figure, and SFDR due to the ASE noise introduced by the EDFA. In addition to that, minimizing the optical power losses is crucial for SFDR measurements, so that the IMD3 can then be observed well above the noise floor. To solve this practical issue, a new bias condition is presented in this section that minimizes the optical power losses in the DPMZM while also simultaneously linearizing the DPMZM. The top MZM in the DPMZM is biased at $V_{b1} = 0.34\ V\pi$, and the bottom MZM is biased at quadrature. The phase shifter is set to 0° so as to enable constructive interference between the two modulated optical signals from the top and bottom MZMs. At this DPMZM bias condition, there is only 2.1 dB loss in addition to the DPMZM insertion loss. This is 11.5 dB, and 20.7 dB lower than the first, and second bias condition respectively. Simulations were carrier out to determine the optimum RF voltage splitting ratio $\propto$ required to cancel the IMD3 component at the designed DPMZM bias condition of $V_{b1}=0.34V\pi$, $V_{b2}=0.5V\pi$, and $V_{b3}=0$. Fig. 3.16 shows the simulation results for the output IF signal power, and the IMD3 power as a function of the RF voltage splitting ratio.

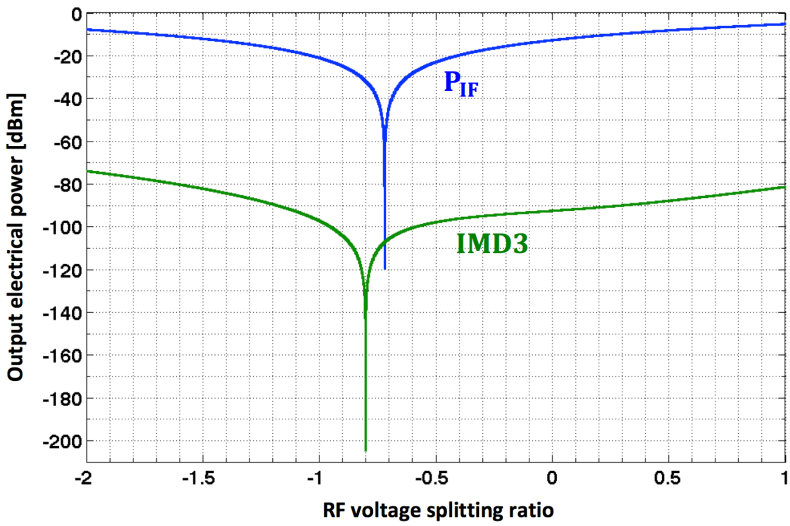

Fig 3.16: Output power spectrum at different RF splitting ratios.

It can be seen from Fig. 3.16 that there exists one real solution for the RF voltage splitting ratio that cancels the IMD3 completely, which occurs for $\propto = -0.81$ i.e. the optimum RF modulation depth into Port 2 of the DPMZM is 81% of the RF modulation depth into Port 1 and it is in anti-phase. There also exist two other solutions, however they are complex and require specific phase relationship between the two input RF signals in Port1 and Port2 of the DPMZM. It can be noted also that the IF product at the optimum ($\propto = -0.81$), which maximises the SFDR, is somewhat smaller than in the case when the SFDR is not maximised i.e. at splitting ratios other than optimum when the DPMZM is not linearised. This can be compensated for by using an EDFA in the mixer link. Also, the degradation in the total noise figure can be overcome by using a low-noise high-gain RF preamplifier at the input of the DPMZM to improve the overall noise figure performance. The performance of the SFDR, conversion efficiency and noise figure as a function of input laser power have been also investigated at V_{b1}=0.34Vπ, V_{b2}=0.5Vπ, V_{b3}=0, and $\propto = -0.81$, and the simulation results are shown in Fig. 3.17.

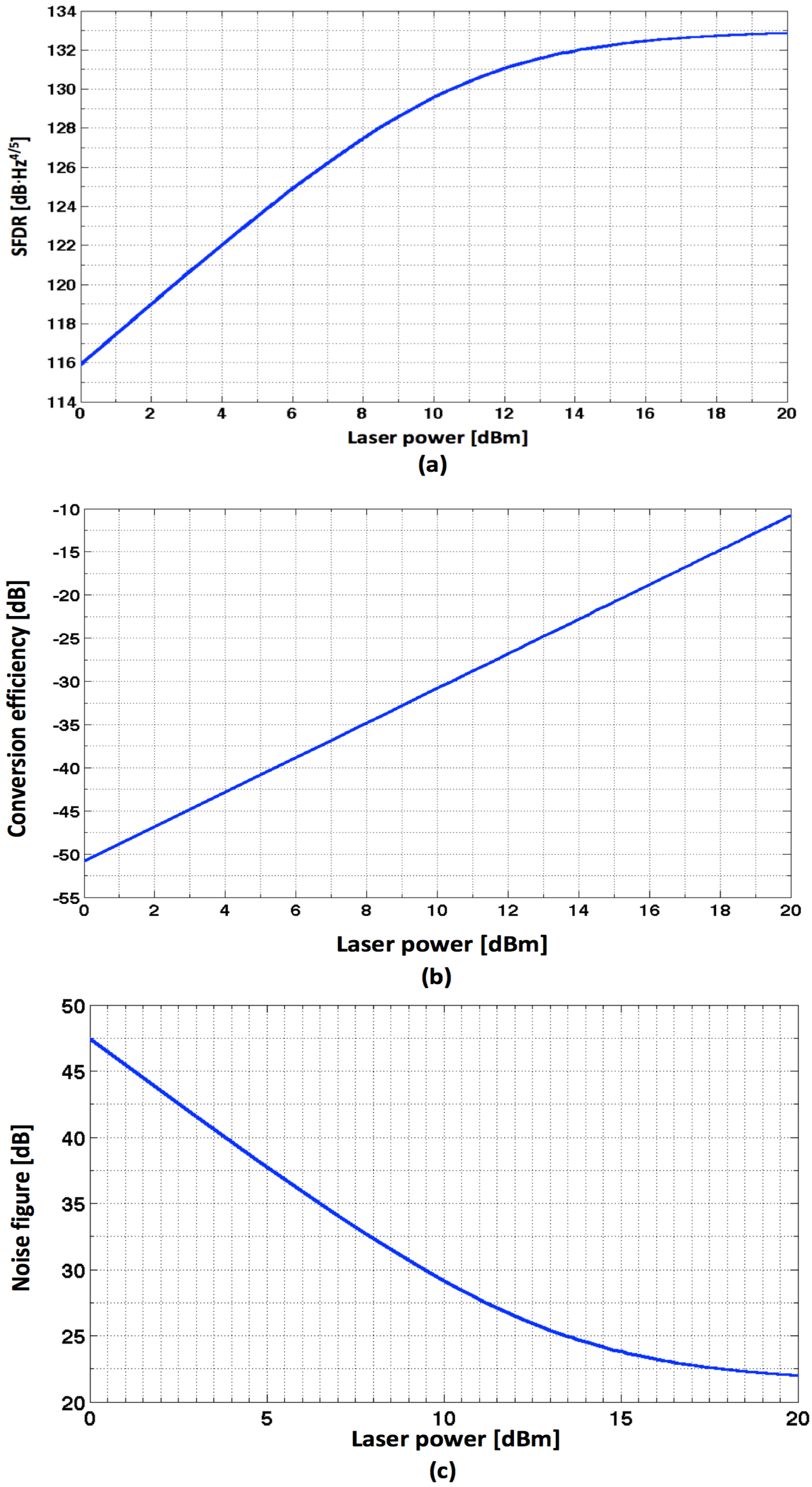

Fig 3.17: Performance of (a) SFDR (b) Conversion efficiency (c) noise figure as a function of input laser power

Fig. 3.17 (a) shows that the SFDR increases linearly with input laser power until approximately P_{in} = 8 dBm. The RIN noise dominates the system noise floor when the laser power exceeds 8 dBm, and hence, the SFDR saturates. At 10 dBm, the SFDR was calculated to be 129.6 dB·$Hz^{4/5}$, and the SFDR further increases to 133 dB·$Hz^{4/5}$ for a laser input of 20 dBm. The performance of the conversion efficiency is shown in Fig. 3.17 (b). At laser power of 10 dBm, the conversion efficiency was calculated to be -31.2 dB, and is further increased to -10 dB at input laser power of 20 dBm. Moreover the noise figure was simulated in Fig 3.17 (c), and was computed to be 28.7 dB, and 22.2 dB at laser power of 10 dBm and 20 dBm respectively. Finally the system noise floor was calculated to be -159.8 dBm/Hz at an input laser power P_{in} = 20dBm and an average power into the photodetector P_{avg} = 4.9dBm. A summary of the system performance of the previous bias schemes is shown in table 3.2.

$\frac{V_{b1}}{V_\pi}$	$\frac{V_{b2}}{V_\pi}$	$\frac{V_{b3}}{V_\pi}$	$\propto$	Conversion Efficiency	Noise Figure	SFDR	DPMZM Loss
0.5	0.814	1	−2	−10 dB	19.6 dB	131 dB·$Hz^{4/5}$	13.6 dB
0.7	0.8	1	−1.3	−21.4 dB	14.8 dB	127.2 dB·$Hz^{4/5}$	22.8dB
0.34	0.5	0	−0.81	−31.2 dB	28.7 dB	129.6 dB·$Hz^{4/5}$	2.1 dB

Table 3.2: Comparison between different bias schemes to improve linearised DPMZM based photonic mixer performance

For experimental considerations, we shall use the bias scheme of V_{b1}=0.34Vπ, V_{b2}=0.5Vπ, V_{b3}=0, and $\propto$ = – 0.81 from now on as it exhibits minimum DPMZM loss, it only requires reasonable amount of EDFA gain to compensate the total optical link loss, and it is the most appropriate for the experimental SFDR measurements so the IMD3 can be observed well above the noise floor. It can be noted also from table 3.2 that all approaches require an out of phase relationship of the RF voltage in port 1 relative to the RF voltage in port 2 of the DPMZM. It was stated earlier that the antiphase can be implemented by using a

180° hybrid coupler. However, the problem of using an electrical 180° hybrid coupler is its frequency dependence nature and that its amplitude and phase response exhibits variations at different signal frequencies. Therefore it is necessary to simulate the tolerance of the SFDR for the linearised DPMZM based photonic mixer at the optimised bias condition so as to determine the signal transmission bandwidth. The tolerance test has been conducted using VPItransmissionMaker photonic simulation software. The structure of the linearised DPMZM based photonic mixer shown in Fig 3.8 was setup in the VPI simulation. The laser power was set to 20 dBm. The DPMZM and the MZM insertion losses were both set to 5 dB. The MZM was driven by an LO with modulation index of m_{LO} = 1.84. The DPMZM was biased at the optimum bias condition of V_{b1}=0.34Vπ, V_{b2}=0.5Vπ, V_{b3}=0, and the RF voltage splitting ratio was set to $\propto = -0.81$. The noise floor was assumed to be −160 dBm/Hz, which is close to the simulated noise floor in Matlab of -159.8 dBm/Hz. The DPMZM linearisation was verified by observing that the simulation results showed that the IMD increased by 5 dB for every 1 dB increase in the input RF signal power at the optimum bias approach, which confirms the validity of the analysis. The tolerance of the maximum SFDR adjustment has also been investigated. This has been done by investigating the tolerance of the SFDR with respect to deviations in the amplitude and phase of the splitting ratio away from the optimum value, which is the most critical effect. The results are shown in Fig. 3.18. The solid lines in Fig. 3.18(a) and (b) shows the tolerance of the SFDR when the DPMZM is biased at the optimum bias condition i.e. $\varphi_1 = 0.34\,\pi, \varphi_2 = 0.5\,\pi,$ and $\varphi_3 = 0$. Fig. 3.27(a) shows that the SFDR peaks 132.2 dB·Hz$^{4/5}$ at the optimum phase of θ = 180° and maintains a value >120 dB·Hz$^{2/3}$ over a phase imbalance of $\pm 2°$. Fig. 3.18(b) shows that the SFDR maintains a value >120 dB·Hz$^{2/3}$ over an amplitude imbalance of ± 0.15 dB. Since the linearisation method for maximum SFDR adjustment is sensitive to changes in the amplitude and phase of the RF signal, we have investigated another linearisation scheme that reduces the sensitivity of the balancing signals by making a trade-off with the maximum SFDR value obtained in the optimum bias approach. The strategy adopted to reduce the sensitivity involves slightly changing one of the RF bias voltages of the DPMZM away from its optimum value: specifically the bias voltage V_{b3} was altered slightly to give $\varphi_1 = 0.34\,\pi$, $\varphi_2 = 0.5\,\pi$, $\varphi_3 = 0.02\pi$ for the higher tolerance approach. The dashed lines in Fig. 18(a) and (b) show this case when the DPMZM is biased for higher tolerance. It can be seen that an SFDR value of >122 dB·Hz$^{2/3}$ is achieved for a phase tolerance of $\pm 3°$ and for an amplitude imbalance tolerance of ± 0.25 dB. Such phase and amplitude tolerances are available from broadband 180° hybrid couplers [53,54].

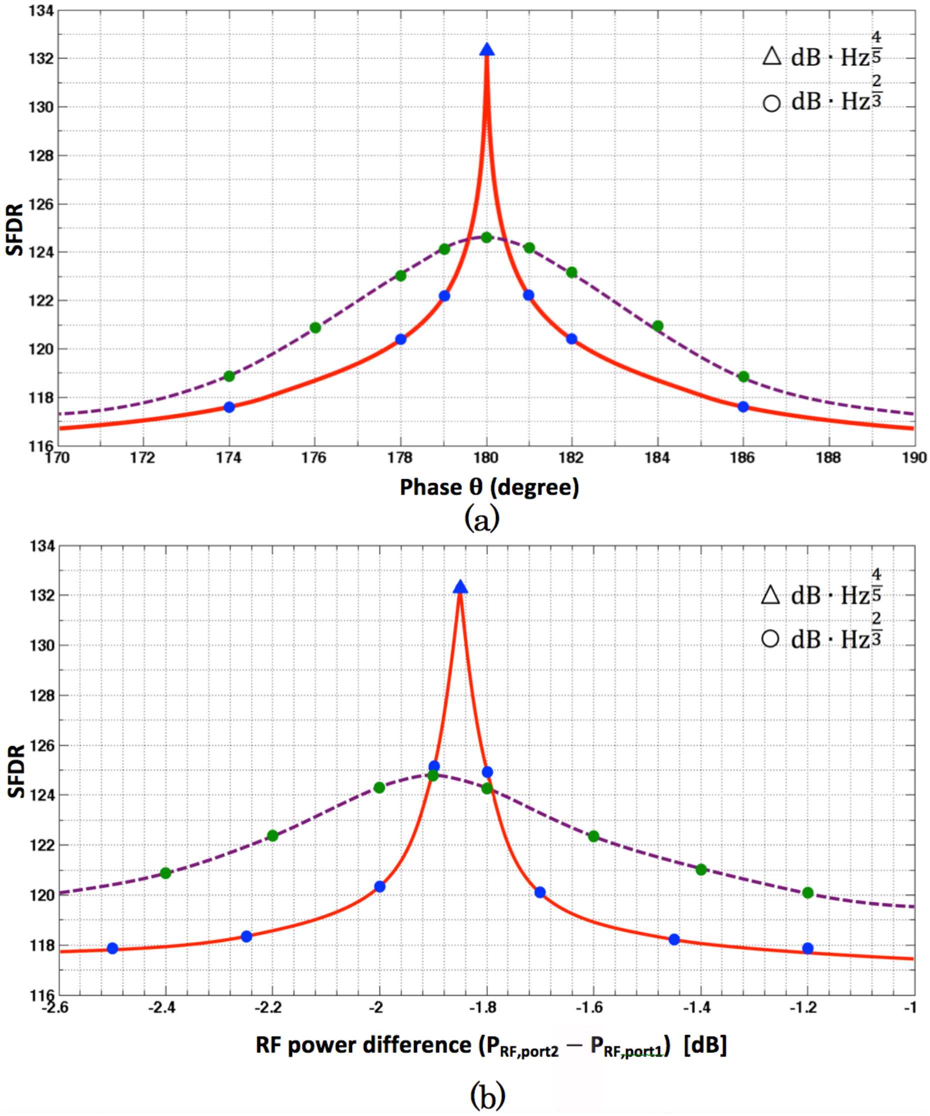

Figure 3.18 DPMZM based photonic mixer SFDR performance for the high tolerance approach with respect to (a) phase variation and (b) amplitude variation. Optimum bias approach (solid) and the high tolerance approach (dash).

The transmission bandwidth for the optimum bias condition for linearisation has also been investigated. The transmission bandwidth with high SFDR performance depends on the bandwidth of the DPMZM, the bandwidth of the photodetector, and the amplitude and phase tracking of the RF power splitter, The DPMZM and photodetector bandwidth can exceed 40 GHz, so the main limitation arises from the power splitter. For a wide transmission bandwidth it is desirable to use a resistive splitter rather than a hybrid coupler, as it provides a flatter phase and amplitude response over a wider frequency range. The anti-phase between the two RF sources can then be implemented by biasing the bottom MZM in the DPMZM at the negative slope to its original bias design. We have investigated the transmission bandwidth using the worst-case amplitude and phase tracking values of a commercially available wideband power splitter [55], using the optimum bias design and with the other simulation parameters the same as above. The result is an SFDR >120.4 dB.Hz$^{2/3}$ over the entire frequency range of DC-18 GHz for the linearised DPMZM based photonic mixer, assuming the worst case maximum phase and amplitude tracking errors specified in [55] over the frequency range of DC-18 GHz. This shows that the proposed linearised mixer structure has the capability of offering wideband high SFDR performance.

3.3.4 Experimental results for the linearised DPMZM based photonic mixer

Experiments were conducted to test the proof of principle of the new photonic mixer structure. Fig. 3.19 depicts the setup for the two tone IMD test on the DPMZM based linearised photonic mixer.

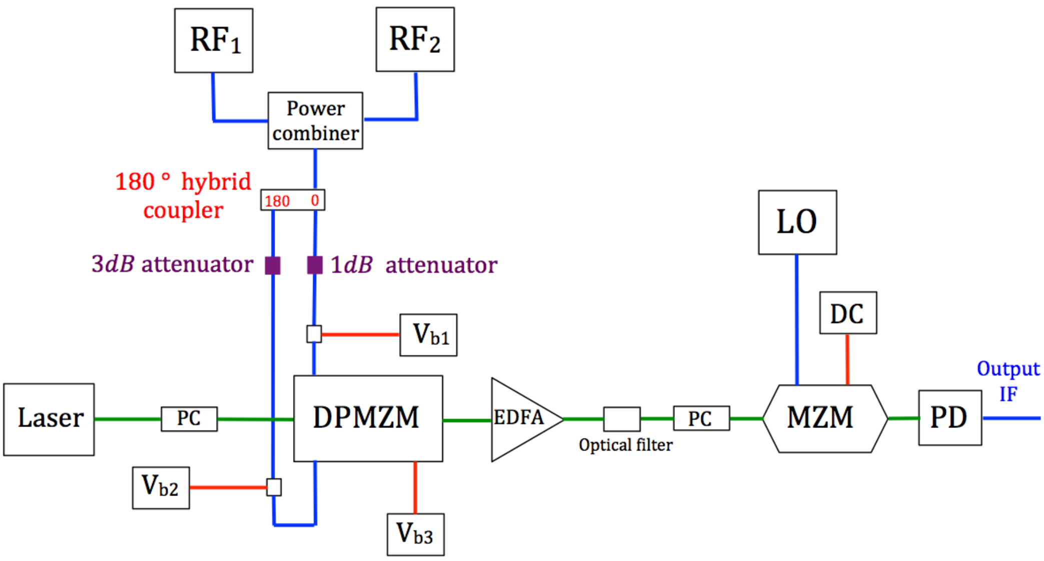

Fig 3.19: Experimental setup of the linearised DPMZM based photonic mixer structure

The optical source was a DFB laser (Fitel) with RIN = -160 dB/Hz. A commercially available integrated DPMZM (Sumitomo) was used that had a bandwidth of 16.7 GHz, and measured insertion loss of 4.8 dB. The optical power of the laser diode was set to be 9.4 dBm, which was limited by the optical power handling capability of the DPMZM. An erbium doped fibre amplifier (EDFA) was used to compensate for the losses together with an optical filter to suppress the amplified spontaneous emission (ASE) noise, and then the light was passed to a quadrature biased MZM (EOSpace) driven by the LO. The insertion loss of the MZM was measured to be 5.4 dB. Finally a photodetector having an optical power handling limit of 10 dBm was used for photodetection. Two polarisation controllers (PCs) were used to align the light polarisation into the DPMZM and the MZM respectively. The DPMZM transfer function for each input port was measured as a function of V_{b1}, V_{b2}, and V_{b3} as shown in Fig. 3.20. These characterisitcs were used to obtain the switching voltage and the bias voltage offset in each port of the DPMZM, which are required to determine the optimum bias condition for cancelling the IMD. This was done by applying 5 dBm optical power into the input of the DPMZM, and the output optical power from the DPMZM was then measured by sweeping one bias voltage while fixing the other two bias voltages to 0 V. Fig. 3.20 (a) shows that the transfer function of the DPMZM with respect to V_{b1} exhibits a bias offset of $V_{offset1} = +0.15$ V, and the modulator switching voltage was determined to be $V_{\pi 1} = 5.55\ V$. Likewise, the DPMZM transfer functions in Fig.3.20 (b) and (c) show bias offsets of $V_{offset\,2} = -1.85$ V, and $V_{offset\,3} = -0.15$ V, and modulator switching voltages of $V_{\pi 2} = 5.8\ V$, and $V_{\pi 3} = 5.65\ V$. A two tone test was performed by using RF input frequencies of f_{RF1} = 2.15 GHz and f_{RF2} = 2.155 GHz. The tones were combined using a high isolation power combiner, and were applied to a 180° hybrid coupler. Two different attenuators (1-dB and 3-dB) were placed at the outputs of the hybrid coupler to obtain the RF splitting ratio, and the two signals were then fed into the DPMZM. The process to determine the three optimum DPMZM voltages during the experiments was as follows. First the DPMZM bias voltages were set corresponding to the theoretical bias condition i.e. $\varphi_1 = 0.34\,\pi,\ \varphi_2 = 0.5\,\pi$ and $\varphi_3 = 0$. However, because the hybrid coupler used in the experiment had a phase difference of 177° between the two output ports at the frequency of operation (instead of 180° as used in the simulation for the linearisation), DPMZM bias voltage of the phase shifter was adjusted to obtain a reduction in the IMD.

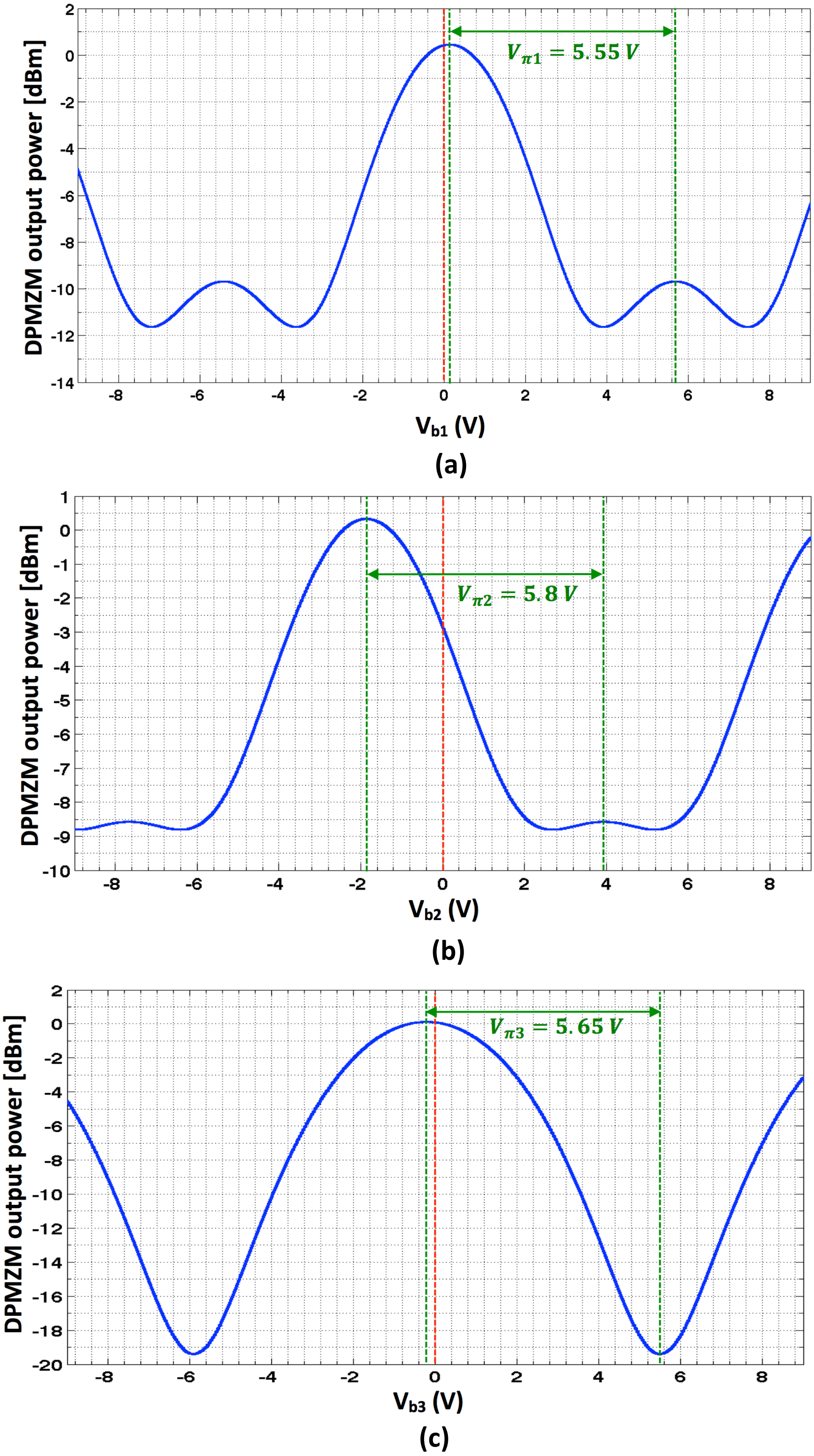

Fig 3.20: Measured transfer function of the DPMZM in (a) port 1 (b) port 2 (c) port 3

The same procedure was then carried out for the bias voltage of the top MZM, and finally the bias voltage of the bottom MZM was adjusted until complete suppression of the IMD was achieved, which could be realised when it was observed that the IMD dropped by 5 dB for every 1 dB drop in the input RF power. The optimum DPMZM bias voltages for cancelling the third order IMD, were found to be V_{b1} = 1.36 V, $V_{b2} = -5.32$ V, and V_{b3} = 0.15 V. This corresponds to $\varphi_1 = 0.22\,\pi, \varphi_2 = 0.59\,\pi,$ and $\varphi_3 = 0.06\,\pi$. The output DPMZM optical power was measured to be 1.6 dBm. The EDFA gain was set to 13 dB, and the input optical power into the MZM was measured to be about 14.6 dBm. The MZM was driven by an LO having a modulation index of 1.84 at an LO frequency of 2 GHz and was biased at quadrature, which corresponded to 2.96 V. The output power after the MZM was measured to be 5 dBm. The output IF singal after photodetection was at the frequencies of f_{IF1} = 150 MHz and f_{IF2} = 155 MHz. The third order IMD products were also observed at the frequencies $f_{IMD3,1}$ = 145 MHz, and $f_{IMD3,2}$ = 160 MHz. The changes in the IF signals and the third order IMDs with respect to the input RF signal power were measured. It was observed that the IMD3 was dropped by 5 dB for every 1 dB reduction in the input RF signal power. This indicates that the linearisation principle works properly under the optimum DPMZM bias voltages.

Fig. 3.21 (a) shows the measured IF spectrum at the optimum bias conditions for linearisation. For comparison, Fig. 3.21 (b) shows the measured IF and IMD products when V_{b1} is changed away from optimum i.e. unlinearised operation. Note that the DPMZM based linearised photonic mixer in Fig. 3.21 (a) provides superior linearity performance when compared to the unlinearised structure shown in Fig. 3.21 (b). The IMD3 was suppressed by more than 37 dB, which consequently increased the SFDR considerably. The mixer noise floor could not be observed at the output because the spectrum analyser noise floor was higher than the noise floor of the actual system. Therefore, the mixer noise floor was measured by placing a low-noise RF amplifier after the photodetector to amplify the noise generated by the system with no RF signal and LO applied to the modulators. Using this technique, the system noise floor was measured to be -157 dBm/Hz, which agrees with the simulated noise floor using the experimental parameters. The noise floor was dominated by the signal-spontaneous beat noise from the EDFA. This low-noise performance was achieved due to the use of a low-RIN laser, and optimising the EDFA location in the setup by placing it in-between the DPMZM and the electro-optic intensity modulator.

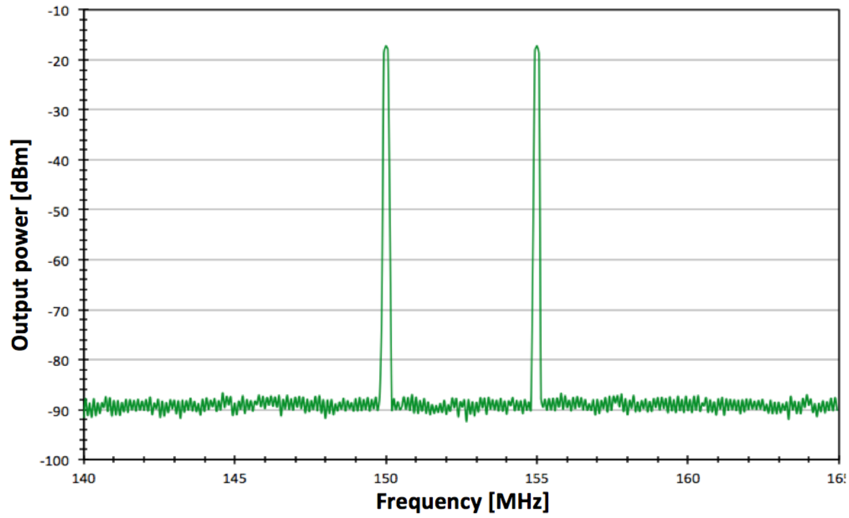

(a)

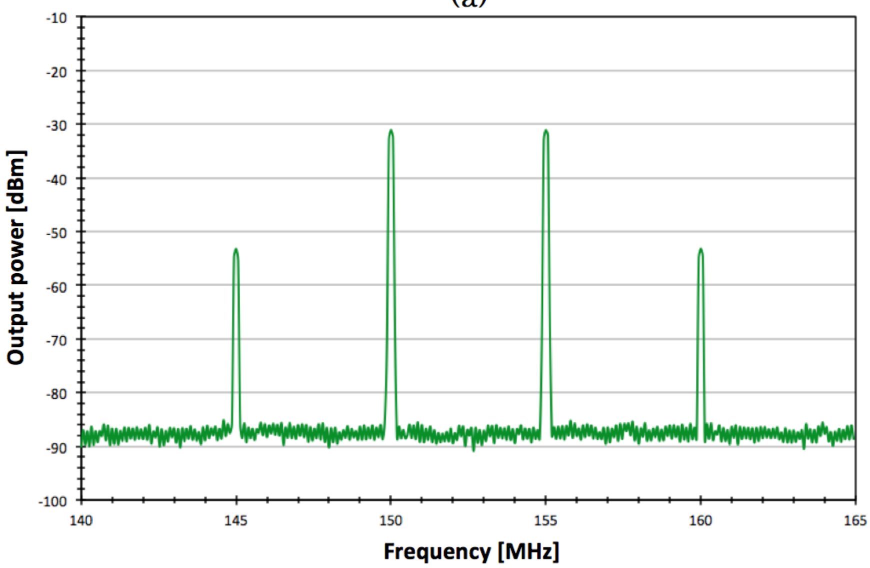

(b)

Fig. 3.21. Output electrical power of the DPMZM based photonic mixer operated (a) in the optimum bias condition ($V_{b1} = 1.36\ V, V_{b2} = -5.32\ V, V_{b3} = 0.15\ V$) and (b) away from the optimum bias condition ($V_{b1} = 0\ V, V_{b2} = -5.32\ V, V_{b3} = 0.15\ V$).

The absence of second order distortion was also experimentally measured. It was observed that second order distortions were not present at the spectrum analyser output when the MZM driven by the LO was biased at quadrature. The measurement is shown in Fig. 3.22. It can be seen that the second order harmonic distortions at frequencies 300 MHz and 310 MHz are fully suppressed, and that the second order IMD at frequency 305 MHz is extremely small (just visible) The absence of second order distortion indicates that the input signal bandwidth can be extended to multioctave operation.

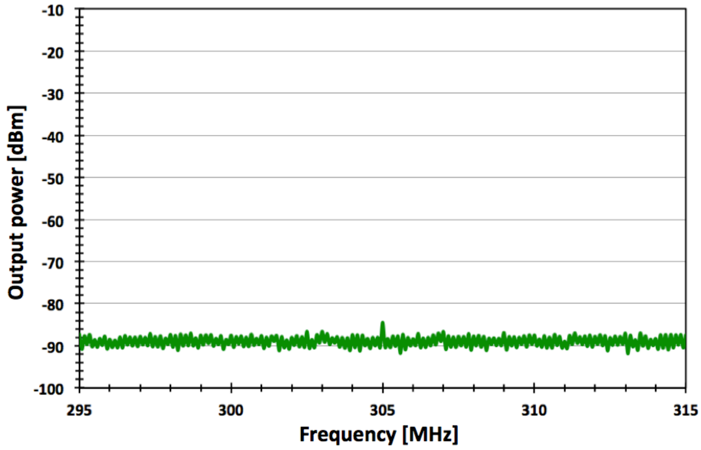

Fig. 3.22. Measured output electrical power of the linearised DPMZM based photonic mixer at the second order distortion frequencies.

The SFDR was determined from the measurements of the the IF signal power, and the IMD3 power at different input RF power. The measured SFDR performance of the linearised photonic mixer is shown in Fig. 3.23. The SFDR was measured to be 127 dB.Hz$^{4/5}$, which to my best knowledge is the highest measured SFDR for a photonic mixer. Further improvement in the SFDR can be made by using a higher-power laser source and a higher optical power handling DPMZM, which can avoid using an EDFA thus lowering the system noise floor. Other proposed linearised microwave photonic mixer such as in [23] has experimentally demonstrated an SFDR performance of 118 dB.Hz$^{2/3}$ which is 9.6 dB lower than the SFDR of the DPMZM based linearised photonic mixer.

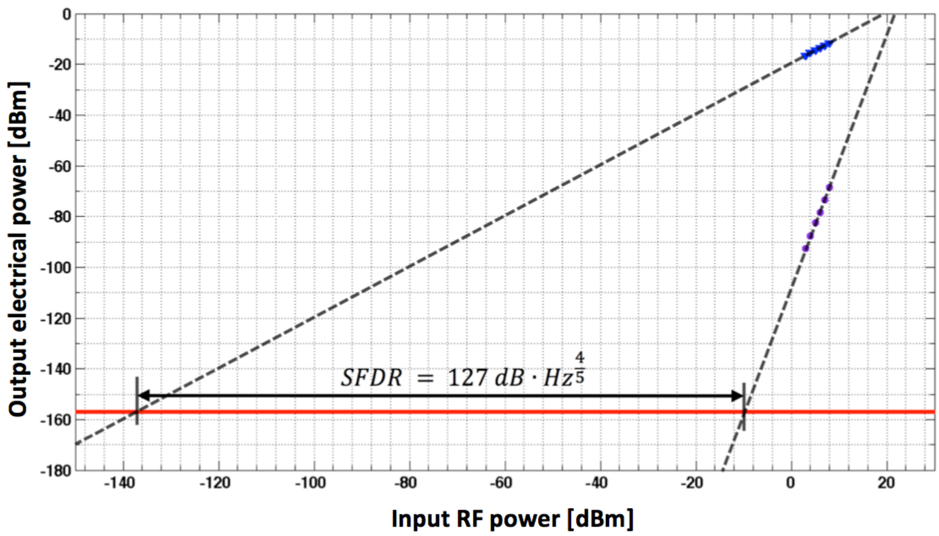

Fig. 3.23. DPMZM based linearised photonic mixer output electrical power versus input RF signal power. Measured IF signal power (▼), measured IMD3 (•), and measured noise floor (—).

The mixer conversion efficiency was measured from the ratio of the measured IF signal power to the measured RF input power, and was found to be -15 dB. The noise figure was measured from the ratio of the measured noise floor to the measured amplified thermal noise and was found to be 31.8 dB. Both these performance parameters can be improved by using higher laser power, and modulators with lower insertion loss, lower switching voltage and higher power handling capabilities. For additional improvement in the noise figure, a low-noise high-gain preamplifier is required at the input of the DPMZM. The SFDR performance demonstrates the largest improvement in the linearised DPMZM based photonic mixer. As the high SFDR performance was obtained at a set of two-tone frequency i.e. $f_{RF1} = 2.15\ GHz$ and $f_{RF2} = 2.155\ GHz$, it is essential to demonstrate the SFDR over different sets of frequencies so as to determine the suitability for broadband operation. This testing was performed using two different approaches i.e. the optimum bias approach, and the high tolerance approach discussed in the previous section. The latter approach differes from the former in one aspect and that is one of the DPMZM bias voltages is slightly adjusted away from its optimum value. In the expirement, the bias voltage at port 1 of the DPMZM V_{b1} was increased by 20 mV away from its optimum value. This is consistent with the simulation result for the high tolerance technique discussed in section 3. The SFDR response with respect to different frequencies was measured and is shown in Fig. 3.24. The SFDR dependence on frequency is mainly due to the use of 180° hyrbid coupler which exhibits different amplitude and phase imbalance at different frequencies, and as was shown in Fig. 3.18, the high tolerance approach offers more tolerance in the SFDR performance than the optimum bias approach in term of phase and amplitude imbalance. Thus the simulation and expiremental results are consistent. Also notice that the high tolerance approach offers an SFDR perforamcne of around 120 dB.Hz$^{2/3}$ from frequency range of $2 - 3.5\ GHz$. The bandwidth can be further extended by using improved hybrid couplers [53-55]. It may also be noted that the experimental results obtained from the DPMZM based photonic mixer using the optimum bias approach and also the higher tolerance approach are repeatable and were demonstrated on different days. Additionally, the second order harmonic distortions were not observed at the mixer output on the spectrum analyser.

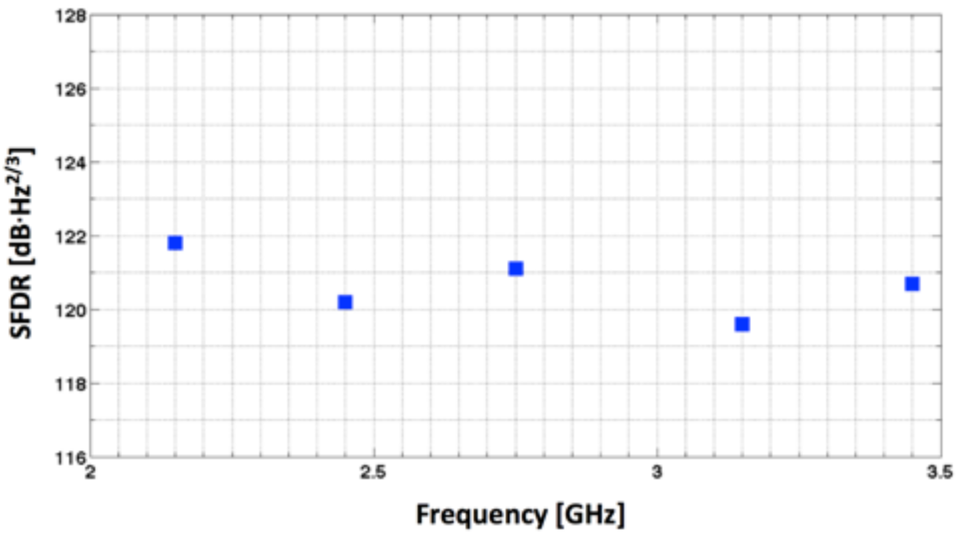

Figure 3.24 Measured SFDR response for the linearised DPMZM based photonic mixer using the high tolerance approach (■).

Finally, an experiment on the conventional dual-series MZM based photonic mixer [4] was performed as a reference for comparison. The experimental setup of the dual-series MZM based photonic mixer is shown in Fig. 3.25.

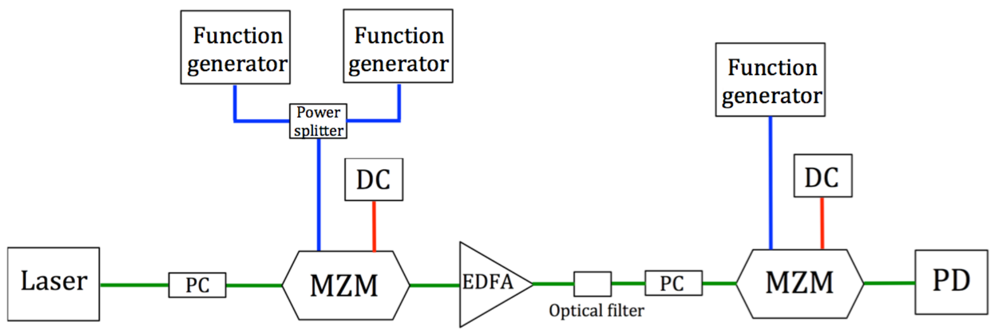

Figure 3.25 Experimental setup for the dual-series MZM based photonic mixer

The same equipment were used as in the linearised DPMZM based photonic mixer experiment except that the DPMZM was replaced by an MZM. The experiment was operated under the same conditions i.e. 9.4 dBm optical power from the DFB laser was launched into the first MZM which was biased at quadrature and was driven by the same two-tone RF signal $f_{RF1} = 2.15\ GHz$ and $f_{RF2} = 2.155\ GHz$; the second MZM was also biased at quadrature and was driven by an LO signal with modulation depth of 1.84 and frequency of $f_{LO} = 2$ GHz. The EDFA gain was controlled so the output average optical power from the second MZM was 5 dBm, which was the same as that in the linearised DPMZM based photonic mixer expirement. The noise floor was measured to be –159 dBm/Hz. The SFDR of the dual-series MZM based photonic mixer was measured to be 104.5 dB·Hz$^{2/3}$ as shown in Fig. 3.26. The experimental result was close to the simulation result of 106 dB·Hz$^{2/3}$. This shows that the new DPMZM based linearised photonic mixer achieves a 22.5 dB increase in the SFDR performance compared to the conventional dual-series MZM based photonic mixer.

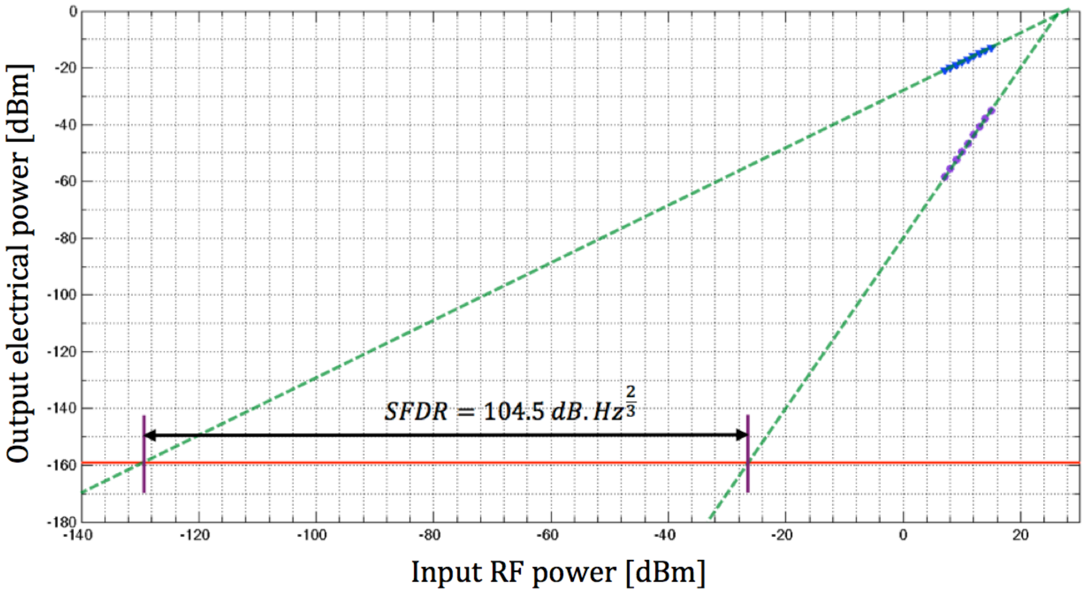

Figure 3.26: Dual-series MZM based photonic mixer output electrical power versus input RF signal power. Measured IF signal power (▼), measured IMD3 (•), and measured noise floor (—).

3.4 Conclusion

In this chapter, a detailed literature review of linearised microwave photonic mixers, including their figure of merits was presented. It has been shown that these previously reported mixer structures are subject to either limited SFDR performance, suboctave bandwidth operation, or poor isolation between the LO and RF ports, and that there is a high demand for a linearised photonic mixer technique that overcome all these bottlnecks. A new linearised photonic mixer structure that can simultaneously achieve a very high SFDR performance, while also enabling multi-octave operation, has been presented. It is based on applying an optimised RF split and an optimised optical phase shift to an integrated DPMZM, which is in series with an MZM driven by the LO. The DPMZM is linearised by fully cancelling third order IMD via controlling the modulator bias voltages and designing the splitting ratio of the RF signals into the modulators inside the DPMZM. This technique also features near infinite isolation between the RF and LO ports, and the ability to function over a multi-octave frequency range. Simulation results have shown different bias operations with the aim of improving the conversion efficiency, or the noise figure while simultaneously achieving high SFDR performance. The tolerance of the linearised DPMZM based microwave photonic mixer has been also investigated with a bias solution to relax the critical tolerance requirements of the linearised approach. Experimental results have demonstrated a record measured SFDR of 127 dB·Hz$^{4/5}$, which is also 22.5 dB higher than that of the conventional dual-series MZM based mixer structure. The main issue of this technique is the critical tolerance performance of the hybrid coupler that is required for the linearization approach which consequently limits the signal transmission bandwidth. In the next chapter, a technique will be presented that overcomes the bandwidth limitation of the linearised DPMZM based photonic mixer.

References

1. C. Lim, A. Nirmalathas, K. Lee, D. Novak, and R. Waterhouse, "Intermodulation distortion improvement for fiber–radio applications incorporating OSSB+C modulation in an optical integrated-access environment," IEEE J. Lightwave Technol. **25**, 1602–1612 (2007).

2. J. Lerdworatawee, and W. Namgoong, "Revisiting spurious-free dynamic range of communication receivers," IEEE Circuits and Systems **53**, 937-943 (2006).

3. Guoqiang Zhang, Shangyuan Li, Xiaoping Zheng, Hanyi Zhang,Bingkun Zhou, and Peng Xiang, "Dynamic range improvement strategy for Mach-Zehnder modulators in microwave/millimeter- wave ROF links," Opt. Express, vol. 20, no. 15, pp. 17214-17219, 2012.

4. G. K. Gopalakrishnan, W. K. Burns, and C. H. Bulmer, "Microwave optical mixing in LiNbO3 modulators," IEEE Microw. Theory Tech., vol. 41, no. 12, pp. 2383–2391, 1993.

5. A. C. Lindsay, A. Knight, and S. T. Winnall, "Photonic mixers for wide Bandwidth RF receiever Applications," IEEE Microw. Theory Tech., vol. 43, no. 9, pp. 2311-2317, 1995.

6. C. K. Sun, R. J. Orazi, and S. A. Pappert, "Efficient microwave frequency conversion using photonic link signal mixing," IEEE Photonics Technol. Lett., vol. 8, no. 1, pp. 154-156, 1996.

7. C. K. Sun, R. J. Orazi, and S. A. Pappert, and W. K. Burns, "A photonic-link millimeter-wave mixer using cascaded optical modulators and harmonic carrier generation," IEEE Photonics Technol. Lett., vol. 8, no. 9, pp. 1166-1168, 1996.

8. K. Ho, S. Liaw, and C. Lin, "Efficient photonic mixer with frequency doubling," IEEE Photonics Technol. Lett., vol. 9, no. 4, pp. 511-513, 1997.

9. R. Helkey, J. Twichell, and C. Cox, "A down-conversion optical link with RF gain," IEEE J. Lightwave Technol., vol. 15, no. 6, pp. 956-961, 1997.

10. K. Kitayama, and R. A. Griffin, "Optical downconversion from millimeter-wave to IF-band over 50-km-long optical fiber link using an electroabsorption modulator," IEEE Photonics Technol. Lett., vol. 11, no. 2, pp. 287-289, 1999.

11. Y. Shi, and J. H. Bechtel, "High isolation balanced photonic microwave mixers," presented at Optical Fiber Communication Conference, San Diego, USA, 21-26 Dec. 1999.

12. D. S. Shin, G. L. Li, C. K. Sun, S. A. Pappert, K. K. Loi, W. S. C. Chang, and P. K. L. Yu, "Optoelectronic RF signal mixing using an electroabsorption waveguide as an integrated photodetector/mixer," IEEE Photonics Technol. Lett., vol. 12, no. 2, pp. 193-195, 2000.

13. G. Jaro, and T. Bereceli, "A new high-efficiency optical-microwave mixing approach," IEEE J. Lightwave Technol., vol. 21, no. 12, pp. 3078-3084, 2003.

14. Y. Shi, W. Wang, and J. H. Bechtel, "High-isolation photonic microwave mixer/link for wideband signal processing and transmission," IEEE J. Lightwave Technol., vol. 21, no. 5, pp. 1224-1232, 2003.

15. M. Bystrom, Y. Li, N. Vacirca, P. Herczfeld, and W. Jermison " A coherent fiber-optic link with optical-domain down-conversion and digital demodulation," presented at the International Topical Meeting on Microwave Photonics, Vectoria, BC, October 2006.

16. Y. Li, P. Herczfeld, A. Rosen, M. Bystrom, and T. Berceli, "Optical domain down-conversion of microwave signals for high dynamic range microwave fiber optic links," presented at the International Topical Meeting on Microwave Photonics, Grenoble, France, 3-5 October 2007.

17. A. Karim, and J. Devenport, "High dynamic range microwave photonic links for RF signal transport and RF-IF conversion," IEEE J. Lightwave Technol., vol. 26, no. 15, pp. 2718-2724, 2008.

18. B. Haas, and T. E. Murphy, " A carrier-suppressed phase-modulated fiber optic link with IF downconversion of 30GHz 64-QAM signals," presented at the International Topical Meeting on Microwave Photonics, Valencia, Spain, 14-16 October 2009.

19. D. Zibar, A. Caballero, N. G. Gonzalez, C. G. Schaeffer, and I. T. Monroy, "Digital coherent receiver employing photonic downconversion for phase modulated radio-over-fiber links," presented at Microwave Symposium Digest, Boston, USA, 7-12 June 2009.

20. C. Bohemond, T. Rampone, and A. Sharaiha, "Performances of a photonic microwave mixer based on cross-gain modulation in a semiconductor optical amplifier," IEEE Journals & Magazines, vol. 29, no. 16, pp. 2402-2409, 2011.

21. T. E. Murphy, and V. R. Pagan, "Phase modulated radio-over-fiber link with electro-optic downconversion using a delay-line interferometer", Proc. SPIE 7936, RF and Millimeter-Wave Photonics, 79360L (February 21, 2011);

22. R. Wang, A, Bhardwaj, and Y.Li "Efficient RF frequency down-conversion using coupled quantum well optical phase modulator," IEEE Photonics Technol. Lett., vol. 23, no. 10, pp. 645-647, 2011.

23. C. Bohemond, P. Morel, A. Sharaiha, T. Rampone, and B. Pucel, "Experimental and simulation analysis of the third-order input interception point in an all-optical RF mixer based on a semiconductor optical amplifier," IEEE J. Lightwave Technol., vol. 29, no. 1, pp. 91-96, 2011.

24. E. H. W. Chan, and R. A. Minasian, "Microwave photonic downconverter with high conversion efficiency," IEEE J. Lightwave Technol., vol. 30, no. 23, pp. 3580-3585, 2012.

25. R. Zhu, B. Hraimel, and X. Zhang, "Analysis of simultaneous photonic frequency downconversion and optical subcarrier modulation in an electroabsorption modulator," IEEE J. Lightwave Technol., vol. 30, no. 3, pp. 344-354, 2012.

26. H. Yang, J. Sun, and Q. Du, "All-optical frequency downconversion based on cross-phase modulation in high nonlinearity dispertion-shifted fiber for WDM radio over fiber application," Opt. Express, vol. 20, no. 7, pp. 8047-8054, 2012.

27. E. H. W. Chan, and R. A. Minasian, "Microwave photonic downconversion using phase modulators in a Sagnac loop interferometer," IEEE J. sel. Topics in Quantum Electronics, vol. 19, no. 6, 2013.

28. E. H. W. Chan, and R. A. Minasian, "High conversion efficiency microwave photonic mixer based on stimulated brillouin scattering carrier suppression technique," Opt. Lett., vol. 38, no. 24, pp. 5292-5295, 2013.

29. B. Masella, B. Hraimel, and X. Zhang, "Enhanced spurious-free dynamic range using mixed polarization in optical single sideband Mach–Zehnder modulator," J. Lightwave Technol. 27, 3034-3041 (2009).

30. C. Middleton and R. DeSalvo, "Suppressed carrier techniques for multi-octave high dynamic range microwave photonic links," Proc. SPIE, 7386, 738626 (2009).

31. H. Roussell and R. Helkey, "Optical frequency conversion using a linearized LiNbO3 modulator," IEEE Microw. Guided Wave Lett. Vol. 8, no. 11, pp.408–410, 1998.

32. E. W. H. Chan, K. E. Alameh, and Robert A. Minasian, "A photonics-based wideband linearized mixer," Microwave and optical technol. Lett. 39, 500-502 (2003).

33. B. M. Haas, and T. E. Murphy, "Linearized downconverting microwave photonic link using dual-wavelength phase modulation and optical filtering," IEEE J. Photonics 3, 1–12 (2011).

34. P. Li, R. Shi, M. Chen, H. Chen, S. Yang and S. Xie, "Linearized photonic IF downconversion of analog microwave signals based on balanced detection and digital signal post-processing," International Topical Meeting on Microwave Photonics, Noordwijk, Netherlands, 11-14 September 2012.

35. S. Li, X. Zheng, H. Zhang, and B. Zhou, "Highly lineari millimeter-wave over fiber transmitter with subcarrier upconversion," in CLEO:2011 - Laser Applications to Photonic Applications, OSA Technical Digest (Optical Society of America, 2011), paper JWA3.

36. V. R. Pagan, B. M. Haas, and T. E. Murphy, "Linearized electrooptic microwave downconversion using phase modulation and optical filtering," Opt. Express 19, 883-895 (2011).

37. C. Middleton, S. Meredith, R, Peach, and R. DeSalvo, "Photonic frequency conversion for wideband RF-to-IF down-conversion and digitization," Avionics, Fiber-Optics and Photonics Technology, San Diego, USA, 4-6 October 2011.

38. S. K. Korotky and R. M. Ridder, "Dual parallel modulation schemes for low-distortion analog optical transmission," IEEE J. Sel. Areas Commun. 8, 1377–1381 (1990).

39. L. M. Johnson, and H. V. Roussell, "Reduction of intermodulation distortion in interferometric optical modulators," Opt. Lett., vol. 13, no. 10, 928-930, 1988.

40. Z. Q. Lin, and W. S. C. Chan, "Reduction of intermodulation distortion of interferometric optical modulators through incoherent mixing of optical waves," Electronics. Lett., vol. 26, no. 23, 1980-1982, 1990.

41. A. Djupsjobacka, "A linearized concept for integrated-optic modulators," IEEE Photonics Technol. Lett., vol. 4, no. 8, pp. 869-872, 1992.

42. W. B. Bridges, and J. H. Schaffner, "Distortion in linearized electrooptic modulators," IEEE Microw. Theory Tech., vol. 43, no. 9, pp. 2184–2197, 1995.

43. A. Ferreira, T. Silveira, D. Fonseca, R. Ribeiro, and P. Monteiro, "Highly linear integrated optical transmitter for subcarrier multiplexed systems," IEEE Photonics Technol. Lett., vol. 21, no. 7, pp. 438-440, 2009.

44. T. Wang, Q. Chang, and Y. Su, "Generation of linearized optical single sideband signal for broadband radio over fiber systems," Chinese Opt. Lett., vol. 7, no. 4, pp. 339-343, 2009.

45. A. Prescod, B. Dingel, and N. Madamopoulos, " Traveling wave optical modulator with high dynamic range (<<130 dB) at large modulation frequencies," Sarnoff Symposium, Princeton, NJ, March 30 - April 1, 2009.

46. G. Zhu, W. Liu, and H. Fetterman, "A broadband linearized coherent analog fiber-optic link employing dual parallel mach-zehnder modulator," IEEE Photon. Technol. Lett., vol. 21, no. 21, pp. 1627–1629, 2009.

47. S. Li, X. Zheng, H. Zhang, and B. Zhou, "Highly linear radio-over-fiber system incorporating a single-drive dual-parallel mach-zehnder modulator," IEEE Photon. Technol. Lett., vol. 22, no. 24, pp. 1775–1777, 2010.

48. S. K. Kim, W. Liu, Q. Pei, L. R. Dalton, and H. R. Fetterman, "Nonlinear intermodulation distortion suppression in coherent analog fiber optic link using electro-optic polymeric dual parallel mach-zehnder modulator," Opt. Express, vol. 19, no. 8, pp. 7865-7871, 2011.

49. P. Liu, B. J. Li, and Y. Trisno, "In search of a linear electrooptic amplitude modulator," IEEE Photon. Technol. Lett., vol. 3, no. 2, pp. 144-146, 1991.

50. G. E. Betts, "Linearized modulator for suboctave-bandpass optical analog links," IEEE Microw. Theory Tech., vol. 42, no. 12, pp. 2642-2649, 1994.

51. E. I. Ackerman, "Broad-band linearization of a Mach-Zehnder electrooptic modulator," IEEE Microw. Theory Tech., vol. 47, no. 12, pp. 2642-2649, 1999.

52. A. Ferreira, T. Silveira, D. Fonseca, and R. Ribeiro, "External modulator linearization techniques for high performance radio over fiber transmission systems," Transparent optical networks, Azores, Portugal, 28 June-2 July 2009.

53. N. Yang, C. Caloz, and K. Wu, "Broadband compact 180° hybrid derived from the Wilkinson divider", IEEE Trans, Microw. Theory Tech. **58**, 1030-1037 (2010).

54. A. Moscoso-Martir, J.G. Wanguemert-Perez, I. Molina-Fernandez, E. Marquez-Segura, "Slot-coupled multisection quadrature hybrid for UWB applications", IEEE Microw. and Wireless Comp. Lett. **19**, 143-145, (2009).

55. Aeroflex Weinschel, "1534 broadband resistive power splitter", http://www.aeroflex.com/ams/weinschel/pdfiles/wmod1534.pdf

CHAPTER 4 A Wideband Microwave Photonic Mixer With Enhanced Conversion Gain And High Spurious Free Dynamic Range

4.1 Introduction

The requirements for high SFDR and high conversion efficiency are vital in applications such as antenna remoting for phased array beamforming and radar systems. This chapter presnts a wideband linearised photonic mixer that can simultaneously achieve good SFDR performance and enhanced conversion efficiency while also enabling broadband signal operation. The structure is based on a combination of two functions i.e. the linearisation process which is done in a single drive DPMZM to obtain high SFDR performance, and the carrier suppression function, which is achieved by exploiting the loss spectrum generated from the physical process of stimulated Brillouin scattering (SBS) in optical fibre, to consequently allow enhanced conversion efficiency. The use of a signle drive DPMZM unit enables broadband operation by eliminating the need for a hybrid coupler, hence overcoming the limitations associated with the linearised DPMZM based photonic mixer presented in the previous chapter.

This chapter is organised as follows. Section 4.2 will introduce the fundamental concepts that are relevant to the development of the new proposed structure i.e. the SBS carrier suppressed based linearised photonic mixer. Section 4.3 will present a brief literature review on the previous work done to improve the conversion efficiency by carrier suppression, either through SBS or other means. Section 4.4 will presnet a new wideband linearised photonic mixer based on SBS carrier suppression, together with detailed mathematical analysis, simulations and experimental results. Finally, a conclusion is made in section 4.5.

4.2 Fundamental concepts for the SBS carrier suppressed based linearised photonic mixer

There are two fundamental principles that need to be introduced in order to understand the basic mechanism behind the SBS carrier suppressed based linearised photonic mixer.

The first concept is the use of carrier suppression techniques to improve the conversion efficiency, and the second concept is the use of SBS, in particular, to perform the carrier suppression function. These two concepts are presented in section 4.2.1 and 4.2.2 respectively.

4.2.1 Enhanced conversion efficiency based on carrier suppression

It was shown in chapter 2 that an effective way to enhance the conversion efficiency in a photonic mixer is to increase the optical power incident on the photodetector. However, due to the limited optical power handling capability of a photodetector, further increasing the average optical power will result in saturating the photodetector, and hence the conversion efficiency cannot be further maximised. The average optical power in a conventional microwave photonic mixer consists of the optical carrier power, the RF sidebands, the LO sidebands and higher order sidebands e.g. harmonics, and IMDs. The higher order sidebands do not contribute much in the average optical power, and their effect can be negligible. On the other hand, the optical carrier has the dominant impact on the average optical power. As shown in Fig 4.1 (a), the downconversion process is obtained by the beating of the RF sidebands with the LO sidebands, which after photodetection, will generate the desired IF signal. The optical carrier contains no information, and does not contribute to the downconversion process, while consuming most of the total average optical power. Assuming the photodetector can handle 10 dBm optical power, only a small portion will be dedicated to the RF and LO sidebands, hence the conversion efficiency will be limited. However, if the optical carrier is eliminated from the system, as shown in Fig 4.1(b), the average power is decreased, but more space for improvement will be available for the LO, and RF sidebands. Using an EDFA, or a higher laser power, the RF and LO amplitudes can be further amplified until the average power reaches the photodetector limit i.e. 10 dBm. In this case, the RF and LO sidebands are the dominant contributions to the average power, hence, the IF amplitude will be further maximised and consequently the conversion efficiency will be enhanced.

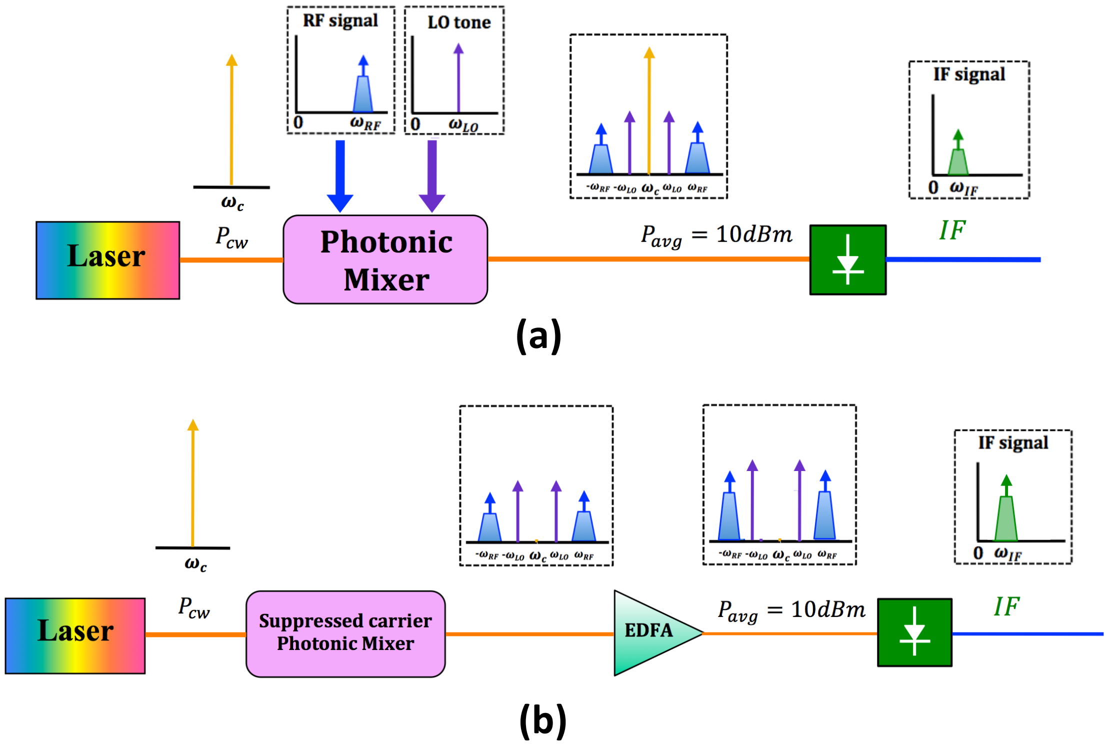

Fig.ure 4.1: Illustration of the enhanced conversion efficiency based on carrier suppression technique. (a) Photonic mixer link with carrier (b) suppressed carrier photonic mixer link

This approach of improving the conversion efficiency through carrier suppression has been already investigated in [1-7], However, the methods, in which the optical carrier is suppressed, are different. In the next section we will briefly introduce the concept of stimulated Brillouin scattering, and show how it is possible to suppress the carrier using the loss spectrum generated from the SBS process.

4.2.2 Carrier suppression using stimulated Brillouin scattering

Stimulated Brillouin scattering (SBS) in optical fibre arises from the interaction between an acoustic wave, a Stokes wave, and a pump wave. The Stokes wave and the pump wave counter-propagate in the optical fibre resulting in a moving interference effect that induces an acoustic wave through the electrostriction effect [8-9]. The refractive index of the fibre associated with the acoustic wave exhibits a periodic perturbation, which creates a travelling Bragg grating to photons. As a result, there is a transfer of power between the pump to the Stokes wave, which simultaneously strengthens the acoustic wave. The result of this interaction is the generation of a narrow-band gain and loss spectrum in the Stokes wave at the difference and sum of the pump frequency and the Brillouin frequency. In a single mode fibre, the Brillouin frequency is given by

$$\Omega_B = \frac{2nv_A}{\lambda_p} \tag{4.1}$$

where n is the fibre refractive index, v_A is the speed of sound, and λ_p is the pump wavelength [8]. Typical values of a Brillouin frequency shift in single mode silica optical fibre at 1550 nm range approximately between 9-12 GHz. The non-linear process of SBS, and the use of the SBS gain and loss spectrum have significant implications in the field of optical fibre technology and particularly in photonic signal processing. For example, the use of Brillouin gain is attractive to implement optical amplifiers due to its ability to offer high levels of gain for relatively low pump powers [10-11]. However, the narrow-band gain spectrum restricts the bandwidth of the signals to be amplified. Remarkably enough, this limitation is turned into advantage as far as photonic signal processing is concerned. In many applications for photonic signal processing, it is desirable to modify only a selected part of the spectrum of a signal without affecting the rest of the spectrum. Thus SBS process allows performing useful functions, such as implementing a frequency shifter [12], a widely tunable filter [13], and a phase shifter [14]. Of particular interest here is the use of SBS nonlinear effect to perform carrier suppression. Assume that the Stokes and the pump are travelling in opposite directions, and that the polarization direction of the pump and the Stokes are maintained the same e.g. by using a polarization maintaining fibre. Due to the SBS process, the pump wave will generate a Brillouin gain spectrum at the Stokes wave centered at a frequency downshifted by the Brillouin frequency shift in the fibre, and will also generate the Brillouin loss spectrum centered at a frequency upshifted by the Brillouin shift. Thus if the pump wave is designed to be at a frequency downshifted by the Brillouin frequency, the Brillouin loss spectrum will be present at the carrier frequency which will then minimize the carrier power. This process is illustrated in Fig. 4.2.

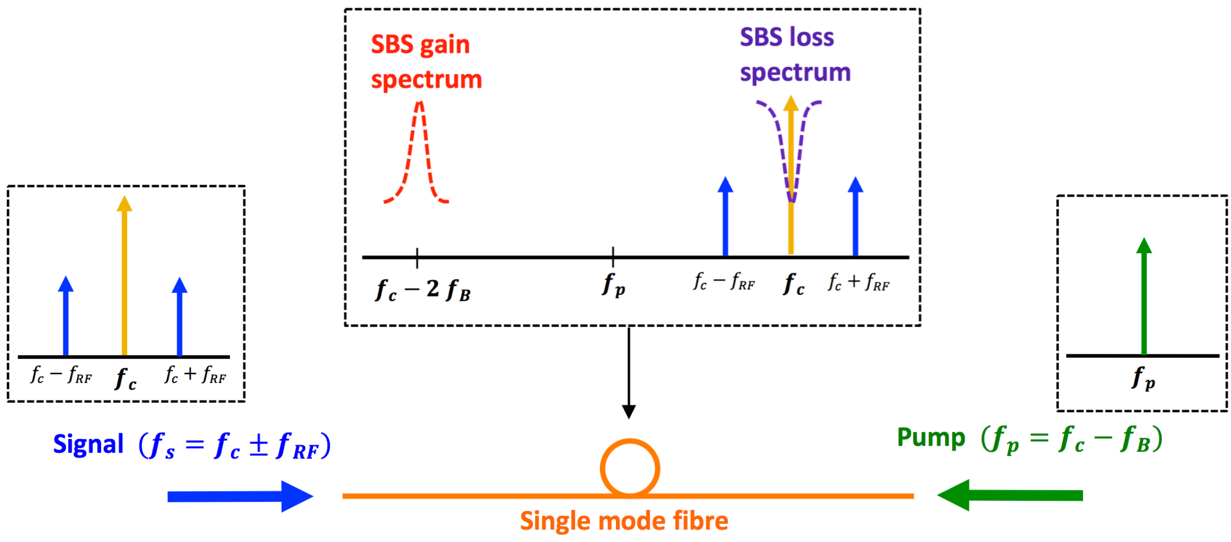

Fig. 4.2 Illustration of the process of carrier suppression based on stimulated Brillouin scattering

The narrowband characteristics of the SBS gain and loss spectrum are highly useful in this particular example, because the optical carrier needs to be suppressed without affecting any other spectral components such as the RF signals. It should be noted that the amount of carrier suppression depends on both the length of single mode fibre as well as in the intensity of the pump wave. In other words, the SBS gain and loss spectra increase by increasing either the length of the single mode fibre or the pump power, and the opposite is true. It has been also demonstrated in [9] that the gain and loss spectra have a Lorentzian profile for low pump powers, however, as the pump power is increased the loss and gain spectra become broader. For carrier suppression at high pump power, the loss spectrum will minimize the carrier but will also introduce SBS noise. The SBS noise will then have significant impact on other spectral components, however, it can be substantially reduced as will be evident later on. The use of SBS for carrier suppression has been investigated previously in [15-16].

4.3 Previous work on carrier suppressed link for enhanced conversion efficiency

There have been several works on suppressed carrier photonic mixer that aim to improve the mixer performance particularly the conversion efficiency. One of these approaches is the use of dual-series phase modulators based photonic mixer with fibre Bragg grating (FBG) at the end of the link, which acts as a notch filter to suppress the optical carrier [1]. In this technique, the FBG used had a bandwidth of 14 GHz, which stipulates that the RF signal and the LO must be spaced away from the carrier by at least 7 GHz in order to avoid any attenuation. This sets a lower boundary limit on the transmission bandwidth. Also the center wavelength of the FBG notch filter must be fixed and must be insensitive to environmental changes in order to realize large suppression level of the optical carrier, and avoid any contact with the signal. Furthermore, the rejection level of the FBG used in this technique was 22.5 dB, which means that the amount of carrier suppression in is limited. For this technique to be efficient, the optical filter must have a very narrow bandwidth with a very sharp roll off and high stopband rejection level at the carrier wavelength, which also must be stable. Such filter requirements are impractical.

Another technique was based on the use of single drive DPMZM connected in series with a MZM [2]. The MZM was driven by the LO, and was biased at the minimum transmission point to suppress the carrier. However, this has the disadvantage of generating second order LO harmonics that, after beating with the RF, will generate second order intermodulation, and second order IF at the output of the photodetector. As a result the bandwidth of the signal will be limited to suboctave so as to prevent any interference between the desired IF signal and the second order distortion products. Additionally, the LO modulation depth need to be 4 times greater than the LO modulation index of the quadrature biased modulator so as to achieve the same conversion efficiency performance. This is an additional electrical power penalty. Furthermore, the bias drift issue associated with commercially available MZM will cause instability in the carrier suppression process, and thus the carrier may gradually appear at the output of the photodetector after some time.

Another photonic mixer technique that exploits the advantage of carrier suppression to improve the conversion efficiency is the use of an integrated DPMZM in which the RF signal is applied to one port of the DPMZM, and the LO is applied to the other port [3]. This approach builds on the technique in [17] that uses dual parallel MZM with manual phase adjustment; however, the integrated DPMZM approach overcomes the coherent interference problem in [17], and provides a robust operation due to the built in phase shifter in the DPMZM. The optical carrier power is suppressed through two different DPMZM bias conditions. The first DPMZM bias condition is to bias the top and bottom MZM (inside the DPMZM) at the minimum point, which inherently suppresses the optical carrier at the output of the DPMZM without the need to control the phase shifter. The second bias condition is to bias the top and bottom MZMs at the quadrature point and to adjust the bias voltage of the phase shifter so that the optical carriers at the two arms of the DPMZM are out of phase. Both bias conditions were found to yield the same conversion efficiency performance. For the same average optical power into photodetector, the suppressed carrier DPMZM photonic mixer approach provides 23.7 dB improvement in the conversion efficiency when compared to the conventional dual-series MZM based photonic mixer. Although the idea achieves an improved conversion efficiency performance, however, it has the limitation that the downconversion operation is performed in a single unit, which did not permit the modulators driven by the RF signal and the LO to be located in different locations where one is at the remote location and the other is at the base station, as is required in applications such as electronic warfare receivers, and other antenna remoting systems [18].

A different idea of improving the conversion efficiency in a carrier suppressed microwave photonic mixer is the use of two travelling wave electrooptic phase modulators (PMs) inside Sagnac loop interferometer [4] as shown in Fig. 4.3. The optical carrier suppression process is inherent from the Sagnac loop structure. A laser light is launched into the Sagnac loop input. The Sagnac loop is constructed using a 50:50 optical coupler. The loop consists of two PMs with their electrodes connected in opposite directions. One of the PM's is driven by the LO while the other is driven by the RF signal. The laser light is split equally at input of the Sagnac loop and half of the light travels in the clockwise (CkW) direction, and the other half travels in the counter clockwise direction (CCkW).

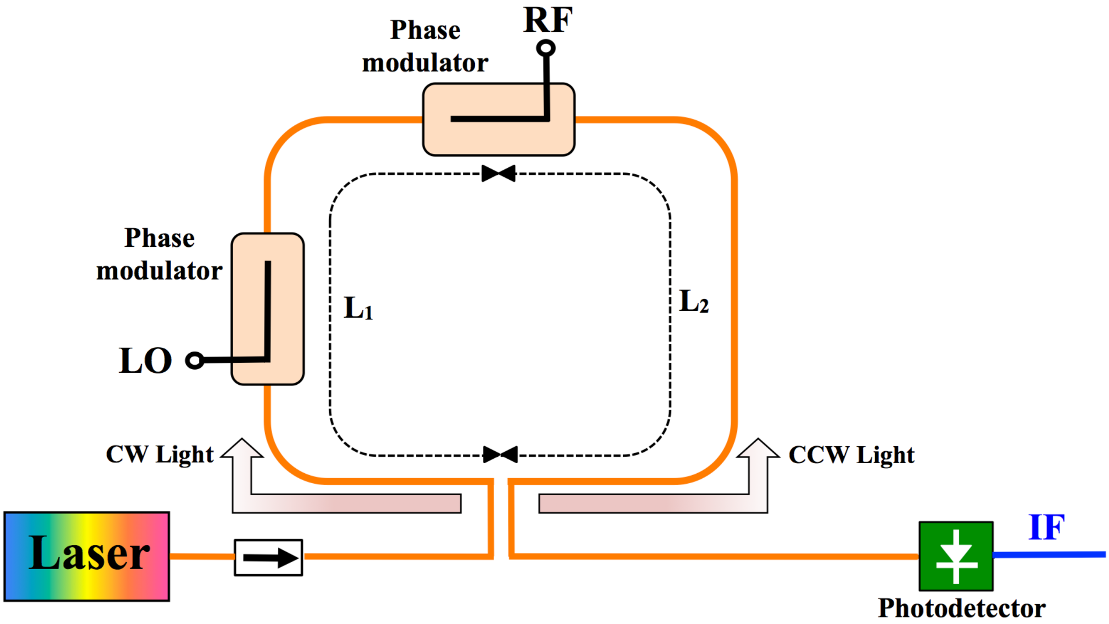

Figure 4.3: Structure of the sagnac loop phase modulation based photonic mixer

The CkW light is fully modulated by the LO, and partially modulated by the RF due to the velocity mismatch effect, while the CCkW light is fully modulated by the RF, while partially modulated by the LO. Because the light coupled from one waveguide to another waveguide in an optical coupler exhibits 90° phase shift, therefore the CkW light and the CCkW light will be 180° out of phase at the output of Sagnac loop. Since the two lights are produced from a common laser source, the majority of the optical carrier is suppressed, while the rest is reflected back to the laser source and is absorbed by the use of an isolator at the input. The RF and LO sidebands of the two phase modulated signals will be also out of phase at the output of the Sagnac loop. By using a high laser power, or an EDFA, the RF and LO amplitude can be further maximised, thus, improving the IF amplitude after the RF beat with the LO at the photodetector. Consequently the conversion efficiency is also improved. Experimental results demonstrated over 26dB improvement in the conversion efficiency when compared to the conventional dual series MZM based microwave photonic mixer. All the components used in the design of the Sagnac loop structure, including the two PMs, the optical coupler, and the optical fibre must be polarization maintaining in order to obtain a robust operation.

One of the unique photonic mixer approaches that has been introduced in [5] exploits the SBS loss spectrum to suppress the optical carrier and consequently improve the conversion efficiency. The topology is similar to [1] except that the FBG notch filter is replaced by the SBS filter which can provide a substantially narrower bandwidth and higher carrier rejection level. The structure is shown in Fig. 4.4.

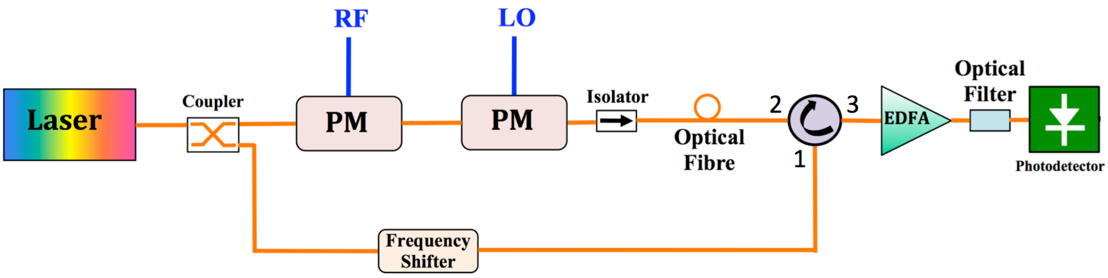

Figure 4.4 Structure of the dual-series phase modulators based on SBS carrier suppression technique

The laser light is split into two paths. The light travelling the upper path passes through two PMs in which one is modulated by the RF and the other is modulated by the LO. The output signal of the two PMs (the Stokes wave) consists of the antiphase RF sidebands and the antiphase LO sidebands. Notice that if the carrier is not suppressed, then there will be no output after photodetection. The light travelling in the lower path passes through a frequency shifter, which downshifts the carrier frequency by the Brillouin frequency. The downshifted light (the pump) is then injected into the other end of the optical fibre via an optical circulator. The pump at the output of the first port of the circulator travels in the opposite direction to the Stokes wave in the single mode fibre. The SBS process takes place and the Brillouin loss spectrum will be introduced in the Stokes wave at the optical carrier frequency, and hence this minimizes the carrier of the phase-modulated signal. At the second output of the circulator, a carrier suppressed phase modulated signal is produced which then is amplified by an EDFA so that the RF and LO sidebands are maximised till the average optical power reaches the power handling capability of the photodetector. The optical filter after the EDFA is used to filter out the amplified spontaneous emission (ASE) noise. The amplified carrier suppressed phase modulated signal beats at the photodetector and high IF output is generated after photodetection. As a result, high conversion efficiency is obtained. Experimental results demonstrated over 26 dB improvement in the conversion efficiency when compared to the conventional dual series MZM based microwave photonic mixer. The drawback of this structure is that it generates second order spurious distortion i.e. second order harmonic distortions and second order intermodulation distortions. Consequently the bandwidth of the signal will be limited to suboctave operation.

4.3.1 Summary and Discussion

The previously reported suppressed carrier photonic mixers that have high conversion efficiency have been limited in their performance as summarized below:

- The mixer technique in [1] is limited by the nonidealities of the FBG notch filter, which has a broad bandwidth, and low stopband rejection level. This can limit the lower operating frequency of the mixer, and the amount of carrier suppression.
- The mixer technique in [2] is limited to suboctave signal operation due to the low biased MZM, which will generate second order distortions, and second order IF. Also it requires a very high LO modulation index which 4 times greater than a quadrature biased MZM in order to achieve the same conversion efficiency performance
- The mixer technique in [3] requires the LO and the RF to be applied to a single DPMZM unit which prevents the modulators being driven by the RF signal and the LO that are located in different locations e.g. where one is at the remote location and the other is at the base station, as is required in applications such as electronic warfare receivers, and other antenna remoting systems.
- The mixer technique in [4] does not operate well at lower frequency and can introduce some ripples in the response.
- The mixer technique in [5] also suffers from the generation of second order distortions which will limit the mixer to suboctave operation

- In addition to the aforementioned disadvantages, all the previous mixer structures showed limited SFDR performance, since they only attempted to improve the conversion efficiency.

Thus it is evident that the previous mixer structures suffer from various impairments that can severely limit their usage in real world applications, or the possibility to be realized in future applications. In this regard, and in order to solve the previous issues, we present in the next section an all-new linearised microwave photonic mixer based on SBS carrier suppression, which can effectively overcome all the previous disadvantages, while also offering a high SFDR and a high conversion efficiency simultaneously. Moreover the new structure offers a broadband operation, and enables a multioctave signal bandwidth. Furthermore, the structure has infinite isolation between the LO and RF signal, and enables the LO to be located in different location than the RF signal.

4.4 A Novel Wideband Microwave Photonic Mixer With Enhanced Conversion Gain And High Spurious Free Dynamic Range Based on SBS Carrier Suppression

4.4.1 Introduction

This section presents a novel wideband linearised photonic mixer structure based on SBS carrier suppression. The structure can effectively overcome the fundamental issues in the previous suppressed carrier photonic mixer structures, such as the limited SFDR performance, the restriction to suboctave signal bandwidth, the ineffective carrier suppression, and the poor isolation between the LO and RF ports. The new structure can provide enhanced conversion efficiency through carrier suppression technique and can also suppress the IMD3 to consequently achieve good SFDR performance, while simultaneously enabling multioctave operation, and essentially infinite isolation between the RF and LO ports. It is based on a SBS suppressed-carrier double sideband LO MZM in series with an integrated single drive DPMZM to which an optimised bias condition is applied. The use of a single drive DPMZM enables broadband signal operation by eliminating the need of an electrical hybrid coupler. Simulation results show an SFDR of 120.4 dB·Hz$^{4/5}$, and a conversion gain of 8.45 dB, corresponding to 15 dB, and 8.8 dB improvements respectively when compared to the conventional dual series MZM based photonic mixer. The SFDR result was obtained at 10 dBm laser power, and the conversion efficiency result was obtained at 20 dBm laser power. Experimental results demonstrate a measured SFDR performance of 120.8 dB·Hz$^{4/5}$, and a conversion efficiency of -13.4 dB, which corresponds to 16 dB, and 1.6 dB improvement respectively when compared to the conventional photonic mixer structure. The experimental results were obtained at laser power of 9.5 dBm, and an average optical power of 5.6 dBm incident on the photodetector.

This chapter is organized as follows. Section 4.4.2 provides the principle of operation of the SBS carrier suppressed based linearised photonic mixer. Section 4.4.3 presents the mathematical analysis and the Matlab simulation results. Section 4.4.4 presents the VPI simulation results. Section 4.4.5 presents the experimental results, and finally a conclusion is made in section 4.4.6.

4.4.2 Principle of operation

Fig 4.5 shows the structure of the SBS carrier-suppressed based linearised photonic mixer.

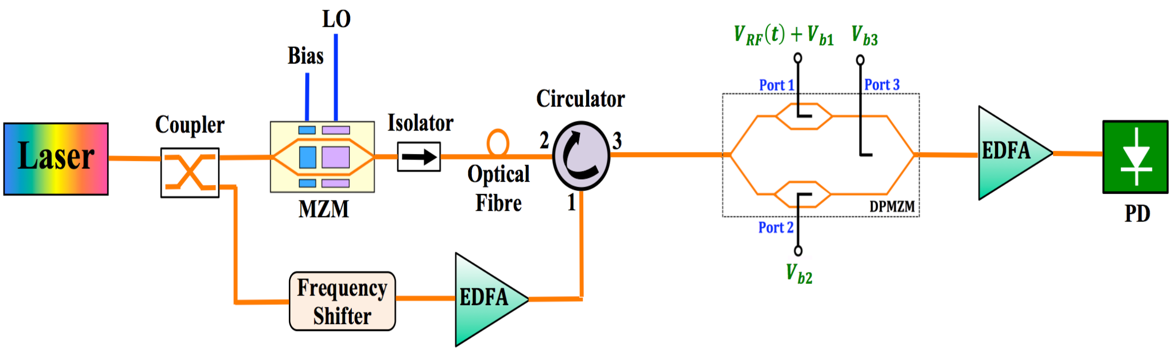

Figure 4.5 Structure of the SBS carrier suppressed based linearised photonic mixer

It consists of two subsystems, which are separated by the optical circulator. The first subsystem, after the laser, provides carrier suppression through the SBS process. The output of the first subsystem is a double sideband suppressed carrier (DSB-SC) LO modulated signal. The second subsystem, after the circulator, provides the linearisation process, which is achieved using a single-drive DPMZM [2]. We shall consider each subsystem as a photonic signal processor with the first acting as a carrier suppression processor on the optical carrier, and the second as a linearizer with an RF input. The multiplication of these two processors results in a photonic mixer processor that can provide high mixer performance. The laser light is split into two paths with a 50:50 optical coupling ratio. The light travelling in the upper path passes through a MZM which is driven by the LO, and which is biased at the quadrature point, which results in the generation of an optical carrier, and two LO sidebands. Note that no even order distortions are generated from the quadrature biased MZM. The output of the MZM is a DSB+C LO modulated signal which is referred to as the Stokes wave, and it passes through an isolator in the forward direction into the single mode fibre. On the other hand, the light travelling in the lower path passes through a frequency shifter, which downshifts the carrier frequency by the Brillouin frequency of the optical fibre. The downshifted light (the pump) is then amplified by an EDFA, and is then injected into the other end of the optical fibre through an optical circulator. The pump coming from port 2 of the circulator travels in the opposite direction to the Stokes wave in the single mode fibre. The SBS process occurs and the Brillouin loss spectrum is introduced in the Stokes wave at the optical carrier frequency. The interaction between the Brillouin loss spectrum and the optical carrier results in reduction of the carrier power. The amount of carrier suppression depends on the EDFA gain used to amplify the pump, and the length of the single mode fibre, which is inserted between the isolator and the circulator. The signal at the output of port 3 of the circulator is a DSB-SC LO modulated signal which is fed to the single drive integrated DPMZM. The DSB-SC signal splits equally in the DPMZM, and is modulated in the top MZM by the RF signal, while it remains unmodulated in the lower MZM. The third order IMD in the optical field is only generated by the top MZM, whose value depends on the input RF modulation depth as well as the bias condtion of the top MZM. The DSB-SC travelling in the lower arm of the DPMZM only exhibits variations in its amplitude and phase which are controlled by the bias voltage of bottom

MZM, and the bias voltage of the phase shifter respectively. The modulated signal in the upper arm and the unmodulated LO in the lower arm are then coherently combined to form the output electric field, which consists of the RF, the LO and higher order distortion products. The DPMZM output modulated optical signal needs to be amplified by an EDFA so that the RF and LO sidebands are maximised until the average optical power incident on the photodetector reaches the power handling capability of the photodetector. The amplified carrier suppressed modulated signal beats at the photodetector and a high IF output is generated as well as the third order IMD. An important point to make is that, after photodetection, the electrical third order IMD amplitude is the sum of two different IMD origins. The first origin is due to the IMD3 generated by the top MZM in the DPMZM, and the second origin is due to the cross beating between the IMD3 generated by the top MZM, and the unmodulated LO sidebands in the lower arm of the DPMZM. Through an optimised DPMZM bias condition, the first origin IMD3 can be made to have the equal amplitude and opposite sign to the second origin IMD3. Thus the total IMD3 component is substantially reduced, and the SFDR performance of the SBS carrier-suppressed based linearised photonic mixer is improved. The key points in the principle of operation of the SBS carrier suppression based linearised photonic mixer are summarised below.

- The linearisation process is achieved by only optimising the DPMZM bias conditions so as to make the two IMD3 origins to have opposite phase and equal magnitude [2]. Hence significantly reducing the total IMD3 component in the electrical domain. This will greatly enhance the SFDR performance.
- The carrier suppression process is achieved by utilising the Brillouin loss spectrum generated from the SBS process. For a fixed average optical power into photodetctor, this technique i.e. carrier suppression enables the amplitudes of the LO and the RF signal to be maximised. As a result, the output IF is increased and consequently the conversion efficiency is enhanced.
- Biasing the MZM driven by the LO at quadrature enables the realisation of multioctave signal operation due to the elimination of the second order distortion products.

- Applying the LO and the RF signal into separate units enables the RF to be located at the remote location, and the LO to be located at the base station, which is essential requirement in electronic warfare receivers, and other antenna remoting systems.
- The use of single drive DPMZM enables broadband signal operation by eliminating the need of an electrical hybrid coupler (which was required in the previous structure) which has critical frequency dependent amplitude and phase charactersitics.

4.4.3 Mathematical Analysis and Matlab Simulation Results

This section presents the mathematical analysis and the Matlab simulation results of the SBS carrier suppressed based linearised photonic mixer structure. We shall consider the use of a single drive DPMZM in which the two MZMs are operated in push-pull configuration. Also we consider the optical coupler to be in a 90:10 ratio. Referring to Fig. 4.5, the input optical field into the DPMZM is given by

$$E_{in,MZM} = \sqrt{0.9}\, E_{in} \tag{4.2}$$

The optical field at the output of the MZM, and after carrier suppression is given by

$$E_{out,MZM} = \sqrt{t_{ff1}} E_{in,MZM} \begin{bmatrix} \cos\left(\frac{\pi V_b}{2V_\pi}\right) \cdot J_0(m_{LO}) \cdot (1-\gamma) + 2\cos\left(\frac{\pi V_b}{2V_\pi}\right) \cdot \sum_{k=1}^{\infty} (-1)^k J_{2k}(m_{LO}) \cos(2k\omega_{LO}t) \\ -2\sin\left(\frac{\pi V_b}{2V_\pi}\right) \cdot \sum_{k=0}^{\infty} (-1)^k J_{2k+1}(m_{LO}) \cos\big((2k+1)\omega_{LO}t\big) \end{bmatrix} \tag{4.3}$$

where t_{ff1} is the insertion loss of the MZM, V_b is the MZM bias voltage, V_π is the MZM switching voltage, $J_m(x)$ is the Bessel function of m-th order of the first kind, and γ is the carrier suppression ratio and is between 0 and 1 where 0 indicates no carrier suppression and 1 indicates full carrier suppression. When the MZM is biased at quadrature, equation (4.3) becomes

$$E_{out,MZM} = \frac{\sqrt{2\, t_{ff1}} E_{in,MZM}}{2} \Bigg[J_0(m_{LO}) \cdot (1-\gamma) + 2\sum_{k=1}^{\infty} (-1)^k J_{2k}(m_{LO}) \cos(2k\omega_{LO}t) - 2\sum_{k=0}^{\infty} (-1)^k J_{2k+1}(m_{LO}) \cos\big((2k+1)\omega_{LO}t\big) \Bigg] \tag{4.4}$$

For simplicity of the analysis, we shall consider equation (4.4) as a function of optical power rather than optical field, and expand the Bessel function to only obtain the DC terms and the first order LO sideband terms. The output MZM optical power is given by

$$P_{out,MZM} = E_{out,MZM} \cdot \overline{E_{out,MZM}}$$

$$= \frac{t_{ff1}\, P_{in,MZM}}{2}\big[1 + (\gamma^2 - 2\gamma) \cdot {J_0}^2(m_{LO})$$

$$+ \{4\,\gamma\;J_0(m_{LO})\,J_1(m_{LO}) - 2J_1(2m_{LO})\}\cos\,(\omega_{LO}t)\big] \tag{4.5}$$

where $\overline{E_{out,MZM}}$ is the complex conjugate of the optical field at the output of the MZM. Equation (4.5) shows that the MZM output optical power is dominated by either the LO sidebands, or the carrier power. When $\gamma = 1$, the output MZM optical power will be dominated by the LO sidebands, and when $\gamma = 0$, the output MZM optical power is mainly dominated by the carrier power. Also the analysis shows that equation (4.5) is free from second order distortions products. From (4.5), we can obtain that the output MZM average optical power is given by

$$P_{out,MZM,avg} = \frac{t_{ff1}\, P_{in,MZM}}{2}\big[1 + (\gamma^2 - 2\,\gamma) \cdot {J_0}^2(m_{LO})\big] \tag{4.6}$$

Also we can obtain from (4.5) the output optical power due to the first order sidebands

$$P_{out,MZM,LO} = \frac{t_{ff1}\, P_{in,MZM}}{2}[4\,\gamma\;J_0(m_{LO})\,J_1(m_{LO}) - 2J_1(2m_{LO})] \tag{4.7}$$

The output MZM optical power $P_{out,MZM}$ passes through a circulator and to the input of the single drive DPMZM. The output DPMZM optical power is given by

$$P_{out,DPMZM} = \frac{t_{ff2} \cdot P_{out,MZM}}{8}\big[2 + cos\big(2m_{RF}(t)\big) + cos(2\varphi_2) + 4\,cos\big(m_{RF}(t)\big)\,cos(\varphi_2)\,cos(\varphi_3)\big] \tag{4.8}$$

where t_{ff2} is the DPMZM insertion loss, $m_{RF}(t) = \; m_{RF}\,cos(\omega_{RF}t) + \varphi_1$ is the input to port 1 of the DPMZM as shown in Fig. 4.5, $m_{RF} = \pi(V_{RF}/V_{\pi,n})$ is the RF modulation index, V_{RF} is the input RF signal amplitude, $V_{\pi,n}$ is the half wave voltage of the n-th MZM, $\varphi_n = \pi(V_{bn}/V_{\pi,n})$ is the phase difference between the two arms of the n-th MZM, V_{bn} is the DC bias voltage into Port n of the DPMZM, and ω_{RF} is the angular frequency of the RF signal. Investigating equation (4.8) for the first order RF sidebands, and replacing $P_{out,MZM}$ by $P_{out,MZM,LO}$, the output IF optical power after the DPMZM, and the EDFA can be obtained and is given by

$$P_{out,IF} = G_{EDFA} \frac{t_{ff2} \cdot P_{out,MZM,LO}}{8} [2\, a\, J_1(2m_{RF}) + 2b\, J_1(m_{RF})]$$

$$= G_{EDFA} \frac{t_{ff1}\, t_{ff2} \cdot P_{in,MZM}}{8} [\, a\, J_1(2m_{RF}) + b\, J_1(m_{RF})] \times [4\, \gamma\;\, J_0(m_{LO})\, J_1(m_{LO}) - 2J_1(2m_{LO})] \quad (4.9)$$

where $a = sin(2\varphi_1)$ and $b = 4 \sin(\varphi_1) \cos(\varphi_2) \cos(\varphi_3)$ are coefficients related to the bias condition of the DPMZM, and G_{EDFA} refers to the EDFA at the end of the mixer link as illustrated in Fig. 4.5. For a small RF signal analysis, (4.9) can be further simplified to

$$P_{out,IF} = G_{EDFA} \frac{t_{ff1}\, t_{ff2} \cdot (P_{in,MZM}) . m_{RF}}{16} (2a + b) \times [4\, \gamma\;\, J_0(m_{LO})\, J_1(m_{LO}) - 2J_1(2m_{LO})] \quad (4.10)$$

The output average power into photodetector is given by

$$P_{avg} = G_{EDFA} \, . \, P_{out,MZM,avg} . \frac{t_{ff2} \cdot P_{out,MZM}}{8} [2 + cos(2\varphi_1) + cos(2\varphi_2) + 4\, cos(\varphi_1)\, cos(\varphi_2)\, cos(\varphi_3)]$$

$$= G_{EDFA} \frac{t_{ff1}\, t_{ff2} \cdot P_{in,MZM}}{16} [2 + cos(2\varphi_1) + cos(2\varphi_2) + 4\, cos(\varphi_1)\, cos(\varphi_2)\, cos(\varphi_3)]$$
$$\times \left[1 + (\gamma^2 - 2\,\gamma) \cdot {J_0}^2(m_{LO})\right] \quad (4.11)$$

Now that equation (4.8), (4.10), and (4.11) are derived, we can proceed with the analysis to evaluate the performance of the conversion efficiency and the SFDR.

4.4.3.1 Conversion Efficiency Analysis

An important point to make is that using the carrier suppression technique to obtain high conversion efficiency is only applicable when comparing the same amount of the average optical power into photodetector to other mixer techniques. In other words, it is important to consider the conversion efficiency of the mixer with and without carrier suppression at a fixed average power into photodetector. Therefore the carrier suppression technique may need the use of an EDFA or a higher power laser in order to achieve the same average power into photodetector as when the carrier is present. For this reason we will first determine the requirement of EDFA gain to maintain the same average optical power into photodectectors for the two cases. The average optical power for the case when the carrier is suppressed was derived in equation (4.11). The average optical power for the case when the carrier is present i.e. when $\gamma = 0$ is given by

$$P_{avg+C} = \frac{t_{ff1}\, t_{ff2} \cdot P_{in,MZM}}{16} [2 + cos(2\varphi_1) + cos(2\varphi_2) + 4\, cos(\varphi_1)\, cos(\varphi_2)\, cos(\varphi_3)] \qquad (4.12)$$

Assuming a high laser power that can overcome all the losses in the system, an EDFA is not needed when the carrier is present. Equating the equation (4.11) with equation (4.12) and solving for G_{EDFA}, the required EDFA gain to obtain the same average optical power into photodetector for the two cases is given by

$$G_{EDFA} = \frac{1}{1 + (\gamma^2 - 2\,\gamma) \cdot {J_0}^2(m_{LO})} \qquad (4.13)$$

Clearly it can be seen from (4.13) that for a fixed LO modulation index, the higher the carrier suppression ratio γ, the higher the requirement for the EDFA gain to maintain the same average optical power into photodetector. Also as the LO modulation index increases, the EDFA gain requirement decreases. The EDFA gain G_{EDFA} in dB is plotted as a function of the carrier suppression ratio γ for LO modulation indices of $m_{LO} = 0.2$, 0.4, 0.6, 0.8, 1, 1.4, and 1.8. This is shown in Fig. 4.6.

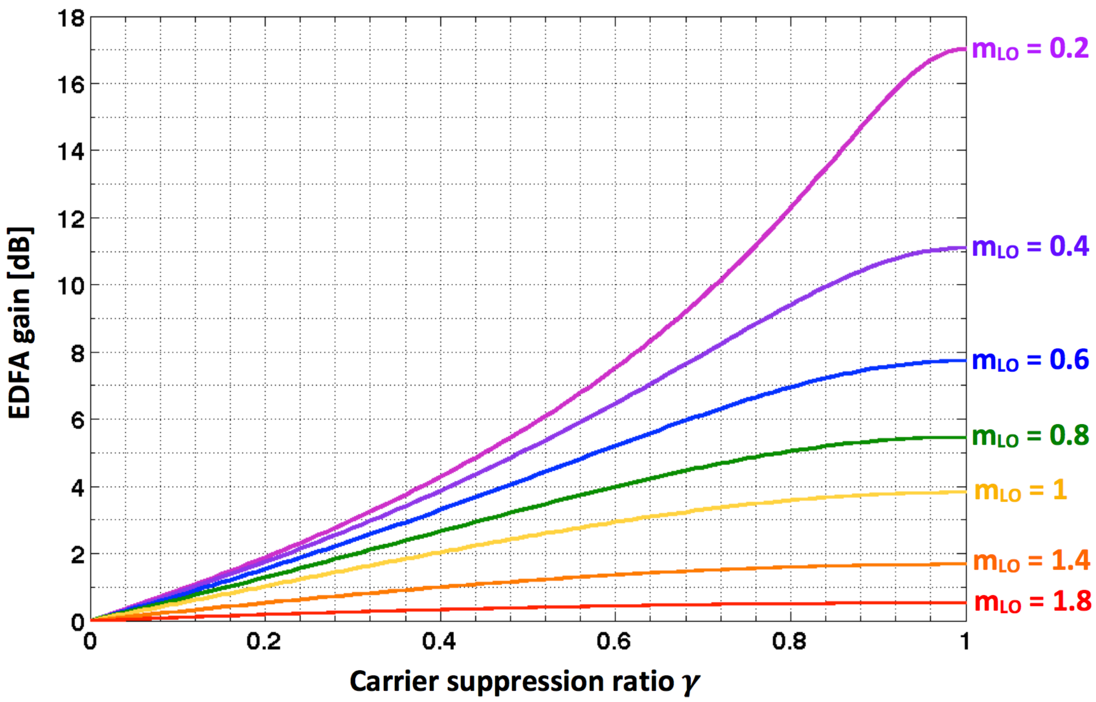

Figure 4.6: Plot of the EDFA gain as a function of the carrier suppression ratio for different LO modulation index

The conversion efficiency of the SBS carrier suppressed based linearised photonic mixer can be obtained from (4.10). The output IF electrical power is given by

$$P_{out,IF} = G_{EDFA}{}^2 \frac{t_{ff1}{}^2 \, t_{ff2}{}^2 \cdot P_{in}{}^2 . m_{RF}{}^2}{32} (2a + b)^2 \times [4\,\gamma\; J_0(m_{LO})\, J_1(m_{LO}) - 2J_1(2m_{LO})]^2 \Re^2 R_L \qquad (4.14)$$

where R_L is the photodiode load resistance and $\Re$ is the photodiode responsivity. Consequently the conversion efficiency is given by

$$G_{conv} = G_{EDFA}{}^2 \frac{t_{ff1}{}^2 \, t_{ff2}{}^2 \cdot P_{in}{}^2 \pi^2}{16\, V_\pi{}^2} (2a + b)^2 \times [4\,\gamma\; J_0(m_{LO})\, J_1(m_{LO}) - 2J_1(2m_{LO})]^2 \Re^2 R_L R_{in} \qquad (4.15)$$

where R_{in} is the modulator input resistance. As a comparison, the conversion efficiency of the same mixer structure but with the carrier present, and without the use of EDFA is given as

$$G_{conv+C} = \frac{t_{ff1}{}^2 \, t_{ff2}{}^2 \cdot P_{in}{}^2 \pi^2}{16\, V_\pi{}^2} (2a + b)^2 \times [2J_1(2m_{LO})]^2 \Re^2 R_L R_{in} \qquad (4.16)$$

The ratio between the conversion efficiency of the suppressed carrier technique to the conversion efficiency when the carrier is present is given by

$$\eta = \frac{G_{conv}}{G_{conv+C}} = G_{EDFA}{}^2 \left[\frac{2\,\gamma\; J_0(m_{LO})\, J_1(m_{LO}) - J_1(2m_{LO})}{J_1(2m_{LO})} \right]^2 \qquad (4.17)$$

Using the assumption that the two optical average power are fixed for both cases, the EDFA gain can be replaced by the term shown in (4.13), and the conversion efficiency ratio becomes

$$\eta = \frac{G_{conv}}{G_{conv+C}} = \left[\frac{2\,\gamma\; J_0(m_{LO})\, J_1(m_{LO}) - J_1(2m_{LO})}{J_1(2m_{LO}) \times \{1 + (\gamma^2 - 2\,\gamma) \cdot J_0{}^2(m_{LO})\}} \right]^2 \qquad (4.18)$$

Clearly, when $\eta = 1$, there is no improvement in the conversion efficiency of the suppressed carrier photonic mixer when compared to the one operating with the carrier. When $\eta < 1$, there is a degradation in the conversion efficiency of the suppressed carrier photonic mixer. Thus it is desirable to make η as high as possible (η >>1) in order to demonstrate high conversion efficiency. There are two parameters that can be controlled to alter η, which are the LO modulation index, and the carrier suppression ratio. The conversion efficiency ratio η has been plotted as a function of the carrier suppression ratio γ, and at different LO modulation depths i.e. m_{LO} = 0.05, 0.1, 0.2, 0.3, 0.4, 0.5, and 0.6. The results are shown in Fig. 4.7.

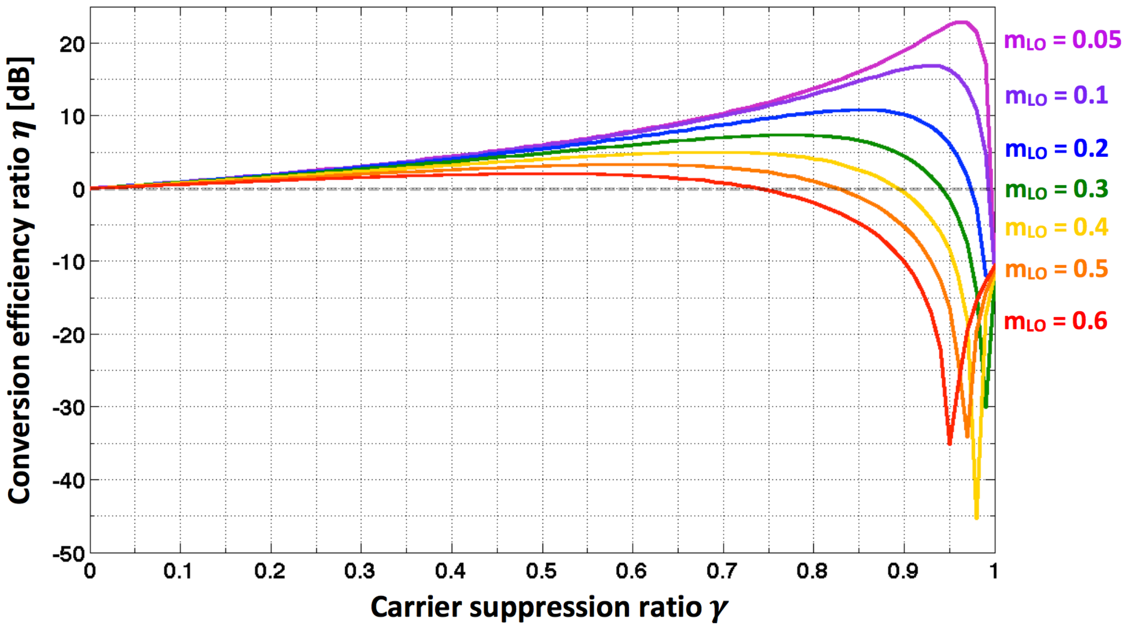

Figure 4.7: Plot of the conversion efficiency ratio as a function of the carrier suppression ratio for different LO modulation index

It can be seen from Fig. 4.7, that an effective way to maximise the conversion efficiency is to use as low LO modulation index as possible, and increase the conversion efficiency ratio so that the carrier power remains below the LO. At high LO modulation index i.e. ($m_{LO} > 0.6$), the carrier suppression technique to improve the conversion efficiency does not hold any longer. This is clearly evident in Fig. 4.7 where at relatively high LO modulation index e.g. $m_{LO} = 0.6$, there is not much improvement in the conversion efficiency ratio. However, at low LO modulation index $m_{LO} < 0.6$, there is a significant improvement in the conversion efficiency ratio. The LO modulation index value that is chosen for the design of the SBS suppressed carrier photonic mixer is $m_{LO} = 0.2$. Note that higher LO modulation index values will yield better conversion efficiency, however, we need to ensure that the LO is well above than the carrier. The conversion efficiency ratio using $m_{LO} = 0.2$ peaks at $\gamma = 0.85$ (corresponds to 8.24 dB carrier suppression). The peak value is $\eta = 10.82$ dB which means that the conversion efficiency of the suppressed carrier photonic mixer is 10.82 dB higher than the conversion efficiency of the photonic mixer operating with the optical carrier. Referring to Fig. 4.6 or equation (4.13), the required EDFA gain (for $m_{LO} = 0.2$, and $\gamma = 0.85$) is 13.77 dB. Now that all the parameters are obtained, the conversion efficiency of the SBS carrier suppressed based photonic mixer can be determined. The DPMZM bias condition are optimised for maximum output IF optical power. Notice from (4.9) that the IF power depends on the coefficient $(2a + b)$ which further depends on the bias condition of the DPMZM. The IF coefficient can be expressed as

$$\Gamma_{IF} = 2\, sin(2\varphi_1) + 4\sin(\varphi_1)\cos(\varphi_2)\cos(\varphi_3) \tag{4.19}$$

The IF coefficient is maximum when $\varphi_1 = \frac{\pi}{4}, \varphi_2 = 0,$ and $\varphi_3 = 0$. This yields a value of $\Gamma_{IF} = 4.83$. In the simulation of the conversion efficiency, both the insertion loss of the MZM and the DPMZM were set to 0.316 corresponding to 5dB loss. The EDFA gain was set to 13.77 dB, the LO modulation index was set to 0.2, the carrier suppression ratio was set to 0.8, the input and load resistance were set to 50 Ω, and the photodiode responsivity was set to 1. The simulation results for the conversion efficiency of the SBS carrier suppressed based photonic mixer are shown in Fig. 4.8. As a reference, the conversion efficiency of the same structure operating with the carrier, and the dual-series MZM based photonic mixer were simulated. All the three structures were operated under the same condition i.e. a fixed average power into photodetector, and all the MZM units operate in push-pull configurations. The SBS carrier suppressed based photonic mixer demonstrated a 10.8 dB and 8.8 dB conversion efficiency improvement compared to the same structure operating with carrier and the dual-series MZM based photonic mixer respectively. At 20 dBm laser power, the average power into photodetector was computed to be 7.2 dBm for all the three structures. The SBS carrier suppressed mixer demonstrated a conversion gain of 8.4 dB, while the same structure with carrier demonstrated a conversion loss of 2.4 dB, and finally the dual-series MZM based photonic mixer showed a conversion loss of 0.4 dB. Further improvement in the SBS carrier suppressed based photonic mixer structure can be obtained by the concurrent design of lower LO modulation index, higher carrier suppression ratio, and higher EDFA gain.

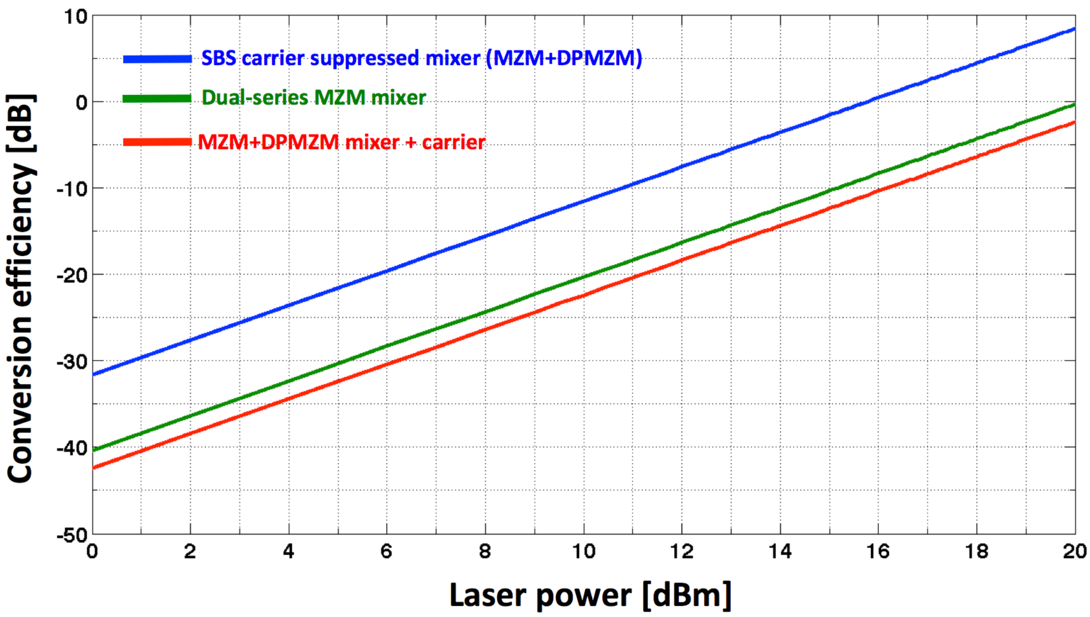

Figure 4.8: Plot of the conversion efficiency performance for the SBS carrier suppressed based photonic mixer with full and no suppression of the carrier, and the dual-series MZM based photonic mixer

We have also investigated the conversion efficiency when the DPMZM is linearised. A detailed discussion on DPMZM linearisation will be presented in the next section. There exist many different bias solutions that successfully linearize the DPMZM transfer function so as to eliminate the third order IMD. However, the design of the optimum DPMZM bias condition for linearisation considers also the minimum penalty in conversion efficiency due to linearisation. An optimum bias solution was found to be $\varphi_1 = 0.42\,\pi$ $\varphi_2 = 0$, and $\varphi_3 = \pi$, which will simultaneously eliminate the third order IMD, and cause only 4.4 dB penalty in the conversion efficiency when compared to the optimised bias condition for maximum conversion efficiency. Thus the conversion efficiency of the SBS carrier suppressed based linearised photonic mixer was computed (at $\varphi_1 = 0.42\,\pi$ $\varphi_2 = 0$, and $\varphi_3 = \pi$) to be 4 dB conversion gain which is still higher than the conversion efficiency of the dual-series MZM based photonic mixer.

4.4.3.2 SFDR and Noise Analysis

In this section, the expressions for the SFDR limited by the cubic nonlinearity, and the SFDR limited by the quintic nonlinearity are obtained. The SFDR performance of the SBS carrier suppressed based linearised photonic mixer is evaluated, and compared with the dual-series based MZM photonic mixer. It should be noted that the SFDR analysis of the single drive DPMZM has been investigated previously in [2], however, the DPMZM bias voltages were only designed to cancel the third order IMD to improve the SFDR performance. There was no attempt to improve the conversion efficiency. The analysis here takes into consideration the optimized conditions for high conversion efficiency i.e. ($m_{LO} = 0.2, \gamma = 0.85$, and $G_{EDFA} = 13.77$ dB). Revisiting equation (4.8) for a two-tone RF signal expressed as $m_{RF}(t) = m_{RF}\, cos(\omega_1 t) + m_{RF}\, cos(\omega_2 t) + \varphi_1$ where ω_1 and ω_2 are the two closely spaced RF angular frequencies, the output electrical signal after photodetection will consist of the two tone IF signals at frequencies $\omega_1 - \omega_{LO}$ and $\omega_2 - \omega_{LO}$ as well as the in-band third order IMD at frequencies $2\omega_1 \pm \omega_2 - \omega_{LO}$. The mixer SFDR performance is limited by the presence of the third order in-band IMD, which is the largest distortion product. Thus it is important to find an expression for the amplitude of the third order IMD to evaluate the SFDR performance. The output third order IMD power in the optical field is given by

$$P_{o,IMD3} = G_{EDFA} \frac{t_{ff1}\, t_{ff2} \cdot P_{in,MZM}}{16} [4\, \gamma\; J_0(m_{LO})\, J_1(m_{LO}) - 2J_1(2m_{LO})] \times \Gamma_3 \tag{4.20}$$

where Γ_3 is the IMD coefficient at the frequencies $2\omega_1 \pm \omega_2 - \omega_{LO}$, and is given by

$$\Gamma_3 = a\, J_2(2m_{RF}) J_1(2m_{RF}) + b\, J_2(m_{RF}) J_1(m_{RF}) \tag{4.21}$$

The first term in equation (4.21) represents the third order IMD in the optical field generated by the top MZM in the DPMZM. This term is called the self-beating IMD of the top MZM. The second term is due to the beating between the IMD3 generated by the top MZM in the optical domain, and the unmodulated LO sidebands in the lower arm of the DPMZM. This term is also called the cross-beating IMD. Expanding (4.21) for only the cubic term, which is the dominant term when a moderate RF signal is considered, the following expression is obtained.

$$\Gamma_3 = \frac{m_{RF}{}^3}{16}(8a+b) - \frac{m_{RF}{}^5}{384}(32a+b) \quad (4.22)$$

Clearly the dominant cubic term can be eliminated when 8a+b = 0. This relationship can be shown in terms of DPMZM bias voltages as

$$8\sin(2\varphi_1) + 4\sin(\varphi_1)\cos(\varphi_2)\cos(\varphi_3) = 0 \quad (4.23)$$

Using the trigonometric relationship $\sin(2\varphi_1) = 2\sin(\varphi_1)\cos(\varphi_1)$, equation (4.23) can be rewritten as

$$4\cos(\varphi_1) + \cos(\varphi_2)\cos(\varphi_3) = 0 \quad (4.24)$$

Clearly there exist many bias solutions that satisfy equation (4.24). Of particular interest is the bias solution $\varphi_1 = 0.42\,\pi$ $\varphi_2 = 0,$ and $\varphi_3 = \pi$, which not only eliminate the cubic nonlinear term, but also reduce the penalty of conversion efficiency to only 4 dB loss when compared to the condition for maximised conversion efficiency. Once the cubic term is cancelled, the residual quintic term in IMD coefficient in equation (4.23) becomes dominant especially at higher RF signal levels. Consequently, the SFDR, limited by the quintic nonlinearity, is given by

$$SFDR = \left(\frac{P_{IF,FOI}}{N_{total}}\right)^{\frac{4}{5}} \quad (4.25)$$

where N_{total} is total noise power at the output of the SBS carrier suppressed based linearised photonic mixer, which includes the laser intensity noise, the photodiode thermal noise, the shot noise, and the signal spontaneous noise. The noise due to SBS is not considered in the analysis. The output IF fifth order intercept power $P_{IF,FOI}$ can be expressed as

$$P_{out,IF} = G_{EDFA}{}^2 \frac{t_{ff1}{}^2\, t_{ff2}{}^2 . P_{in}{}^2 . \kappa_{FOI}}{32}(2a+b)^2 \times [4\,\gamma\ J_0(m_{LO})\, J_1(m_{LO}) - 2J_1(2m_{LO})]^2 \Re^2 R_L \quad (4.26)$$

where κ_{FOI} is the fifth order intercept point and is given by

$$\kappa_{FOI} = \sqrt{192\frac{2a+b}{32a+b}} \quad (4.27)$$

The SFDR limited by the quintic nonlinearity can be improved by increasing the output IF fifth order intercept power. This can be done by either increasing the laser power P_{in}, increasing the fifth order intercept point κ_{FOI}, optimising the LO modulation index m_{LO}, or increasing the IF coeffecient i.e. $(2a+b)^2$. Using the same parameters used for the conversion efficiency simulation, and setting the DPMZM bias condition to be $\varphi_1 = 0.42\,\pi$ $\varphi_2 = 0$, and $\varphi_3 = \pi$, the SFDR is simulated as a function of laser power as shown in Fig. 4.9.

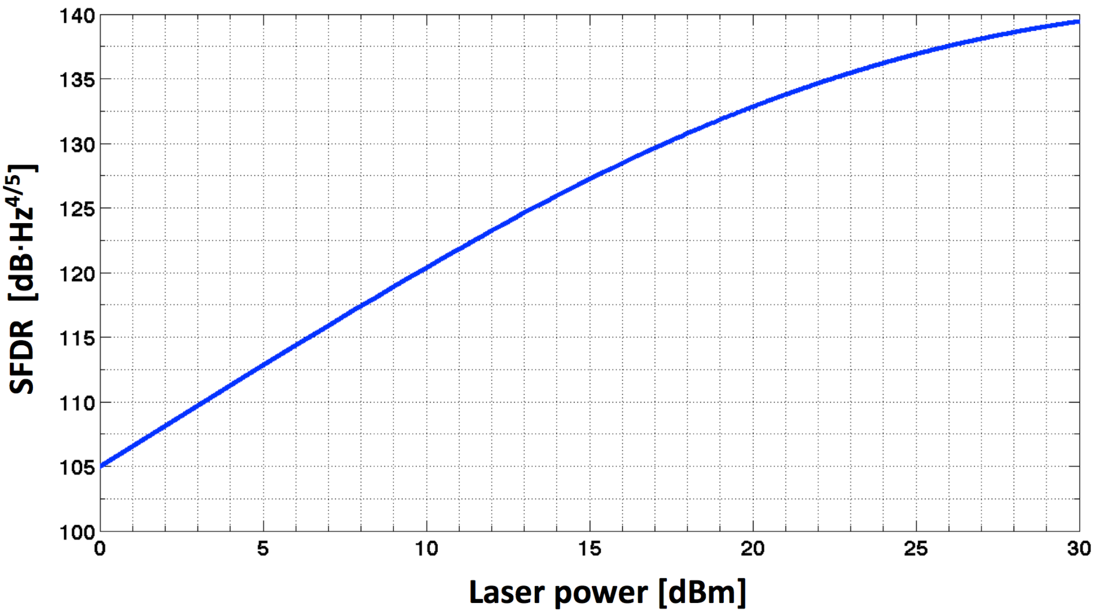

Figure 4.9: Simulation of the SFDR with respect to laser power for the SBS carrier suppressed based linearised photonic mixer

The SFDR increases as the laser power increases. The saturation effect is not apparent before 20 dBm laser power. This is expected, as the carrier suppression method will substantially minimize the RIN noise contribution as well as the shot noise. The SFDR was calculated to be 120.4 dB·Hz$^{4/5}$ at input laser power of 10 dBm, and average optical power into photodetector of -10 dBm. The SFDR is improved to 132.8 dB·Hz$^{4/5}$ at input laser power of 20 dBm, and average optical power of 0 dBm. Fig. 4.10 shows other performance parameters. In Fig. 4.10 (a) the average optical power into photodetector is plotted as a function of the laser power, and can be referred to whenever needed. Fig. 4.10(b) shows the noise floor simulation result. At 10 dBm laser power, the noise floor was calculated to be -167 dBm/Hz, and was dominated by the thermal noise as shown in Fig 4.10 (e). The conversion efficiency result for the linearised case is shown in Fig 4.10(c).

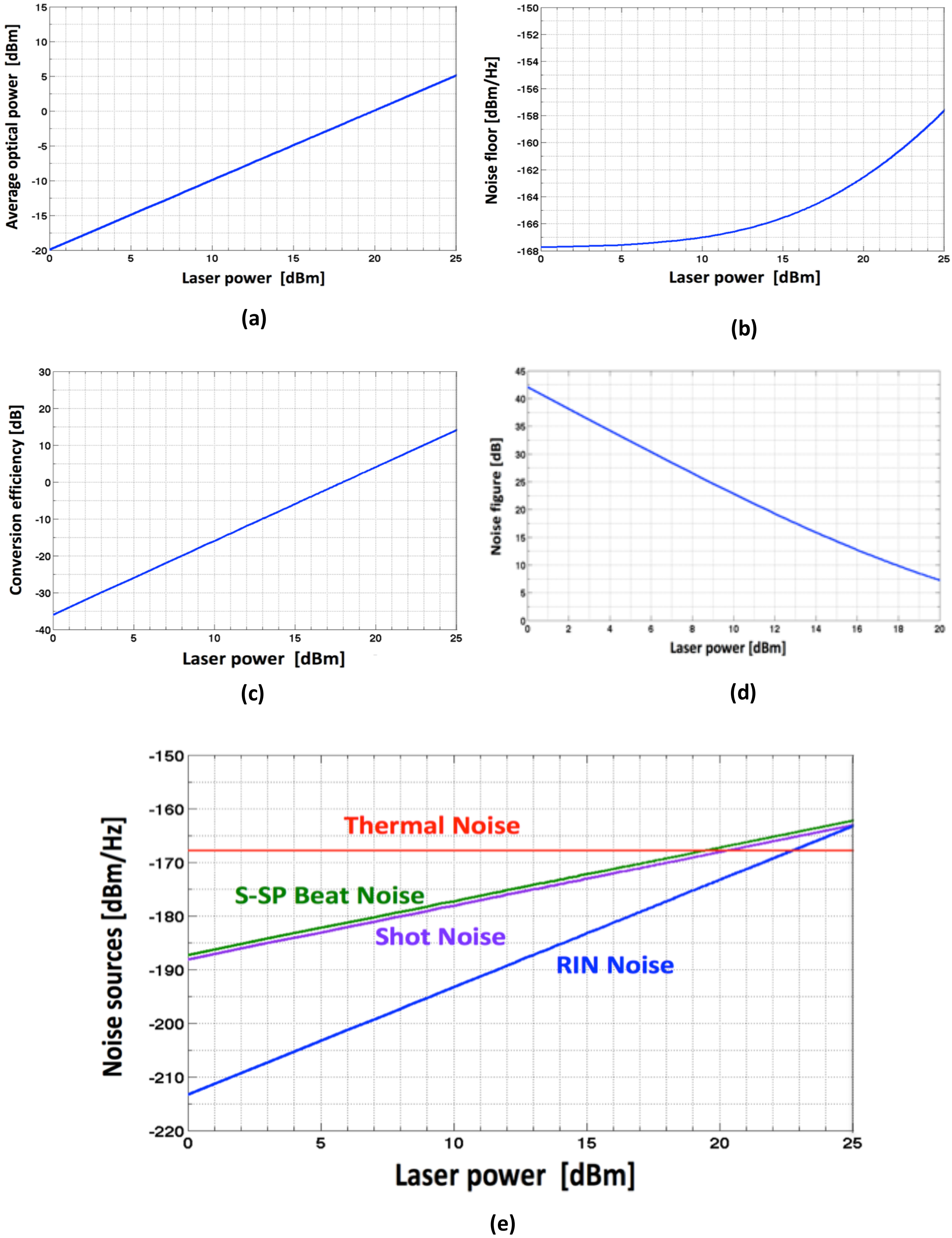

Figure 4.10: plot of (a) the average optical power (b) the noise floor (c) the conversion efficiency (d) the noise figure and (e) the noise source, as a function of laser power

Clearly there is only 4 dB penalty in the conversion efficiency compared to the high conversion efficiency technique. Note that this is not always the case, as other bias solutions can linearize the DPMZM, yet, they degrade the performance of the conversion efficiency significantly. The DPMZM bias voltages were designed in such a way to cancel the third order IMD and simultaneously minimize the conversion efficiency penalty. The conversion efficiency was calculated to be -15 dB at 10 dBm laser power. The noise figure has been also simulated as shown in Fig 4.10(d). The noise figure was calculated to be 22.5 dB at 10 dBm laser power. Finally, the different noise sources in the SBS carrier suppressed based photonic mixer have been simulated in Fig. 4.10(e). The noise includes laser intensity noise, shot noise, thermal noise, and signal spontaneous noise. Theoretically, the laser intensity noise dominates the noise floor at high enough laser power since it is quadratically proportional to the laser power. However, since the carrier power is significantly suppressed, the impact of laser intensity noise will become insignificant. As shown in Fig4.10 (e), the dominant noise before 20 dBm laser power is the thermal noise. As the laser power increases further beyond 20 dBm, the laser intensity noise will come into effect and will dominate the system noise floor.

4.4.4 VPI simulation results of the carrier suppressed based linearised photonic mixer

The objective of VPI simulation is to verify that the idea of the SBS carrier suppression based linearized photonic mixer works successfully and that it achieves good SFDR and conversion efficiency performance. The first task of the VPI simulation is to ensure that the carrier is suppressed using the SBS process and to investigate the optimum EDFA gain that results in clear spectral lines without introducing SBS pedestal noise. The second task is to investigate the optimum LO modulation index that yields high IF when using high RF signal power to measure the SFDR. The third task involves verifying that linearization is achieved by observing that the slope (in dB) of the IMD component is 5:1 in comparison to the IF component. Accordingly the SFDR, and conversion efficiency of the SBS based linearized mixer will be determined.

4.4.4.1 Simulation of carrier suppression based on SBS

The front subsystem of the SBS carrier suppressed based linearised photonic mixer was initially invistigated to test SBS carrier suppression of the LO as shown in Fig. 4.11.

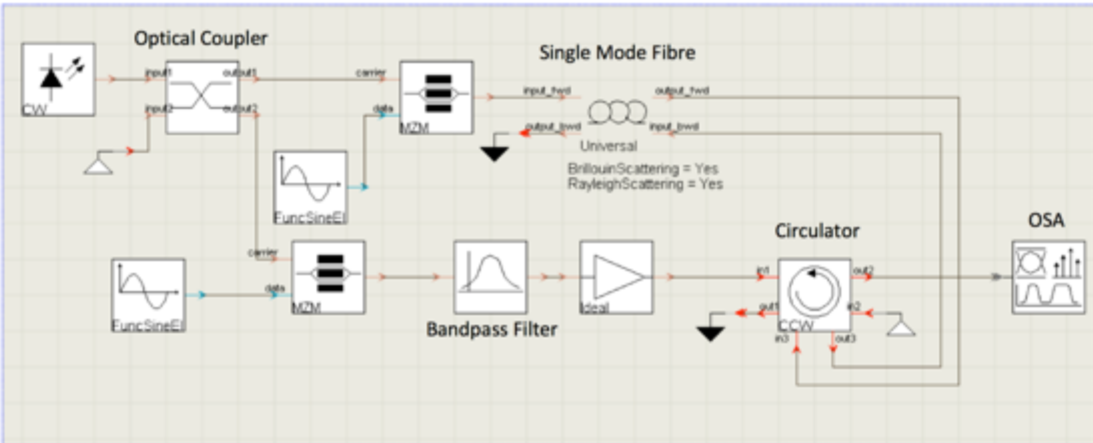

Figure 4.11: VPI simulation setup of carrier suppression based SBS technique

The laser power was set to 10mW, the coupling ratio was set to 50:50, the MZM driven by the LO was biased at quadrature (bias = $\frac{V_{\pi}}{2}$) and was driven by an LO with frequency 15 GHz, the LO modulation index was set to be close to 0.2, the pump frequency was set to 10.5 GHz, the lower MZM was biased at minimum, the bandpass filter was centered at the lower sideband frequency i.e. $f_c - 10.5$ GHz, which corresponds to the carrier being downshifted by the Brillouin frequency. This specific setup (instead of simply using frequency shifter) was used in order to be consistent with the experimental setup. The output of the bandpass filter was a single sideband suppressed carrier signal. The pump gain was varied with three different values i.e. 10dB, 20dB and 30dB. The parameter of the Brillouin scattering was turned on in the universal fiber and the Brillouin frequency was set to 10.5 GHz. Fig. 4.12 (a), (b) and (c) shows the output at the circulator when using pump gain of 30 dB, 20dB and 10dB respectively. It can be seen from Fig. 4.12(a), that when the pump gain is 30dB, very large carrier suppression is obtained. The carrier is suppressed till 35dB below the LO. However the large pump gain caused significant SBS pedestal noise at the base of the LO lines and the carrier. This SBS noise is unwanted and therefore a large suppression of the carrier is not desirable. Fig. 4.12(b) shows the output signal from the circulator when the EDFA pump gain is 20dB. The carrier is still suppressed, however, it is now 18 dB below the LO modulation sidebands.

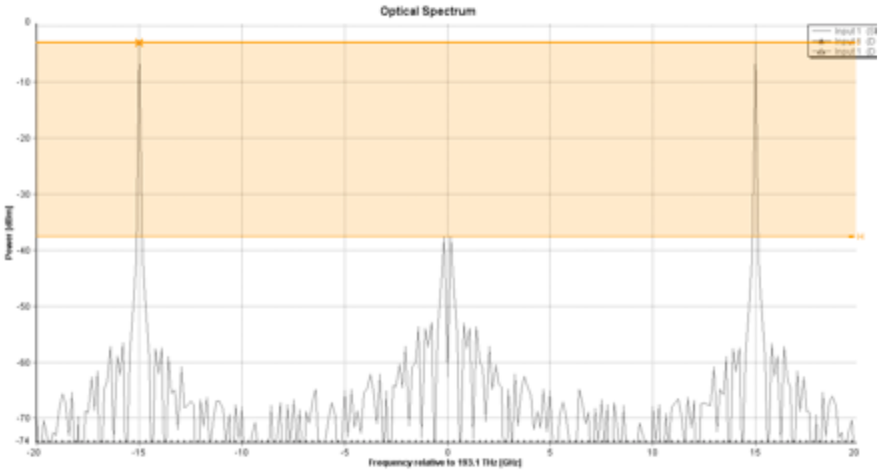

(a)

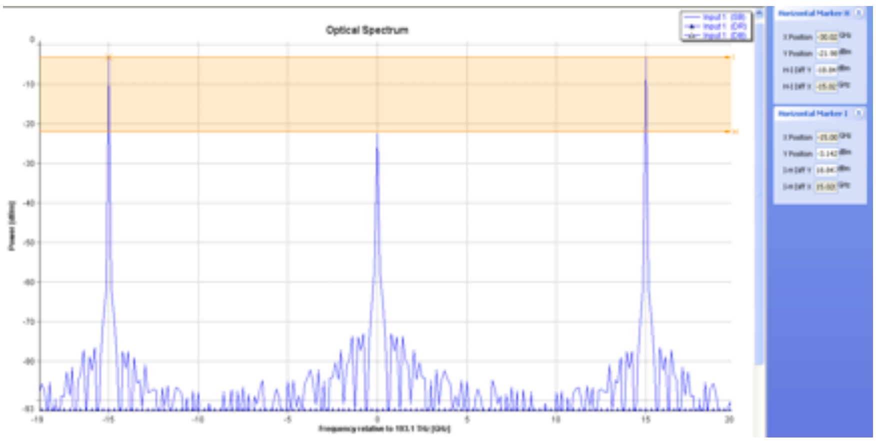

(b)

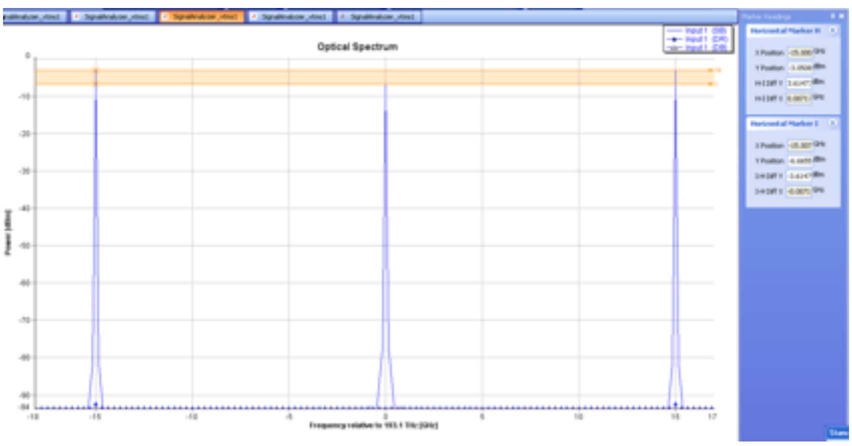

(c)

Fig. 4.12 Output DSB-SC signal from the circulator at pump gain of (a) 30 dB (b) 20 dB and (c) 10 dB

It can be also seen that the SBS pedestal noise is decreased as the pump gain decreases. There is a clear dependence of the SBS noise on the pump gain. A solution was found that achieves carrier suppression below the LO modulation sidebands and at the same time produces clear spectral lines that are free of SBS noise as shown in Fig. 4.12(c). The EDFA pump gain was set to 10 dB. At this condition, the carrier was still maintained below the LO modulation sidebands by 3.6 dB and the SBS noise was completely eliminated. This is exactly what was done in the experiment to get rid of the SBS pedestal noise.

4.4.4.2 VPI simulation of the SFDR

Fig. 4.13 shows the complete set-up for the SBS carrier suppression based linearized photonic mixer.

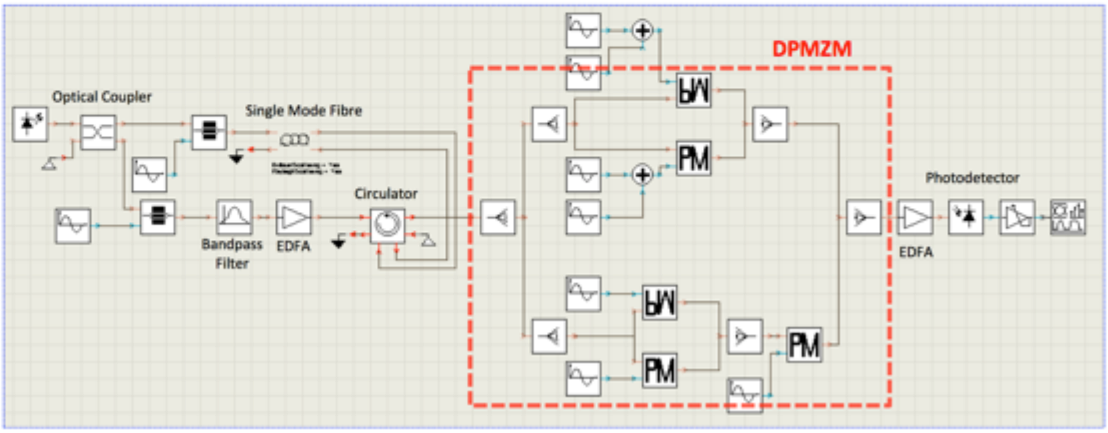

Figure 4.13: VPI simulation setup of the SBS carrier suppression based linearized mixer

The output optical power from the circulator was fed into the single drive DPMZM which was driven by a two tone RF signal at $f_{RF,1}$= 16 GHz and $f_{RF,2}$= 16.05 GHz. The RF power was initially set to 7 dBm. The bias condition for the DPMZM was set to φ_1= 0.46π, φ_2 = $\pi/3$ and φ_3 = π, which also satisfies the linearisation condition (4.24), however, the conversion efficiency performance is slightly less than the DPMZM bias condition for linearisation discussed in the Matlab simulation. The output modulated signal from the DPMZM was then amplified by 20 dB to maintain an average optical power into photo detector to be 5.6 dBm. The output spectrum from the signal analyzer consisted of the downconverted IF signal at frequencies f_{IF1}= 1 GHz and f_{IF2} = 1.05 GHz and the IMD3 at frequencies $f_{IMD3,1}$ = 0.95 GHz and $f_{IMD3,2}$ = 1.10 GHz. The optimum LO modulation index can be determined by adjusting its value until maximum IF power is obtained. The optimum value was found to be close to 0.13. The IF and IMD3 power were measured at different input RF power. The measurement is summarized in the Table 4.1.

$P_{in,RF}$ [dBm]	P_{IF} [dBm]	P_{IMD3} [dBm]
7	-11.88	-83.94
6	-12.88	-88.90
5	-13.88	-93.87
4	-14.87	-98.84
3	-15.88	-103.83

Table 4.1: Measured input RF power, output IF power and third order IMD

Also Figure 4.14 shows the actual spectrum observed at the signal analyzer at $P_{in,RF}$ ranging from 3 to 7 dBm.

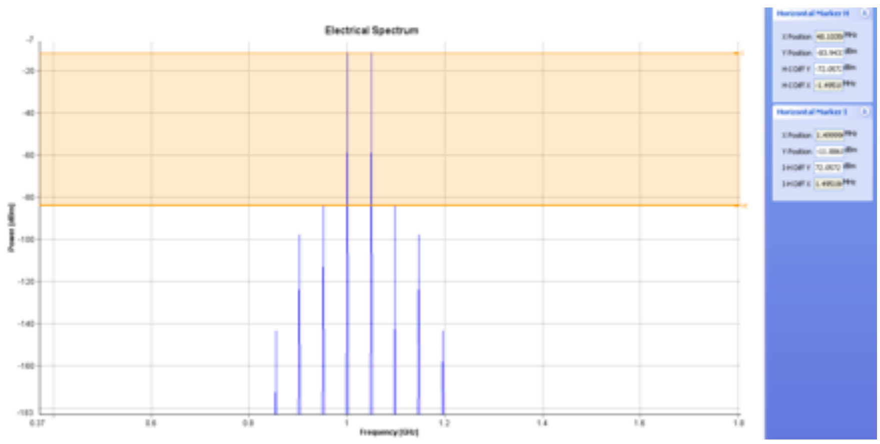

(a)

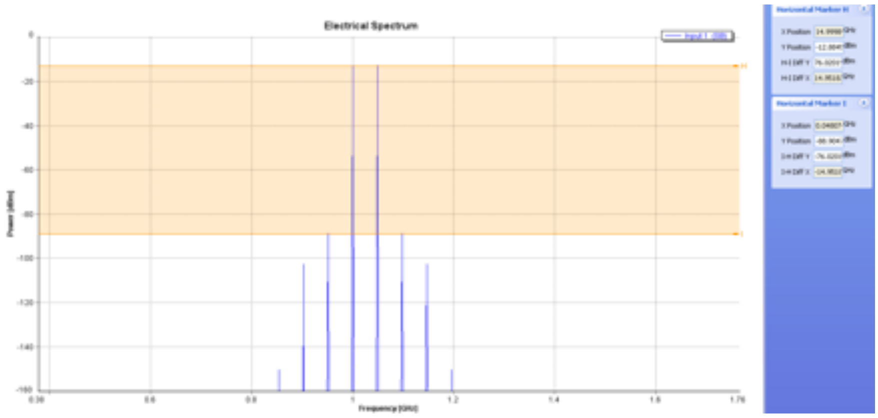

(b)

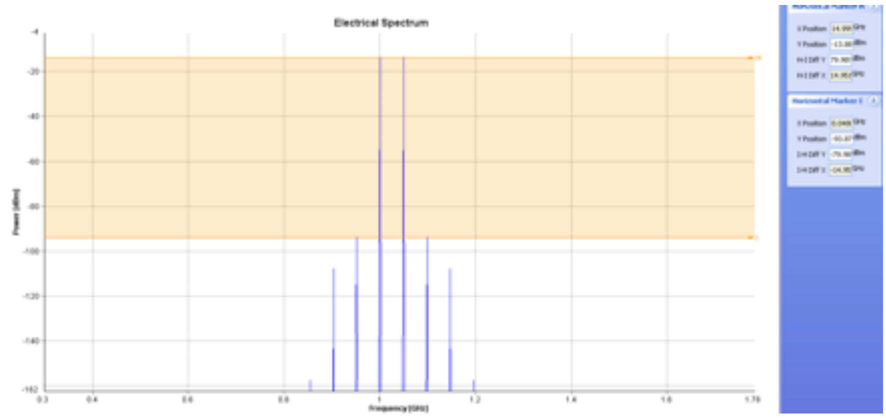

(c)

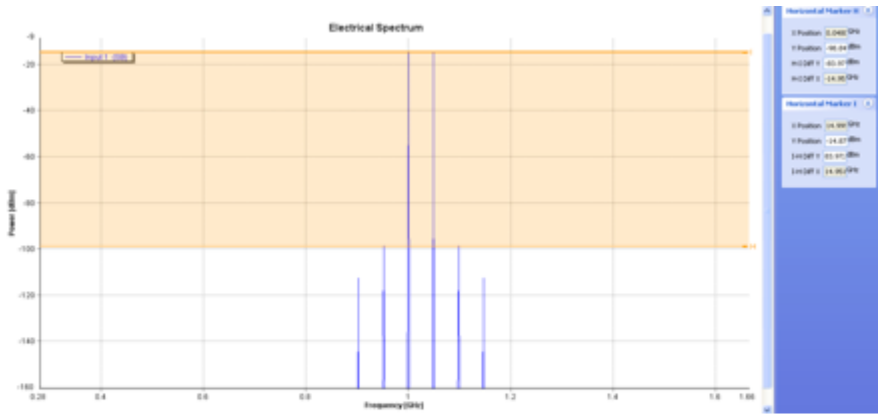

(d)

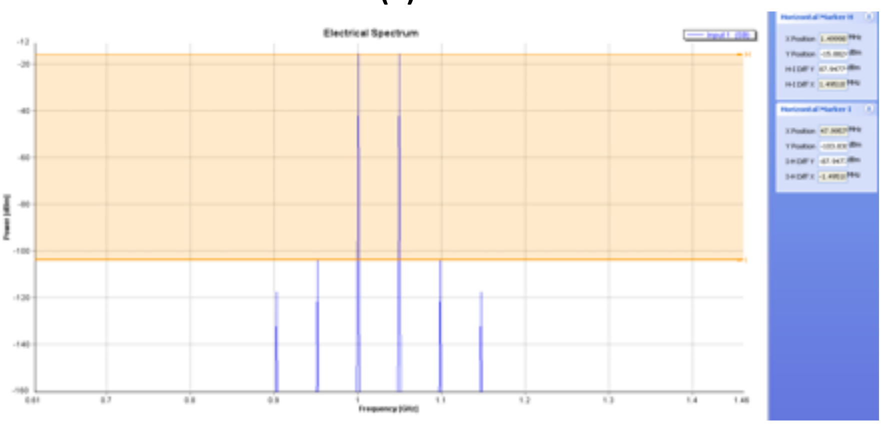

(e)

Figure 4.14: Output IF and IMD spectrum at $P_{in,RF}$ (a) 7dBm (b) 6 dBm (c) 5 dBm (d) 4 dBm and (e) 3 dBm

It can be clearly observed from Figure 4.14 and Table 4.1, that the dominant IMD drops by 5 for every 1 dB change in the RF power. This verifies the linearization principle of the SBS carrier suppression based linearized photonic mixer. The SFDR can then be measured by assuming a noise floor i.e. -147.79 dBm/Hz, which corresponds to the experimental measured noise floor shown in the next section. The noise floor is different from Matlab simulation due to the use of laser source with RIN= -145 dBm/Hz rather than RIN=-160 dBm/Hz. The SFDR was calculated to be 123.2 dB·Hz$^{4/5}$ at an input laser power of 10 dBm and optical average power into photodetector of 5.6 dBm.

4.4.5 Experimental results of the carrier suppressed based linearised photonic mixer

An experiment was conducted to verify the proof of principle of the SBS carrier suppression based linearised photonic mixer. The experimental setup is shown in Fig. 4.15. The optical source used in this experiment was a tunable laser (Santec TSL-210) with RIN= -145 dB/Hz. The optical laser power was set to be 9.5 dBm. A 50:50 optical coupler was used to equally split the optical input into two paths. The optical power travelling in the upper path was fed into an MZM that was driven by a single tone LO at 2 GHz and biased at quadrature. The LO modulation index was set close to 0.2. The MZM insertion loss was measured to be 4.85 dB. The output modulated optical signal (the Stokes wave) was passed through 25km single mode fiber to interact with the pump wave travelling in the counter direction. The optical power travelling in the lower path was modulated by a low biased MZM with pump frequency of 10.54 GHz. The output of the low biased MZM was a double sideband suppressed carrier signal at $f_p = f_c + 10.54$ GHz and $f_{-p} = f_c - 10.54$ GHz. A fiber Bragg grating (FBG) was placed after the MZM so as to filter out the upper sideband of the DSB-SC signal. This was achieved by controlling the tunable laser wavelength so as to align the FBG center frequency to the upper sideband frequency. The resultant output after the FBG is a single sideband suppressed carrier (SSB-SC) signal i.e. the pump wave, which

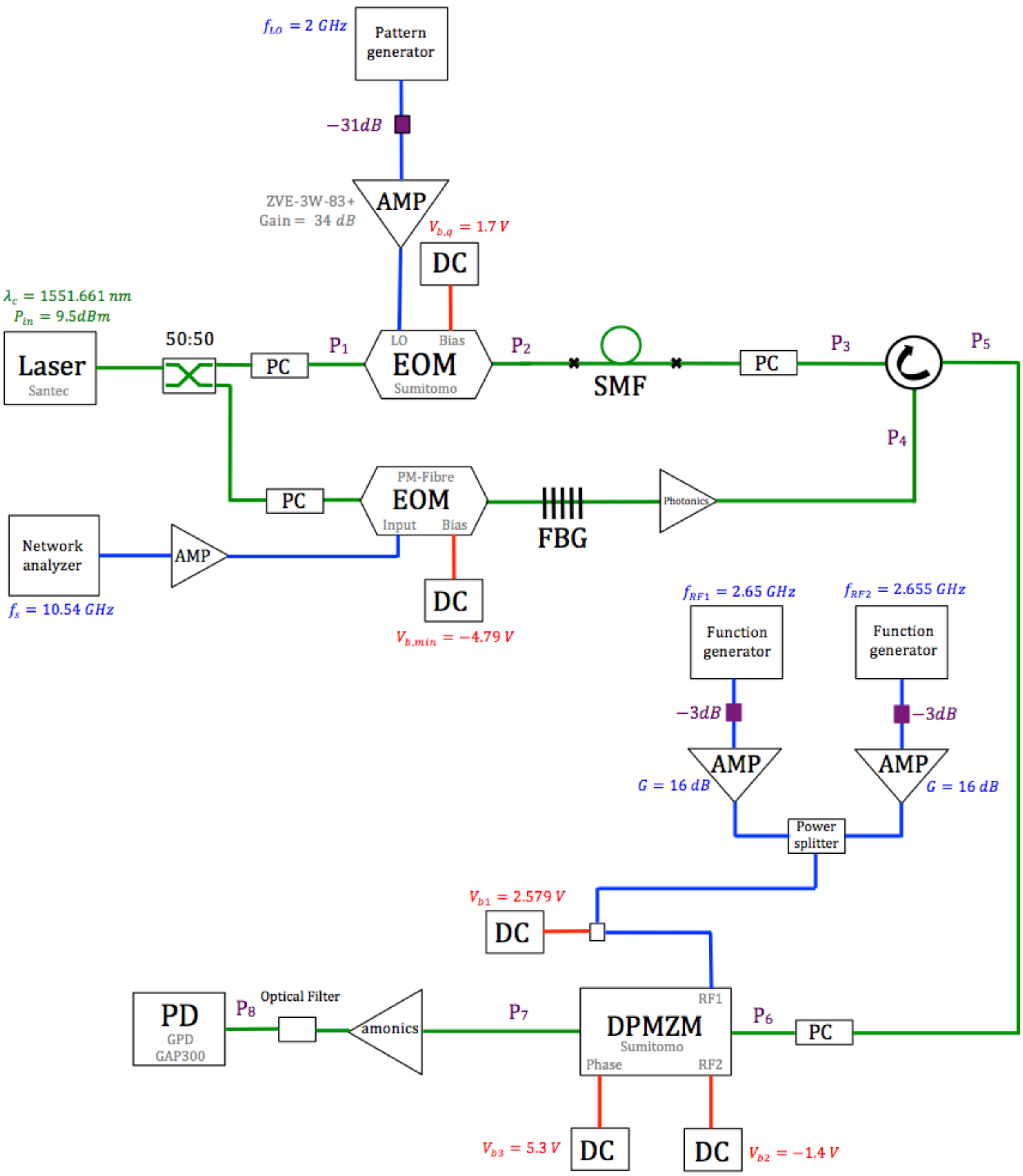

Figure 4.14 Experiment Setup for the SBS suppressed carrier based linearised photonic mixer

was fed to an EDFA (photonics SPLA-B-FC/APC) so as to control the pump power. The pump wave was injected into the other end of the single mode fibre (SMF) via a circulator. It traveled in the opposite direction to the modulated optical signal (the Stokes wave) with a Brillouin frequency shift of exactly 10.54 GHz. Through the SBS process, a loss spectrum was produced at the LO carrier frequency. A polarization controller (PC) was used at the end of the single mode fibre to align the light polarization state of the pump and Stokes wave. The carrier was minimized by its interaction with the loss spectrum. The amount of carrier suppression was controlled through the EDFA gain. The EDFA gain was set to 12 dB so as to make the carrier 3dB below the LO sidebands. The output of the circulator was a DSB-SC LO signal and was fed into the single drive DPMZM. The DPMZM was driven by a two-tone RF signals at f_{RF1} = 2.65 GHz and f_{RF2} = 2.655 GHz. The linearization was obtained by setting the optimum bias condition of the DPMZM to correspond to the theoretical bias condition obtained in the Matlab simulation (i.e. $\varphi_1 = 0.42\,\pi$ $\varphi_2 = 0$, and $\varphi_3 = \pi$). From the DPMZM transfer function, the bias voltages were found to be V_{b1}= 2.579 V, V_{b2}= -1.4 V and V_{b3} = 5.3 V. An EDFA (Amonics AEDFA-PA-35-B-FA) was placed after the DPMZM so as to amplify the output modulated power from the DPMZM. The EDFA gain was set to 22.8 dB so as to make the average power into photodetector to be 5.6 dBm. A tunable optical filter (Newport TBF-1550-1.0) with bandwidth of 1 nm was also inserted before the photodiode to filter out the ASE noise generated from the EDFA. The output of the photodiode is the desired IF downconverted signal. Table 4.2 shows the optical power measurement at different points as illustrated in Fig 4.14.

Optical Power Label	Measured value [dB]
P_1	6.3
P_2	-1.1
P_3	-7.2
P_4	3.2
P_5	-9
P_6	-9.4
P_7	-17.2
P_8	5.6

Table 4.2 Optical power measurements at different locations in the experiment

Fig. 4.15 shows the measured output IF power at 0 dBm input RF power. A clear IF spectral line is obtained free from SBS pedestal noise.

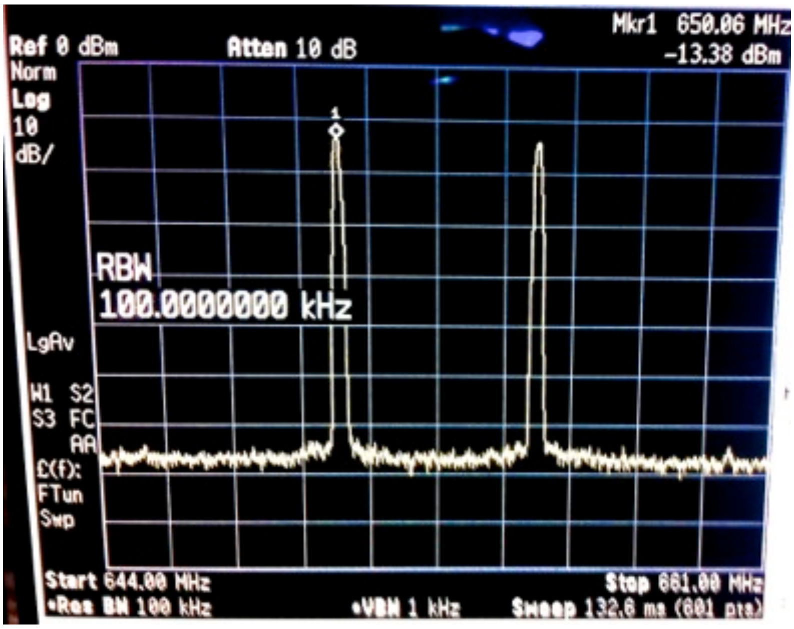

Figure 4.15 Measured IF spectrum at the output of the spectrum analyzer at Pin,RF = 0 dBm.

The output IF power was recorded to be -13.38 dBm at input RF power of 0 dBm. Hence a conversion efficiency of -13.38 dB was measured at 2.65 GHz RF signal, which matches the simulation results obtained in the Matlab simulation. The system noise floor was also measured. The method used to measure the noise floor is shown in Fig. 4.16

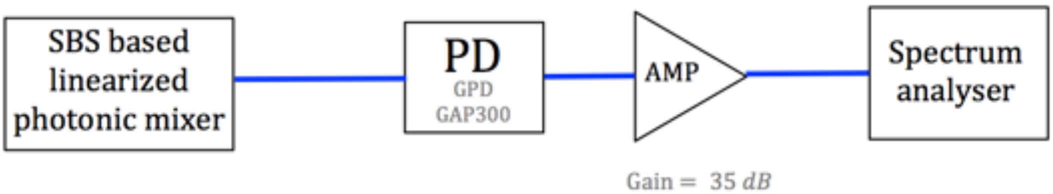

Fig. 4.16 The method to measure the system noise floor in the SBS based linearized photonic mixer

An RF amplifier with a gain of 35 dB was added after the photodetector to amplify the noise floor of the whole system so as to make it visible above the noise floor of the spectrum analyzer. The noise floor was first measured when the booster RF amplifiers after the two-tone input were turned on and it was found to be $-103.45 - 35 = -138.45$ dBm/Hz. However these RF amplifiers were not low-noise and they introduce substantial noise themselves. Hence, in order to consider the case if low-noise RF amplifiers at the RF input were available and were used, the RF amplifiers were turned off, and the noise floor was re-measured and was found to be −112.79 − 35 = −147.79 dBm/Hz as shown in Fig. 4.17. The dominant noise contribution to the noise floor was found to be the laser intensity noise. This is primarily due to the use of the Santec laser, which had a relatively high RIN level of -145 dB/Hz.

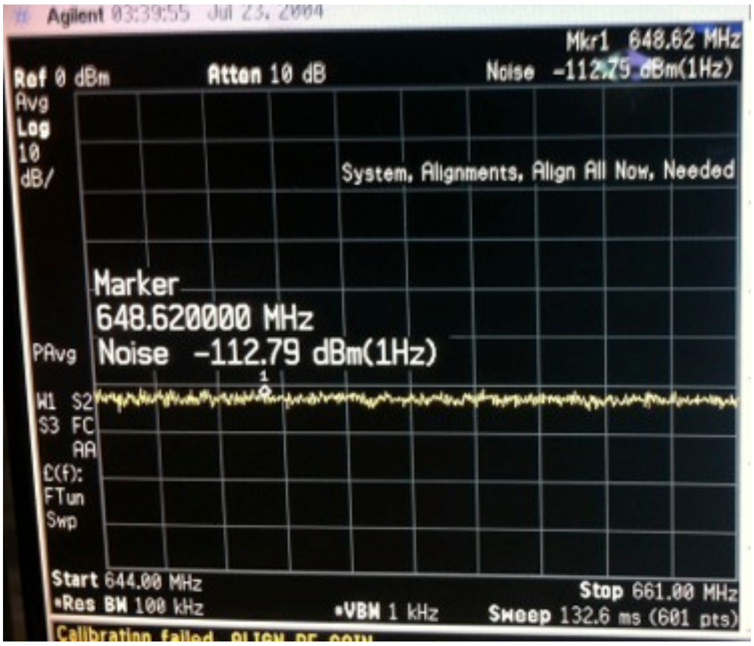

Figure 4.16 measurement of the output noise floor of the SBS suppressed carrier based linearised photonic mixer

The change in the IF signals and the third order IMDs with respect to the input RF signal power was measured under the optimum DPMZM bias condition, which is V_{b1}= 2.579 V, V_{b2}= −1.4 V and V_{b3} = 5.3 V. It was observed that the IMD3 was dropped by 5 dB for every 1 dB reduction in the input RF signal power. This verified that the linearisation principle was successfully achieved using the optimum DPMZM bias voltages. Table 4.3 shows four measurements of the IF and IMD3. The resolution bandwidth on the spectrum analyzer was reduced from 100 kHz to 1 kHz in the measurements in order to enable the IMD3 components to be observable at the lower power levels.

$P_{in,RF}$ [dBm]	P_{IF} [dBm]	$IMD3$ [dBm]
2	-11.85	-70.05
1	-12.51	-74.96
0	-13.38	-79.55
-1	-14.33	-84.54

Table 4.3 Measured IF and IMD3 output at different input RF power.

Based on the IF and IMD3 measurements as well as the noise floor measurement, the SFDR was determined to be 120.8 dB.Hz$^{4/5}$ as shown in Fig. 4.17.

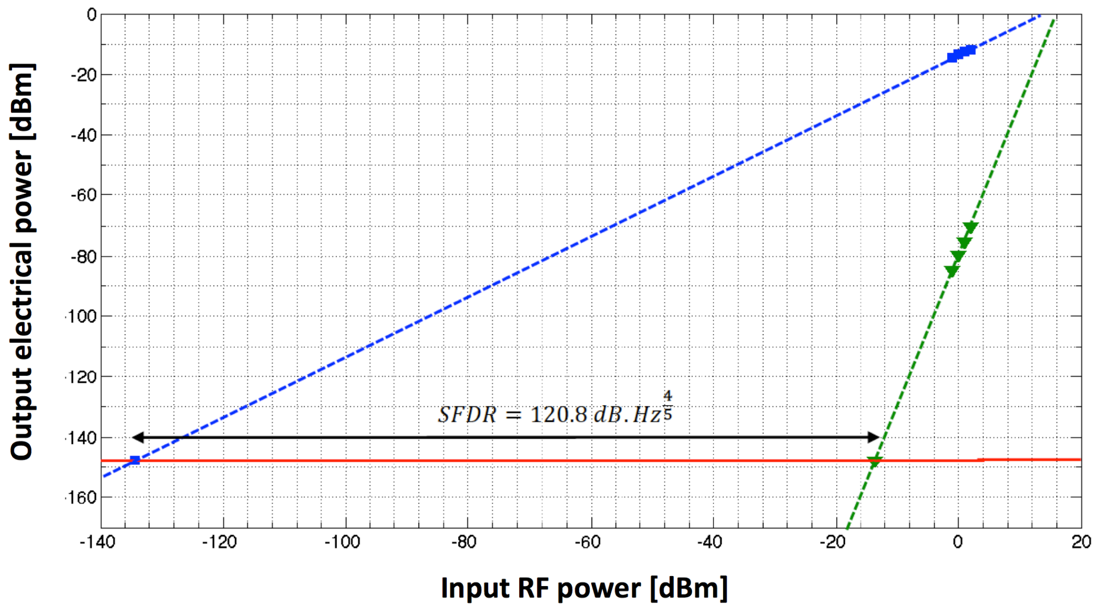

Fig.ure 4.17. SBS suppressed carrier based linearised photonic mixer output electrical power versus input RF signal power. Measured IF signal power (■), measured IMD3 (▼), and measured noise floor (—).

The SFDR result matches Matlab and VPI simulation results, which indicates the validity of the experimental results. This SFDR result corresponds to 16 dB improvement in the SFDR performance when compared to the dual-series MZM based photonic mixer structure. Further improvement in the SFDR is possible by using a higher-power laser source, by using a lower RIN laser, and by using a higher optical power handling DPMZM, which can avoid using an EDFA thus lowering the system noise floor. In general, the experimental results for the SBS suppressed carrier based linearised photonic mixer showed good agreement with the simulated values of SFDR and conversion efficiency. The measured SFDR of 120.8 dB.Hz$^{4/5}$ is close to the best SFDR reported previously for photonic mixers, and in addition this new structure overcomes the previous limitations by enabling multi-octave wideband operation and essentially infinite isolation between the RF and LO ports.

4.5 Conclusion

In this chapter, a new structure for a linearised photonic mixer based on SBS carrier-suppression and a single-drive DPMZM, has been presented. Following a literature review on carrier suppression methods to improve the conversion efficiency of micorwave photonic mixers, it has been shown that these mixer structures were subject to either limited SFDR performance, suboctave bandwidth operation, ineffective carrier suppression or poor isolation between the LO and RF ports, and that there is a need for a linearised photonic mixer technique that overcome all these limitations. A new wideband linearised photonic mixer structure that can simultaneously achieve a good SFDR performance, and a good conversion efficiency has been presented. The new structure also enables multi-octave operation, and infinite isolation between the LO and RF ports. It is based on a SBS suppressed-carrier double sideband LO MZM in series with an integrated single drive DPMZM to which an optimised bias condition is applied. The use of single drive DPMZM enables broadband signal operation to be obtained by eliminating the need for an electrical hybrid coupler as was necessary in the technique discribed in the previous Chapter. Simulation results showed an SFDR of 120.4 dB·Hz$^{4/5}$, and a conversion gain of 8.45 dB, corresponding to 15 dB, and 8.8 dB improvements respectively when compared to the conventional dual series MZM based photonic mixer. Experimental results have demonstrated a measured SFDR performance of 120.8 dB·Hz$^{4/5}$ obtained at laser power of 9.5 dBm, and an average optical power of 5.6 dBm, and can be improved further by using a higher power laser and by using a lower RIN laser. These results are close to the best previously reported SFDR for photonic mixers, and moreover this new structure overcomes the previous limitations by enabling multi-octave wideband operation and essentially infinite isolation between the RF and LO ports.

References

1. B. Haas, and T. E. Murphy, " A carrier-suppressed phase-modulated fiber optic link with IF downconversion of 30GHz 64-QAM signals," presented at the International Topical Meeting on Microwave Photonics, Valencia, Spain, 14-16 October 2009.

2. S. Li, X. Zheng, H. Zhang, and B. Zhou, "Highly linear radio-over-fiber system incorporating a single-drive dual-parallel mach-zehnder modulator," IEEE Photon. Technol. Lett., vol. 22, no. 24, pp. 1775–1777, 2010.

3. E. H. W. Chan, and R. A. Minasian, "Microwave photonic downconverter with high conversion efficiency," IEEE J. Lightwave Technol., vol. 30, no. 23, pp. 3580-3585, 2012.

4. E. H. W. Chan, and R. A. Minasian, "Microwave photonic downconversion using phase modulators in a Sagnac loop interferometer," IEEE J. sel. Topics in Quantum Electronics, vol. 19, no. 6, 2013.

5. E. H. W. Chan, and R. A. Minasian, "High conversion efficiency microwave photonic mixer based on stimulated brillouin scattering carrier suppression technique," Opt. Lett., vol. 38, no. 24, pp. 5292-5295, 2013.

6. J. Ni, L. Liu, S. Zheng, X. Jin, H. Chi, and X. Zhang, "Performance improvement in phase-modulation radio over fiber link through carrier suppression using stimulated Brillouin scattering," CJMW, Hangzhou, China, 20-22 April 2011.

7. L. Liu, S. Zheng, X. Zhang, X. Jin, and H. Chi, "Performance improvement in radio over fiber link through carrier suppression using stimulated Brillouin scattering," Opt. Express, vol. 18, no. 11, pp. 11827-11837, 2010.

8. A. B. Ruffin, "Stimulated brillouin scattering: an overview of measurements, system impairments, and applications," Technical Digest: Symposium on Optical Fiber Measurements, Boulder, USA, 28-30 Sept 2004.

9. A. Loayssa, D. Benito, and M. J. Grade, "High-resolution measurement of stimulated Brillouin scattering in single-mode fibres," IEEE Optoelectronics, vol. 148, no. 3, pp. 143-148 2001.

10. P. Bayvel, P. Radmore, and I. P. Giles, "All-fibre Brillouin amplifiers in single mode fibres and fibre ring resonators," IEEE Colloquium on Optical Amplifiers for Communications, London, UK, 27 Oct 1989.

11. R. W. TKACH, and A. R. Chraplyvy, "Fibre Brillouin amplifiers', Opt. Quantum Electron., vol. 21, pp. S105-S112, 1989.

12. E. H. W. Chan, and R. A. Minasian, "All-optical frequency shifter based on stimulated Brillouin scattering in an optical fiber," IEEE J. Photonics, vol. 6, no. 2, 2014.

13. W. Zhang, and R. A. Minasian, "Widely tunable single-passband microwave photonic filter based on stimulated Brillouin Scattering," IEEE Photon. Technol. Lett., vol. 23, no. 23, pp. 1775–1777, 2011.

14. A. Loayssa, and F. J. Lahoz, "Broad-band RF photonic phase shifter based on stimulated Brillouin scattering and single-sideband modulation," IEEE Photon. Technol. Lett., vol. 18, no. 1, pp. 208-210, 2006.

15. Y. Shen, X. Zhang, and K. Chen, "A simple filter based on stimulated Brillouin scattering for carrier-suppression of microwave photonics signals," Proc. Of SPIE, vol. 5625, pp. 109-116, 2005.
16. Y. Shen, X. Zhang, and K. Chen, "Optical carrier-suppression of microwave signals with stimulated Brillouin scattering in long fiber ring," Microw. Opt. Technol. Lett., vol. 43, no. 3, pp. 258-260, 2004.

17. R. Helkey, J. Twichell, and C. Cox, "A down-conversion optical link with RF gain," IEEE J. Lightwave Technol., vol. 15, no. 6, pp. 956-961, 1997.

18. M. E. Manka, "Microwave photonics electronic warfare technologies for Australian defence," in Proc. IEEE Int. Top. Meet. Microw. Photon., pp. 1–2, 2008.

CHAPTER 5 Conclusion

5.1 Summary

Photonic signal processing offers unprecedented features for processing high bandwidth signals. It puts forward a new prospect for overcoming the inherent bottlenecks caused by limited sampling speeds in conventional microwave signal processors [1]. The motivation emerges from the great potential of exploiting the unique, high time-bandwidth product, low loss, and immunity to electromagnetic interference (EMI) capabilities of photonic signal processing [2]. Microwave photonic signal processing is considered an attractive alternative approach for processing wideband microwave signals compared to the conventional microwave systems. Amongst the different types of photonic signal processors, the microwave photonic frequency downconverter is important in many communication systems and particularly in antenna remoting systems [3].

Two new microwave photonic downconverters have been presented in this thesis. These new structures have resulted in enhanced SFDR and conversion efficiency performance compared to the previously reported microwave photonic approaches.

The achievements of the work completed in this thesis are summarized below.

- A new linearised photonic mixer structure that can simultaneously achieve a very high SFDR performance, while also enabling multi-octave operation, has been presented. It is based on applying an optimised RF split and an optimised optical phase shift to an integrated DPMZM, which is in series with an MZM driven by the LO. The DPMZM is linearised by fully cancelling third order IMD via controlling the modulator bias voltages and designing the splitting ratio of the RF signals into the modulators inside the DPMZM. This technique also features near infinite isolation between the RF and LO ports, and the ability to function over a multi-octave frequency range. Simulation results have shown different bias solutions with the aim of improving the conversion efficiency or the noise figure while simultaneously achieving high SFDR performance. The tolerance of the linearised DPMZM based microwave photonic mixer has been also investigated and a bias solution was obtained to relax the critical tolerance requirements of the linearised approach. Experimental results have demonstrated a record measured SFDR of 127 dB·Hz$^{4/5}$, which is also 22.5 dB higher than that of the conventional dual-series MZM based mixer structure.

- A new linearised photonic mixer structure that uses carrier suppression together with wideband linearization has been presented. The new structure also enables multi-octave operation, and infinite isolation between the LO and RF ports. It is based on the stimulated Brillouin scattering effect to suppress the LO carrier which is then input to an integrated single drive DPMZM to which an optimised bias condition is applied. The use of single drive DPMZM enables broadband signal operation by eliminating the need for an electrical hybrid coupler as was needed in the previous approach. Simulation results showed an SFDR of 120.4 dB·Hz$^{4/5}$, and a conversion gain of 8.45 dB, corresponding to 15 dB, and 8.8 dB improvements respectively when compared to the conventional dual series MZM based photonic mixer. Experimental results have demonstrated a measured SFDR performance of 120.8 dB·Hz$^{4/5}$, which corresponds to 16 dB improvement when compared to the conventional dual-series MZM based mixer structure.

5.2 Future Work

Although high SFDR, and high conversion efficiency photonic downconverters were demonstrated, a number of issues need to be addressed in the future to further improve the performance of the two proposed photonic mixer structures. With respect to the linearised DPMZM based photonic mixer structure, the critical sensitivity of the RF split in terms of amplitude and phase caused a reduction in the signal transmission bandwidth under the optimised DPMZM bias condition. A technique was demonstrated to relax the SFDR tolerance with respect to the phase and the amplitude characteristics of the RF voltage split, though at the expense of a reduction in the SFDR performance. Thus future work should be focused on improving the tolerance requirements of the linearised approach without causing a penalty in the dynamic range performance. Regarding the SBS suppressed carrier based linearised photonic mixer, the experimental results obtained for the noise floor was much higher than the simulated noise floor, which led to a degradation in noise figure. One reason for this is that the SBS noise, which was not accounted for in the simulation, also contributes to the total noise floor. The Brillouin-induced depletion caused a pedestal noise on the carrier. This pedestal noise was minimized by reducing the pump power. However, the SBS noise needs to be studied and considered in future work to optimize the noise performance and carrier suppression characteristics.

Other than using intensity modulation direct detection (IM/DD) techniques to linearize the photonic mixer, there have also been emerging linearisation techniques, using phase modulation direct detection (PM/DD). The modulators in PM/DD techniques are simple in design and do not require active bias circuits. Moreover through carrier suppression, PM/DD techniques exploit both sidebands of the downconverted IF signal while intensity modulators only utilize one sideband of the signal.

Finally more investigation should be made on methods to linearize, and increase the SFDR of photonic mixer structures through the use of photonic integrated circuits (PICs). The photonic mixer components can be monolithically integrated into a single chip using, for example, Indium Phosphide (InP) as a material platform. Other available technology platforms include Silica, Silicon, Chalcogenides, and so on. This integration of photonic components simplifies optical system design, reduces space and power consumption and improves reliability. Moreover, it also lowers the cost of Optical-to-Electrical-to-Optical (OEO) conversion. PICs also provide the possibility to be combined with electronic integrated circuits and hence maximize system functionality and simplify system operations. All these advantages can be obtained in a very compact and robust chip [4,5].

References

1. R. A. Minasian, "Photonic signal processing of microwave signals," IEEE. Trans. Microw. & Tech., vol. 54, no. 2, pp. 832–846, 2006.
2. J. P. Yao, "Microwave photonics," J. Lightw. Technol., vol. 27, no. 3, pp. 314–335, 2009.
3. C. H. Cox, "Steps towards photonic antennas," International conference on phased array systems and technol., Dana Point, CA, 21-25 May 2000.
4. D. Marpaung, C. Roeloffzen, R. Heideman, A. Leinse, S. Sales, and J. Capmany, "Integrated microwave photonics," Lasers Photon., vol. 7, no. 4, pp. 506-538, 2013.
5. J. Capmany and P. Munoz, " Integrated microwave photonics for radio access networks," J. Lightw. Technol., vol. 32, no. 16, pp. 2849-2861, 2014.

Index – List of Acronyms

A/D	Analog to Digital
ASE	Amplified Spontaneous Emission
CATV	Community Access TV
CkW	Clockwise
CCkW	Counter Clockwise
CW	Continuous Wave
DFB	Distributed Feedback
DSB+C	Double Sideband with Carrier
DSB-SC	Double Sideband Suppressed carrier
DSM	Dual-Series Modulator
DPMZM	Dual Parallel Mach-Zehnder Modulator
EAM	Electro-Absorption Modulator
EDFA	Erbium Doped Fibre Amplifier
EHF	Extremely High Frequency
EMI	Electro-Magnetic Interference
EOM	Electro-Optic Modulator
FBG	Fibre Bragg Grating
FOL	Fibre Optic Link
HD	Harmonic Distortion
IF	Intermediate Frequency
IM/DD	Intensity Modulation Direct Detection
IMD	Intermodulation Distortion
IMD2	Second Order Intermodulation Distortion
IMD3	Third Order Intermodulation Distortion
IMD5	Fifth Order Intermodulation Distortion
InP	Indium Phosphide
LED	Light Emitting Diode
$LiNbO_3$	Lithium Niobate
LO	Local Oscillator
MZM	Mach-Zehnder Modulator
NF	Noise Figure
OEO	Optical-to-Electrical-to-Optical
PC	Polarization Controller
PICs	Photonic Integrated Circuits
PM	Phase Modulator
RF	Radio Frequency
RIN	Relative Intensity Noise
RoF	Radio over Fibre
SBS	Stimulated Brillouin Scattering
SFDR	Spurious Free Dynamic Range
SNR	Signal-to-Noise Ratio
SOA	Semiconductor Optical Amplifier
SSB	Single Sideband
SSB-SC	Single Sideband Suppressed Carrier
UHF	Ultra High Frequency
WDM	Wave Division Multiplexing